# Altimetry for Estimating Snow Depth on Sea Ice: Surface and Satellite Observations from the Canadian Arctic

by

Monojit Saha

A Thesis submitted to

Faculty of Graduate Studies of the University of Manitoba

In partial fulfillment of the requirements of the degree of

MASTER OF SCIENCE

Department of Environment and Geography,

University of Manitoba

Winnipeg, Canada

# Abstract

Snow plays a vital role in near-shore landfast sea ice physical and biological processes. It needs to be monitored in order to understand sea ice processes and also for estimating sea ice thickness. However, snow depth remains difficult to estimate directly from space which forces the sea ice thickness products to use snow depth from model outputs or out of date climatology. Satellite altimetry based dual-radar and coincident laser/radar have been considered for providing regular estimates of snow depth on sea ice. In addition to the limitations associated with the functioning of individual altimeters, snow on landfast sea ice presents its own challenges especially due to the lack of leads. While past studies have mostly focused on approaches suited to pack ice in the Central Arctic, this study aims to provide critical observations from landfast first-year sea ice in the Canadian Arctic. Surface-base altimeter retrievals from snow on sea ice at Churchill, Manitoba is compared to snow on lake ice demonstrate that the position of the Ku-band main scattering horizon is impacted by the presence of brine in the snow pack. The satellite-level study conducted at Dease Strait near Cambridge Bay is the first to assess the possibility of using coincident laser/radar altimeters (Cryo2Ice) for estimating snow depth on land-fast and lead-less sea ice at the Canadian Arctic Archipelago. The retrieved Cryo2Ice snow depths were underestimated by an average of 20.7 % which is slightly higher than the tidal adjustment applied. However, snow geophysical properties and surface roughness are seen to significantly bias Cryo2Ice retrievals. Both surface and satellite based studies point towards the position of the Ku-band main scattering horizon being closer to the air-snow interface as opposed to the generally assumed snow-ice interface. Therefore, findings from this study may be useful for monitoring snow depth on land-fast sea ice using currently available and future satellite altimeters whereby snow depth and sea ice satellite products may be more useful in a landfast sea ice context.

## Acknowledgement

First and foremost, I would like to express my gratitude towards my supervisors Dr. Julienne Stroeve and Dr. Dustin Isleifson for their unwavering support throughout my masters. I want to thank them for helping me throughout many challenges and uncertainties that came along the way. I'm also grateful to my committee members Dr. Zou Kuzyk and Dr. Colin Gilmore for their vital inputs and guidance throughout the program. I'm grateful for financial support from Julienne Stroeve's Canada-150 Research Chair, ArcticNet and University of Manitoba Graduate Fellowship. I want to thank the numerous mentors that have helped me throughout my masters. Drs Mallik Mahmud and Vishnu Nandan for inspiring a clueless undergrad from Bangladesh to take up Arctic Science. I also want to thank Dr. Vishnu Nandan and Dr. Rosemary Willatt for playing instrumental roles as mentors for helping me with both my projects with both their scientific expertise and also as a friend and mentor. Special thanks to Dr. John Yackel for being a mentor on both my field campaigns in Churchill and Cambridge Bay and truly showing the way on tackling the numerous challenges in field work. Dr. Jack Landy for his vital feedback and guidance on satellite altimetry throughout the project. Dr. David Walker not only for his guidance in GIS and Statistics but also as a mentor through the Advanced Geomatics course. My heartfelt gratitude to my friends and colleagues at CEOS especially Fowzia, Patricia, and Vaishali for always lending their support through thick and thin. The support of my parents and my brother Anujit is the main driving force behind everything I achieve, I want to thank them for letting me dream. Last but not the least, my wife Anindita for constantly showering me with love and support and not shying away from making the biggest sacrifices which allows us to grow!

*This thesis is dedicated to my mother,*

*Rekha Saha for inspiring me*

*to be a better person every day*

# Table of Contents

## List of Figures

## Contribution of Authors

Chapter 3 was prepared based on data collected from the Churchill Freeze-Up Campaign. Monojit Saha, Rosemary Willatt, Vishnu Nandan, Robbie Mallett, Tom Newman, David Jensen Julienne Stroeve and John Yackel contributed to collecting snow geophysical, KuKa and Magnaprobe data. Monojit Saha conducted the KuKa data processing using methodology suggested in Willat et al, (2023). Rosemary Willatt provided code which was modified by Monojit Saha for conducting the KuKa data analysis. Vishnu Nandan provided the modelling outputs. Julienne Stroeve and Dustin Isleifson provided vital feedback on conceptualization and research direction.

Chapter 4 was prepared as a paper which has been submitted to *The Cryosphere* for publication. Monojit Saha, Julienne Stroeve and Dustin Isleifson were involved in the conceptualization of the study. Monojit Saha, Julienne Stroeve, John Yackel, Hoi Ming Lam and Vishnu Nandan were involved in planning of the field campaign. Julienne Stroeve acquired the funding for the research. Monojit Saha, John Yackel and Hoi Ming Lam collected the snow and sea ice physical property validation data from the field. Monojit Saha, Julienne Stroeve, Dustin Isleifson, Jack Landy and Vishnu Nandan were involved were involved in formulating the methodology for the analysis. Monojit Saha prepared the original draft. All co-authors were involved in the review and editing process.

# Chapter 1: Introduction

As the planet has warmed, sea ice in the Arctic has been changing not only in extent but also in thickness (Meier & Stroeve, 2022), affecting local- and regional-climate, marine ecosystems and navigation, and traditional ways of living and harvesting. Sea ice extent in summer across the northern Canadian waters has decreased by ~ 7% per decade between 1968 and 2015 (ECCC, 2021). Although sea ice extent has been widely used as an indicator for climate change, sea ice volume (derived from extent and thickness) is arguably a better metric for Arctic sea ice loss (Meier and Stroeve 2022). While sea ice thickness from field campaigns, submarines and moorings provide accurate in-situ estimates, the spatial coverage is limited (Kern et al., 2014). Therefore, satellite- based observations provide both the synoptic and temporal resolutions needed for monitoring sea ice thickness.

Although satellite-based sea ice extent has been monitored since 1979 using passive microwaves, the first basin-scale sea ice thickness product using remote sensing was produced only in 2003 by Laxon et al (2003). Using hydrostatic equilibrium assumption (Laxon et al., 2003), and considering estimates of snow depth, satellite altimetry-derived sea ice freeboard can be converted into ice thickness (Kwok & Cunningham, 2008). Therefore, snow depth is crucial for sea ice thickness estimation. Moreover, providing Arctic communities forecasts of the changing trends in snow depth is important to avoid major sea ice hazards (Eicken & Mahoney, 2015). Changes in snow on sea ice have also been linked to the process of melt pond formation (Eicken et al., 2004). The changing snow on sea ice has also been observed to affect the ringed seal because they need at least 20 cm snow depth on sea ice to build snow caves (Hezel et al., 2012). Moreover, the changing snow cover alters the rate of melt which affects the timing of the phytoplankton bloom (Arrigo et al., 2008). Therefore, in order to monitor the changing snow and sea ice, it is important to produce accurate satellite derived snow depth products which can be used in observational as well as model studies/community applications.

Satellite altimetry is being widely used for monitoring pan-Arctic snow depth and sea ice thickness. Dual-frequency radar altimetry and coincident radar/laser altimetry are two satellite altimetry focused approaches which have been explored for retrieving snow depth on sea ice. The basic assumption in both approaches is that Ku-band microwave has dominant scattering from the snow-ice interface allowing the estimation of the sea ice freeboard which is then differenced from the snow freeboard estimated from Ka-band returns (Dual-frequency radar) or laser returns (coincident radar/laser) coming off the top of the snowpack (Beaven et al., 1995; Kwok et al., 2020; Laxon et al., 2003; Ricker et al., 2014). However, several recent studies have shown that Ku band waveform primarily scatters from within the first few tens of centimetres of the snow and therefore does not reach the snow/sea ice interface (Nandan et al., 2017, 2020; Ricker et al., 2014; Willatt et al., 2010). Snow geophysical conditions such as the snow density (Mallett et al., 2020), temperature (Willatt et al., 2010), salinity (Nandan et al. 2017; 2020), and surface roughness (Landy et al., 2020) affect the position of the dominant scattering horizon of Ku-band microwaves in the snowpack.

Surface based measurements (often limited in spatial coverage) are important for validating satellite measurements using the same frequencies. This study presents observations from a surface based altimeter that uses the same frequencies as satellite-based dual-frequency altimeters operating in Ku-band (Cryosat-2) and Ka-band (AltiKa). The use of dual-frequency radar (Ku and Ka) for estimating snow depths has been tested for both currently active altimeters (Cryosat-2 and AltiKa) and the future Copernicus Polar Ice and Snow Topography Altimeter (CRISTAL) missions. However, critical uncertainties including the penetration of the Ku band into the snowpack, difference in footprint size (Guerreiro et al., 2017) and the choice of retrackers on the Ku/Ka waveform (Lawrence et al., 2018) remain major challenges that need to be addressed. Surface based altimeters play a critical role in collecting validation measurements and improving our understanding of microwave interactions with the snowpack as well as the impacts of in-situ snow conditions on the radar waveform.

At the satellite level, coincident laser/radar approaches which also uses a Ku-band radar (Cryosat-2), have been recently explored due to the Cryo2Ice campaign in August 2020 where the Cryosat-2 orbit has been adjusted to have better coincidence with ICESat-2 in the Arctic followed by a further realignment to have better coincidence over the Antarctic (Kwok et al., 2020; Lawrence et al., 2018). This provides a unique opportunity to test how well snow depth can be retrieved over sea ice using coincident radar and laser altimetry. However, using a combination of Cryosat-2 and ICESat-2 products to estimate snow depth especially on landfast sea ice in the Canadian Arctic is challenging because of the difficulty in assessing the sea surface height with no leads appearing during the winter. Other factors, including land contamination of the radar and laser altimeter signals, and uncertainties associated with the retrieval processes of the two altimeters are critical challenges in estimating snow depth on sea ice from satellite altimetry. The accuracy of Cryo2Ice derived snow depths within the Canadian Arctic Archipelago (CAA) has not been explored previously. Identifying sources of errors is imperative for improving snow depth measurements from Cryo2Ice in the CAA.

While several studies have assumed full penetration of Ku-band in the snowpack and have relied on airborne validation campaigns for ICESat-2 (Operation IceBridge) and Cryosat-2 (CryoVEX) to assess the accuracy of retrieved snow depths, these validation campaigns did not cover landfast ice in the Canadian Arctic.  Therefore, the overall objective of this thesis is to evaluate the dual-frequency (Ku and Ka) radar approach from surface measurements and a coincident laser/radar approach for estimating snow depth on landfast sea ice in the Canadian Arctic from the satellite level. A comprehensive analysis focusing on different aspects that influence uncertainties in snow depth retrievals is conducted using in-situ, surface-based radar and satellite level techniques. Chapter 3 presents the study exploring the dual- frequency radar altimeter approach using surface-based Ku-Ka radar. The interaction of Ku and Ka band radar over brine-wetted snow on sea ice is compared against non-saline snow on lake ice. Chapter 4 explores the coincident radar/laser satellite altimeter approach for estimating snow depth on sea ice. The study presents an in-situ snow depth validation dataset along a coincident Cryo2Ice line on the 29th of April 2022 near Cambridge Bay in the Canadian Arctic Archipelago. The ICESat-2 and Cryosat-2 passes had very high temporal (~1hour) and spatial (~1 km) coincidence which reduces the bias due to geo-location and time of flight difference. Impact of other sources of bias including snow geophysical properties and surface roughness on snow depth retrieved from Cryo2Ice were also assessed.

## 1.1 Thesis Objective

The aim of this thesis is to make critical observations and improve snow depth on sea ice estimates using altimetry on first-year landfast sea ice from both the surface and satellite scale.

The two specific objectives of the thesis are as follows:

(i) Analyze microwave interaction with snow on sea ice using a surface based Dual-frequency Ku-Ka band altimeter using snow on lake ice as a control.

(ii) Retrieve and validate snow depth on sea ice from coincident satellite laser (ICESat-2) and radar (Cryosat-2) altimeters.

Objective (i) is addressed in Chapter 3 and Objective (ii) is covered in Chapter 4.

## References

Arrigo, K. R., van Dijken, G., & Pabi, S. (2008). Impact of a shrinking Arctic ice cover on marine primary production. *Geophysical Research Letters*, *35*(19). https://doi.org/10.1029/2008GL035028

Bunzel, F., Notz, D., & Pedersen, L. T. (2018). Retrievals of Arctic Sea-Ice Volume and Its Trend Significantly Affected by Interannual Snow Variability. *Geophysical Research Letters*, *45*(21), 11,751-11,759. https://doi.org/10.1029/2018GL078867

De Rijke-Thomas, C., Landy, J. C., Mallett, R., Willatt, R. C., Tsamados, M., & King, J. (2023). Airborne Investigation of Quasi-Specular Ku-Band Radar Scattering for Satellite Altimetry Over Snow-Covered Arctic Sea Ice. *IEEE Transactions on Geoscience and Remote Sensing*, *61*, 1–19. https://doi.org/10.1109/TGRS.2023.3318263

ECCC. (2021). *Canadian environmental sustainability indicators: Sea ice in Canada*. Environment and Climate Change Canada = Environnement et changement climatique Canada.

Eicken, H., Grenfell, T. C., Perovich, D. K., Richter-Menge, J. A., & Frey, K. (2004). Hydraulic controls of summer Arctic pack ice albedo. *Journal of Geophysical Research: Oceans*, *109*(C8). https://doi.org/10.1029/2003JC001989

Eicken, H., & Mahoney, A. R. (2015). Chapter 13 - Sea Ice: Hazards, Risks, and Implications for Disasters. In J. F. Shroder, J. T. Ellis, & D. J. Sherman (Eds.), *Coastal and Marine Hazards, Risks, and Disasters* (pp. 381–401). Elsevier. https://doi.org/10.1016/B978-0-12-396483-0.00013-3

Giles, K. A., Laxon, S. W., Wingham, D. J., Wallis, D. W., Krabill, W. B., Leuschen, C. J., McAdoo, D., Manizade, S. S., & Raney, R. K. (2007). Combined airborne laser and radar altimeter measurements over the Fram Strait in May 2002. *Remote Sensing of Environment*, *111*(2), 182–194. https://doi.org/10.1016/j.rse.2007.02.037

Guerreiro, K., Fleury, S., Zakharova, E., Kouraev, A., Rémy, F., & Maisongrande, P. (2017). Comparison of CryoSat-2 and ENVISAT radar freeboard over Arctic sea ice: Toward an improved Envisat freeboard retrieval. *The Cryosphere*, *11*(5), 2059–2073. https://doi.org/10.5194/tc-11-2059-2017

Hezel, P. J., Zhang, X., Bitz, C. M., Kelly, B. P., & Massonnet, F. (2012). Projected decline in spring snow depth on Arctic sea ice caused by progressively later autumn open ocean freeze-up this century: DECLINE IN SNOW DEPTH ON ARCTIC SEA ICE. *Geophysical Research Letters*, *39*(17), n/a-n/a. https://doi.org/10.1029/2012GL052794

Kern, S., Khvorostovsky, K., Skourup, H., Rinne, E., Parsakhoo, Z. S., Djepa, V., Wadhams, P., & Sandven, S. (2014). *About uncertainties in sea ice thickness retrieval from satellite radar altimetry: Results from the ESA-CCI Sea Ice ECV Project Round Robin Exercise* [Preprint]. Sea Ice. https://doi.org/10.5194/tcd-8-1517-2014

Kwok, R., & Cunningham, G. F. (2008). ICESat over Arctic sea ice: Estimation of snow depth and ice thickness. *Journal of Geophysical Research: Oceans*, *113*(C8). https://doi.org/10.1029/2008JC004753

Landy, J. C., Petty, A. A., Tsamados, M., & Stroeve, J. C. (2020). Sea Ice Roughness Overlooked as a Key Source of Uncertainty in CryoSat-2 Ice Freeboard Retrievals. *Journal of Geophysical Research: Oceans*, *125*(5), e2019JC015820. https://doi.org/10.1029/2019JC015820

Lawrence, I. R., Tsamados, M. C., Stroeve, J. C., Armitage, T. W. K., & Ridout, A. L. (2018). Estimating snow depth over Arctic sea ice from calibrated dual-frequency radar freeboards.

*The Cryosphere, 12*(11), 3551–3564. https://doi.org/10.5194/tc-12-3551-2018

Laxon, S., Peacock, N., & Smith, D. M. (2003). High interannual variability of sea ice thickness in the Arctic region. *Nature*. https://doi.org/10.1038/nature02050

Mallett, R. D. C., Lawrence, I. R., Stroeve, J. C., Landy, J. C., & Tsamados, M. (2020). Brief communication: Conventional assumptions involving the speed of radar waves in snow introduce systematic underestimates to sea ice thickness and seasonal growth rate estimates. *The Cryosphere, 14*(1), 251–260. https://doi.org/10.5194/tc-14-251-2020

Meier, W., & Stroeve, J. (2022). An Updated Assessment of the Changing Arctic Sea Ice Cover. *Oceanography*. https://doi.org/10.5670/oceanog.2022.114

Nandan, V., Geldsetzer, T., Yackel, J., Mahmud, M., Scharien, R., Howell, S., King, J., Ricker, R., & Else, B. (2017). Effect of Snow Salinity on CryoSat-2 Arctic First-Year Sea Ice Freeboard Measurements. *Geophysical Research Letters*, *44*(20), 10,419-10,426. https://doi.org/10.1002/2017GL074506

Willatt, R., Laxon, S., Giles, K., Cullen, R., Haas, C., & Helm, V. (2011). Ku-band radar penetration into snow cover on Arctic sea ice using airborne data. *Annals of Glaciology*, *52*(57), 197–205. https://doi.org/10.3189/172756411795931589

Willatt, R., Stroeve, J. C., Nandan, V., Newman, T., Mallett, R., Hendricks, S., Ricker, R., Mead, J., Itkin, P., Tonboe, R., Wagner, D. N., Spreen, G., Liston, G., Schneebeli, M., Krampe, D., Tsamados, M., Demir, O., Wilkinson, J., Jaggi, M., … Oggier, M. (2023). Retrieval of Snow Depth on Arctic Sea Ice From Surface-Based, Polarimetric, Dual-Frequency Radar Altimetry. *Geophysical Research Letters, 50*(20), e2023GL104461. https://doi.org/10.1029/2023GL104461

# Chapter 2 Background

## 2.1 The Changing Arctic Sea Ice

Arctic sea ice extent is decreasing at an accelerated rate across all seasons (Meier & Stroeve, 2022), which is causing massive changes to the associated physical, chemical and biological processes. Between 1978 to 2022, the minimum sea ice extent in September decreased at a rate of -12.7% per decade (Meier and Stroeve 2022). There is also a statistically significant decreasing trend in the maximum sea ice extent in March in the same period. There has also been a dominant shift in the ice regime from thicker and older multi-year ice to thinner and younger first-year ice (Maslanik et al., 2011). The extent of sea ice that is greater than 4 years old has been persistently been less than 500,000 km$^2$ since 2012 (Meier and Stroeve 2022). The spring sea ice melt is occurring earlier while freeze up is occurring later, which is causing higher energy input into the Arctic Ocean (Meier and Stroeve, 2022).

Sea ice is very sensitive to climate change because of the albedo feedback that determines how much solar radiation is absorbed by the sea ice (ECCC, 2021). Therefore, the thermodynamic processes in sea ice are often affected by changes in the overlying atmosphere and the underlying hydrosphere. The younger and thinner sea ice responds more to the atmospheric winds and currents which in turn, leads to greater sea ice motion and accelerated loss of sea ice from the Arctic. Therefore, Arctic sea ice is becoming increasingly more susceptible to thermodynamic forcing, which in turn is increasing its inter-annual variability (Kwok et al., 2009).

## 2.2 Snow on Sea Ice

One of the critical components of the cryosphere climate is snow on sea ice (Petty et al., 2018).

Snow on sea ice acts as an insulator and impacts both the growth and decay of sea ice (Maykut & Untersteiner, 1971). Snow has one of the highest albedo values (~0.7-0.9 for wet to dry snow) of any natural substance on earth and is one of the best thermal insulators per unit thickness (Curry et al., 1995). Therefore, if sea ice grows when air temperatures fall below freezing but there is little snowfall, there will be rapid thermodynamic sea ice growth compared to ice with a snow cover. In the summer, the albedo of snow determines the amount of solar radiation absorption and therefore the initiation and rate of the melt process (Webster et al., 2014). Thinner snow cover promotes the formation of melt ponds (Eicken et al., 2004), which absorb approximately 1.7 times more solar radiation in comparison to bare ice leading to greater sea ice loss (Webster et al., 2014). Therefore, the snow cover plays a vital role in terms of accelerating the loss of Arctic sea ice.

Additionally, the snow accumulating upon newly formed sea ice in the fall modifies the biophysical processes of the sea ice (Sturm & Massom, 2017). Snow depth on sea ice and associated geophysical properties is a determining factor for the growth of sea ice algae (Mundy et al., 2005). Thin snow covers are associated with a decrease in algae production. Snow cover on sea ice is also a major source of freshwater discharged into the ocean, which affects the total freshwater budget (Andersen et al., 2019). Snow cover on sea ice also impacts the air-ice drag coefficient by changing surface roughness, which impacts the heat exchanges occurring between the air and ice (Andreas et al., 2005). Snow on sea ice can also cause surface flooding and snow-ice formation (Granskog et al., 2017).

## 2.3 Properties of Snow on First Year Sea Ice

Sea water initially freezes into unconsolidated frazil, grease, slush and shuga which are all < 10 cm and are classified as new ice. The new ice consolidates into nilas ice which is also <10 cm but is more elastic (Geldsetzer, 2009). Further cooling leads to formation of young ice which is between 10 to 30 cm. Upon further cooling, sea ice becomes >=30 cm which is then considered as First-year sea ice. First-year sea ice can be thought of as a mixture of air, ice, liquid brine and solid salts (Yackel, 2001). After initial formation, the relative proportion of these constituents is the result of the thermodynamic structure within the snow and sea ice volume (Weeks & Ackley, 1986). An idealized phase diagram (Figure 1) was developed by Assur (1958) which tries to generalize the solid, brine and solid salts compositions based on temperature and density. It is also noteworthy that the seasonal evolution of sea ice is the most critical factor determining the general composition of first-year sea ice. For this study, the Winter season is most relevant as the field works conducted in this study were done in December 2021 and April 2022. During this season, first-year sea ice can range between 30 cm and ~200 cm with a typical snow cover between 5 cm and 100 cm (Yackel, 2001). Under winter conditions, we assume that snow is acting as an insulator from the cold surroundings which ultimately limits the growth of sea ice between 1 to 2 metres (Yackel, 2001). This is because of the low thermal conductivity of snow when compared to sea ice owing to the more prevent presence of air in snow.

During winter, snow on sea ice acts as an insulator causing the sea ice to stop growing beyond 1 to 2 metre. Therefore, snow geophysical properties directly impact first year sea ice processes. First-year sea ice is generally very saline but it also drains the salinity very quickly in summer (Vancoppenolle et al., 2006). One of the most significant properties of snow on sea ice is high salinity due to the process of brine wicking. Some of this expelled brine moves upwards towards the surface and therefore a thin brine layer is often present on the surface of sea ice reaching salinities up to 100 ppt (Geldsetzer et al., 2009). Therefore, when snow falls on top of this surface, the brine wicks up the snow layer between the snow grains (Barber et al., 1998). The proportion of these brine inclusions depends on the snow salinity, temperature and density (Drinkwater & Crocker, 1988).

The volume fraction of brine in snow is estimated by Drinkwater & Crocker (1988) according to the following equation:

$$\varphi = \left[\frac{\varphi i * \rho b}{(1-\varphi i)\rho i + \varphi i \rho b)}\right]\frac{\rho s}{\rho b} \text{ (i)}$$

Where, $\varphi$ brine volume fraction of snow is calculated using the $\varphi i$ temperature dependent brine volume fraction in sea ice, $\rho b$ which is the density of brine in g/cm$^3$, $\rho i$ which is the temperature-dependent density of pure ice in g/cm$^3$ and $\rho s$ which is the density of snow in g/cm$^3$. Therefore, with decreasing temperatures, water inside the brine inclusion would freeze which would increase the salt concentration and decrease the liquid brine volume. When the temperature increases, concentrated brine would melt the adjacent snow grains which would increase the brine volume but decrease the salt concentration.

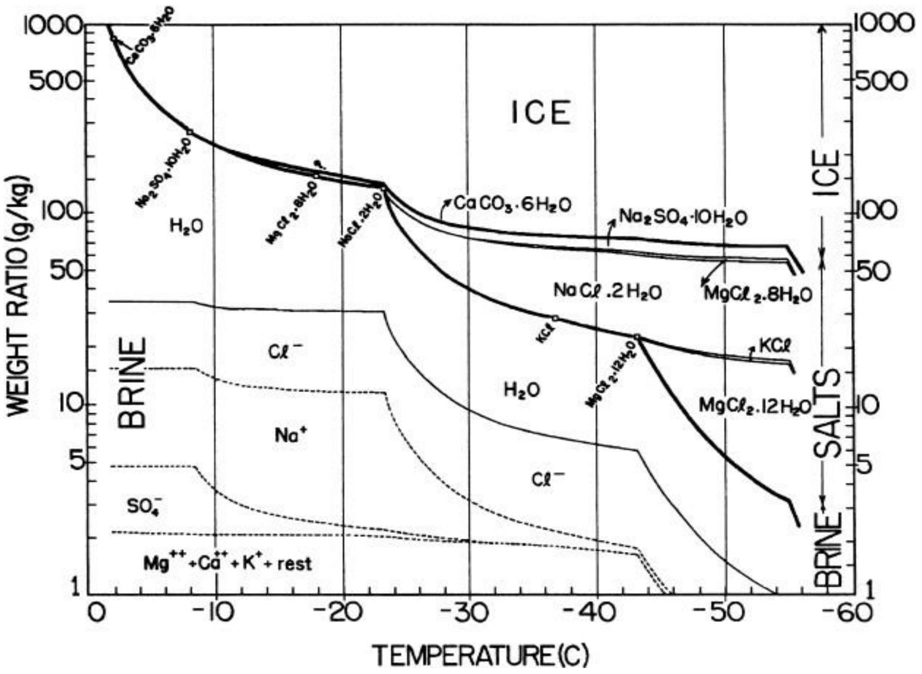

Figure 1 Top diagram shows the Sea ice phase diagram showing the typical compositions in different temperatures and phases after Assur (1958). The diagram shows the idealized salinity profiles for first year sea ice adapted from Yackel, 2019.

### 2.4 Microwave Interaction of Snow on Sea Ice

Microwave interaction with snow on sea ice is largely dependent on the changing dielectric constant of snow. The dielectric properties define material electric conductivity depending on the wavelength and polarization of electromagnetic waves. The complex dielectric constant is expressed according to the following equation:

$$\varepsilon *= \varepsilon' + j\varepsilon'' \qquad \text{(ii)}$$

Where, $\varepsilon *$ is the dielectric constant, $\varepsilon'$ is the dielectric permittivity, $\varepsilon''$ which is the dielectric loss and j is a complex number. The dielectric permittivity is directly related the electromagnetic wave speed in a material, which in turn can tell us how much of an incident wave is reflected at a boundary, and how much is transmitted. A higher permittivity change across a boundary (e.g. the air/snow boundary) means less wave penetration and therefore more reflection. Once a wave is transmitted across a boundary, the dielectric loss tells us how much of the transmitted energy is abosrbed and turned into heat inside the material (e.g. snow). Therefore, higher permittivity means lesser penetration of the microwave and therefore more reflection. The dielectric loss $\varepsilon''$ would represent how much of the penetrated energy would be absorbed within the material.

The large dielectric constant of brine ($\varepsilon * = 70 + j34$) has a significant influence on the combined dielectric properties of brine wetted snow especially (Yackel, 2001). Both the permittivity and loss of energy would increase as the salinity of the snow would increase. However, as the temperature decreases, both the permittivity and loss decreases. In winter, considering a dry snow cover, the vertical distribution of snow salinity and snow density determines the permittivity and loss of microwaves and therefore microwaves (C, X and Ku) completely penetrates the snow pack with little reflection. However, the brine volume at the basal snow layers play a determining factor in the extent of this penetration.

### 2.5 Observing Snow Depth on Sea Ice

The most comprehensive record of snow depth on sea ice was collected during the Soviet North Pole (NP) drifting station in 1937 and 1954-1991, and has been used to produce the Warren's Climatology (Warren et al., 1999). Snow depth used in nearly all sea ice thickness products are computed using a modified Warren's Climatology which reduced the snow depth by 50% over seasonal ice zones (Garnier et al., 2021). However, several studies have identified the snow depth values in modified Warren’s Climatology as being outdated given the rapidly changing climate (Kern et al., 2015; Kurtz & Farrell, 2011). The NP stations recorded snow depth over multi-year sea ice which is significantly different to first-year sea ice which dominates the Arctic (Maslanik et al., 2011). The snow depths from Warren’s climatology are still widely used and are typically halved over first-year sea ice assuming lower snow accumulation (Guerreiro et al., 2016; Tilling et al., 2018). (Forsström et al., 2011) and (Shalina & Sandven, 2018) try to provide improved climatologies especially over seasonal sea ice but the data sources are still from the 1960s, 1970s and 1980s. In 2000, the ice mass balance buoys deployed during the Surface Heat Budget of the Arctic Ocean (SHEBA) campaign helped to provide in-situ measurements of sea ice parameters. The CryoSat Validation Experiment (CryoVEx) and Operation Ice Bridge (OIB) provide essential air-borne snow depth for validation purposes. Between 2019-2020, in-situ snow depth measurements were also collected as part of the internal MOSAIC expedition in the central Arctic (Shupe et al., 2020). While such in-situ measurements are vital for satellite and model validation purposes, the limited spatial and temporal resolution along with the increasing variability in snow means they cannot be considered as representative of the entire arctic for all seasons.

Several snow depth products from modelling and a combination of modelling and satellite observations are also available. Of the reanalysis based products, (Zhou et al., 2021) identifies SnowModel-LG (Liston et al., 2020; J. Stroeve et al., 2020), the NASA Eulerian Snow on Sea Ice Model (NESOSIM), and the Centre for Polar Observation and Modelling (CPOM) snow products as having the highest consistency after validation with in-situ observations. However, challenges lie with the spatial resolution of these modelled products along with the scarcity of in-situ datasets to validate the model outputs.

Snow depths derived from satellites can only provide the required spatio-temporal resolution for time series analysis and modelling (Lawrence et al., 2018). Snow depth estimates from passive microwaves have been widely used for sea ice thickness estimations (Kurtz et al., 2009). Such estimations have been based upon the relationship between snow thickness and passive microwave brightness temperatures. The first snow depth on sea ice was obtained from passive microwave satellite observations by (Markus & Cavalieri, 1998) who used passive microwave brightness observations at 19 and 37 GHz. (Comiso et al., 2003) showed that snow depth could also be estimated using passive microwave data from Aqua/Advanced Microwave Scanning Radiometer-EOS (AMSR-E) but these retrievals were limited to dry snow and snow depths less than 50 cm . (Cavalieri et al., 2012) validated snow depth outputs from AMSR-E with snow depth from obtained from airborne laser and radar altimeters and showed a correlation of 0.59. (Rostosky et al., 2018) later improved these retrievals to include multi-year sea ice as well. However, ( Stroeve et al., 2006) showed that variations due to surface roughness causes several uncertainties for the snow depth derived from AMSR-E.

(Maaß et al., 2013) used radiative transfer model along with brightness temperatures from the L band microwave interferometric radiometer Soil Moisture and Ocean Salinity (SMOS) to determine snow depth. This technique showed good estimations up to 35 cm but showed overestimations as the snow pack got deeper due to the desensitization of brightness temperatures. (Huang et al., 2021) proposed a technique using InSAR (Interferometry SAR) to measure snow depth and sea ice thickness by compensating for the electromagnetic penetration depth changes caused due to snow on sea ice. However, this interferometric technique may produce error due to the drifting of sea ice.

Dual frequency radar altimeters have been explored for accurately estimating snow depth on sea ice. Ka- and Ku-band have been explored for retrieving freeboard, but challenges lie with the ‘retracking’ process whereby the dominant scattering horizons are delineated from the radar waveform (Guerreiro et al., 2016). Guerreiro et al., (2016) suggested the use of both Ku- band (Cryosat-2) and Ka-band (AltiKa) frequencies with the application of an extinction-based model considering different snow grain sizes. However, the product developed by Guerreiro et al., (2016) misses the central Arctic due to the inclination of AltiKa (Rostosky et al. 2018). Gurreiro et al (2016) suggested that Ka-band signals penetrate into the first few centimetres of the snow pack, whereas Ku-band reflected before the snow-ice interface. However, Lawrence et al. (2018) assumed that AltiKa Ka-band does not penetrate the snow pack at all, whereas Cryosat-2 penetrates the snow pack fully.

## 2.6 Satellite Altimetry

Satellite altimeters are active instruments that measure the time between short pulses sent out in nadir direction at an object of interest (Gommenginger et al., 2011). Satellite altimetry measures the distance from the satellite to surface feature (sea ice, sea surface etc.) with which the transmitted signals interacts (Chelton et al., 2001). The altimeter ideally transmits a short pulse with known power towards the target object and a part of this incident wave returns to the satellite after being reflected. The shape of the reflected signal is known as the ‘waveform’ which is representative of the change in reflected power as the radar pulse hits the surface (Gommenginger et al. 2011).

For satellite altimetry applications, the microwave and visible portions of the electromagnetic spectrum are widely used. Radar signals are generally active microwave systems operating between 300MHz to 300 GHz. However, laser altimeters operate in the visible spectrum of the electromagnetic spectrum. Therefore, based on the significant differences in the two frequencies used, the microwaves interact differently with the surface. Laser altimeters typically have a much smaller footprint in comparison to radar altimeters.

Over sea ice, satellite laser and radar altimeters are widely used to estimate sea ice freeboard which can be converted with estimates from climatology to produce sea ice thickness. Laser altimeters are ideally used to estimate the snow (total) freeboard which is the distance between the air-snow interface and the sea surface (Figure 1). However, the interaction of the radar altimeters depends on the frequency being used. For example, Ka- and Ku-band radar altimeters have significantly different dominant scattering horizons. In this study, we are focusing on Ku-band radar altimeters. Therefore, based on the assumption that Ku-band signals penetrate the snowpack on sea ice, radar altimeters are assumed to give the ice freeboard, which is the distance between the snow-ice interface and the sea surface (Figure 1).

Based on the assumption of hydrostatic equilibrium, the sea ice thickness may be obtained from a measure of the sea ice freeboard as shown in Equation (iii). Equation (iii) represents the isostatic balance between the ice floe and snow on top assuming hydrostatic equilibrium.

$$f = \frac{[h_i\,(\rho_w - \rho_i) - h_s\ \rho_s]h_i}{\rho w} \text{ (iii)}$$

In equation (iii), $f$ is the sea ice freeboard, h is the sea ice thickness while ρ is the density while subscripts $_i$ , $_w$ and $_s$ represent ice, water and snow respectively. This shows that the sea ice freeboard is determined by the difference between the ice buoyancy $hi\ (\rho w - \rho i)$ and weight of the snow ($h_s\ \rho_s$). Snow depth is therefore a critical in estimating sea ice thickness (Zygmuntowska et al., 2014). (Zygmuntowska et al., 2014) shows that about 70% of the error in sea ice thickness estimated from ICESat-2 may be contributed due to snow depth with the highest errors occurring between October and November. (Djepa, 2013) shows that considering typical values for snow and ice densities and considering a 5 cm snow depth is used to calculate sea ice which is 109.5 cm thick with an uncertainty of 27.17 cm (24.8%) error.

Satellite radar altimetry has been used to derive radar freeboard, which can then be used with snow depths derived from climatology or passive microwave derived products to estimate sea ice thickness (Giles et al., 2007; Laxon et al., 2003; Laxon et al., 2013). One of the first estimates of sea ice thickness using satellite radar altimetry was carried out by Laxon et al (2003) who used ERS-1 and ERS-2 radar altimetry satellites. This study assumed that the 13.4 GHz Ku-band radar reflection from the satellite originated from the snow-ice surface. Consequently, it was assumed that the elevation measurements provided the sea ice freeboard (Laxon et al., 2003). Laxon et al (2003) showed significant correlation with submarine derived sea ice thicknesses. However, this technique was unable to measure sea ice thickness in thin ice (0.5 to 1 m). Subsequently, the Cryosat-2 Ku-band radar altimeter has been widely used for estimating sea ice freeboard since 2010. (Landy et al., 2022) recently developed an algorithm to retrieve year-round sea ice thickness from Cryosat-2. However, there are several challenges with using Cryosat-2 sea ice freeboard, including errors in retraction of the radar waveform (Ricker et al., 2014), impact of surface roughness (Landy et al., 2020) and snow properties (Nandan et al., 2017) among others.

## 2.7 Dual-Frequency Radar Altimetry for Snow Depth on Sea Ice retrievals

The proposition of using a dual-frequency radar altimetry system for estimating snow depth on sea ice is relatively recent. (Armitage & Ridout, 2015) demonstrated that Cryosat-2 penetrates through most of the snow pack and AltiKa returns from the mid-point of the snow pack. However, this study was conducted based on basin-averaged freeboards and only limited to the spring months. Guerreiro et al., (2016) ran simulation experiments on Ka band AltiKa and Ku-band Cryosat-2 microwave penetration depths against snow grain size under different snow densities and temperature conditions and proposed the combination of Ka-band and Ku band radar systems to retrieve snow depth on sea ice (Guerreiro et al. 2016). The basic assumption proposed was that the Ka-band AltiKa doesn't penetrate the snowpack at all whereas the Ku-band Cryosat- 2 penetrates the snowpack completely and therefore the snow depth could be computed based on simple differencing. (Guerreiro et al., 2017) showed that difference in footprint size and processing technique leads to bias between Cryosat-2 and Envisat both of which operated in Ku-band. This implied that the difference in freeboard between AltiKa and Cryosat-2 may not be solely a result of snow properties but due to difference in footprint size between the two sensors and the use of empirical retrackers (Lawrence et al. 2018). Lawrence et al., (2018) used independent freeboard measurements from Operation IceBridge to calibrate both AltiKa and CS2 freeboard and subsequently used them to compute snow depth on sea ice by accounting for a factor for the reduction in speed of the microwave. However, Lawrence et al., (2018) pointed out that there was a dearth of independent snow depth measurements to validate snow depths from CS2 and AltiKa which was necessary to improve processing techniques and distinguish the sources of bias. Therefore, we realize for both coincident radar and laser altimetry as well as dual-frequency radar altimetry, validation using in-situ field measurements is vital.

### 2.8 Snow on Lake ice as a Control

Therefore, snow on sea ice has unique characteristics that make it an unique physical system. As with snow on sea ice, snow on lake ice impacts the formation and thickness of the lake ice which it covers (Pouw et al., 2023). Snow accelerates the onset of lake freeze- up until the ice is formed when snow accumulation acts as an insulator because of its low thermal conductivity compared to ice (Pouw et al., 2023). Snow on lake ice impacts the timing of the melt and ice free seasons.

Snow on lake ice is different from sea ice. The key difference is that snow on sea ice is saline due to the presence of brine pockets whereas snow on lake ice is fresh (Figure 2). Snow on lake ice has comparable densities to snow on sea ice, which is around 320 kg/m$^3$ (Semmler et al., 2012). However, the presence of brine impacts thermal conductivity of snow on sea ice which is also not present in snow on lake ice. Therefore, snow on lake ice may qualify as a control for understanding the impact of brine on snow in sea ice. In fact, if the sea ice and lake ice are under similar meteorological conditions, the evolution of the two bodies and the impact of the presence and absence of brine may be assessed.

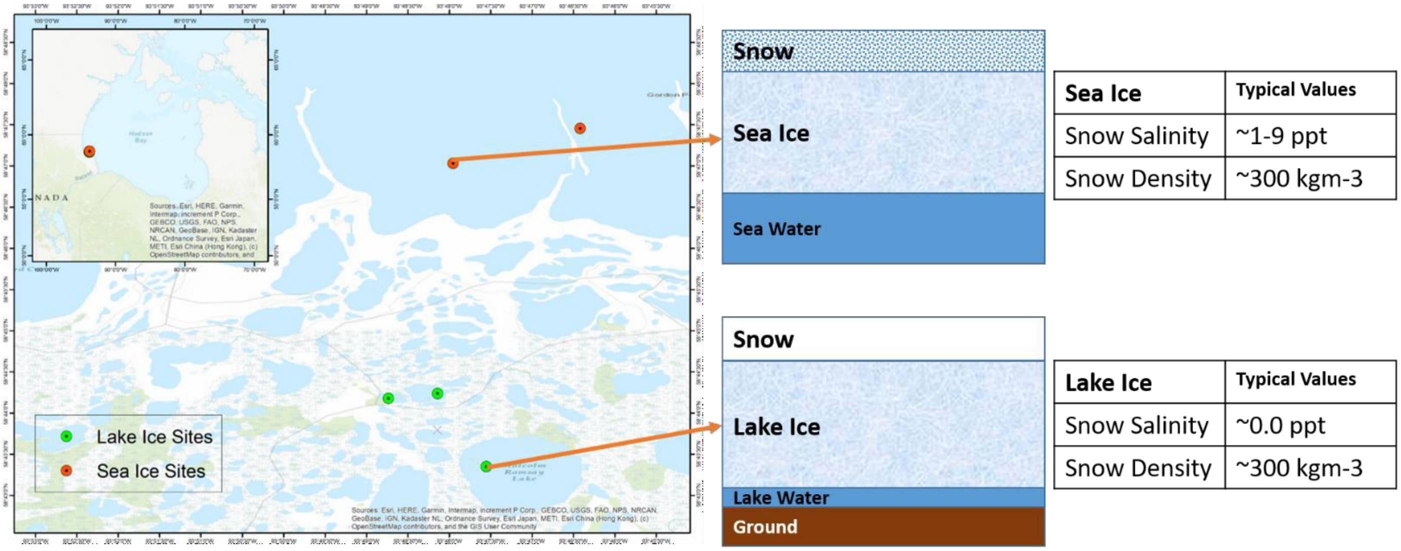

Sources: Esri, HERE, Garmin, Intermap, increment P Corp., GEBCO, USGS, FAO, NPS, NRCAN, GeoBase, IGN, Kadaster NL, Ordnance Survey, Esri Japan, METI, Esri China (Hong Kong), (c) OpenStreetMap contributors, and the GIS User Community

| **Sea Ice** | **Typical Values** |
|---|---|
| Snow Salinity | ~1-9 ppt |
| Snow Density | ~300 kgm-3 |

| **Lake Ice** | **Typical Values** |
|---|---|
| Snow Salinity | ~0.0 ppt |
| Snow Density | ~300 kgm-3 |

Figure 2 Simplified layer structure for sea ice and lake ice including the typical snow salinity and density values for snow on sea ice and lake ice. The salinity and density values are reported from snow sampling done in Churchill, Manitoba in December 2021.

### 2.9 Coincident Radar and Laser Altimetry for Snow Depth on Sea Ice retrievals

Coincident radar and laser altimeters have been proposed to be an efficient method for estimating snow depth on sea ice based on the differences in freeboard. Airborne coincident laser and radar altimeter data were collected over Arctic sea ice during the Laser-Radar Altimetry (LaRA) mission in 2003 (Raney & Leuschen, 2003). Analyzing the results from this airborne campaign, it was concluded that for radar signals interacting with sea ice with snow on top, the dominant scattering horizon was the sea-ice interface rather than the snow surface (Leuschen et al., 2008). Additionally, it was also observed that the laser signal provided snow surface elevation that coincided with the radar signals. These observed phenomena led to the use of coincident laser and radar altimeters to estimate snow depth on sea ice.

(Kwok & Markus, 2018) suggested the benefits of using the combination of ICESat-2 and Cryosat-2 derived freeboards for estimating snow depth on sea ice. Previous applications of Cryosat-2 and ICESat-2 faced the challenge of limited crossovers separated by long time lags with longer overlaps closer to the poles (Kwok & Markus, 2018). Despite having similar orbital inclinations, the difference in altitude between Cryosat-2 and ICESat-2 meant that there were only rare overlaps between the ground tracks (Farrell et al., 2021). (Kwok & Markus, 2018) also made a case for the benefits of adjusting the Cryosat-2 orbit in order to achieve more overlaps with ICESat-2 which ultimately improves both the spatial and temporal coincidence of the two altimeters. Consequently, the CRYO2ICE campaign was proposed. In order to achieve overlaps between the two altimeters, the CryoSat-2 orbit was raised by ~ 900 metres in August 2020. This realignment meant that for once in every19 Cryosat-2 (20 ICEsat-2) cycles, the two altimeters align for few hundred kilometers over the Arctic.

According to the conventional process for estimating snow depth from CRYO2ICE proposed by (Kwok et al., 2020), snow depth (SD) can be calculated from the difference between the total freeboard ($h_f$) and the sea ice freeboard ($h_{fi}$) (Figure 3). The total (snow) freeboard $h_f$ can be estimated from IS2 and can be used in conjunction with sea ice freeboard estimates ($h_{fi}$) to find snow depth ($h_{fs}$) as shown in Equation (iv)

$$SD = h_f - h_{fi} \quad \text{(iv)}$$

The sea ice freeboard is related to the radar freeboard $h_{fi}$(CS2) using the following equation:

$$h_{fi} = h_{fi}(\text{CS2}) + \text{SD}\ (\eta s - 1)\ \text{(v)}$$

The second term in Equation (v) represents the snow depth adjusting for the reduction in Ku-band travelled through the snow pack due to the reduction speed through the snow pack. The refractive index $\eta s$ is related to the speed of light in vacuum ($c$) and the speed of light in the snowpack and the snow density according to Equation (vi)

$$\eta s = \frac{c}{cs * \rho s} \quad \text{(vi)}$$

In Equation (vi), c is the speed of light in free space, cs is the reduced speed of Ku-band radar propagating through the snowpack, and ρs is the snow bulk density.

According to (Ullaby et al., 1987), the refractive index ηs which accounts for the reduction in speed of Ku-band propagation through a dry snowpack can be calculated using the following equation:

$$\eta s = (1 + 0.51 * \rho s)^{1.5} \quad \text{(vii)}$$

Therefore, using snow bulk density from either Warren's climatology or using in-situ data, a reasonably accurate snow refractive index may be computed with the assumption that the snowpack is dry. According to (Kwok et al., 2020), in temperatures below freezing, Ku-band penetrates through the snowpack and the ice freeboard ($h_{fi}$) estimated from Cryosat-2 is presentative of the snow-ice interface and the snow freeboard ($h_f$) estimated from ICESat-2 represents the air-snow interface as the green laser doesn't penetrate the snowpack. Therefore, combining equation (v) and (vii) the snow depth (SD) can be calculated using the following equation:

$$SD = \frac{h_f - h_{fi}}{\eta s} \quad \text{(viii)}$$

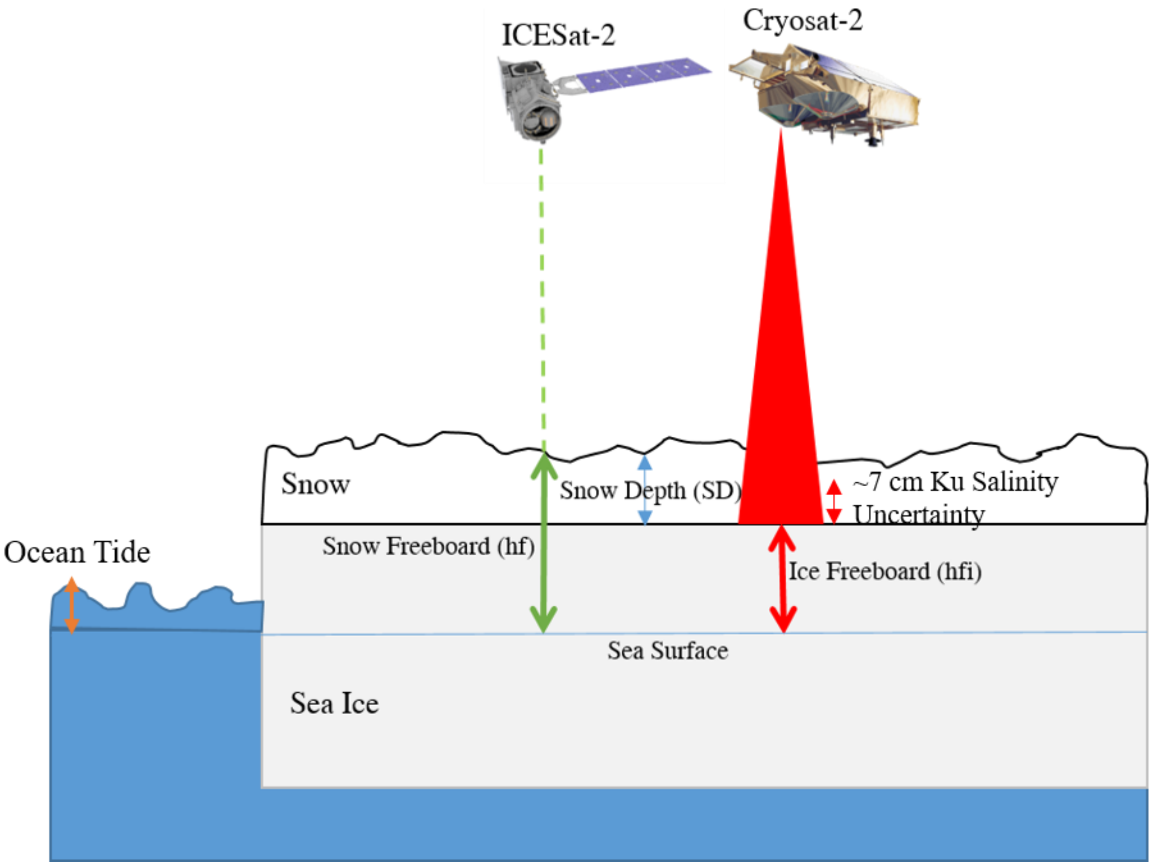

Figure 3 Simplified diagram showing the relation between freeboards and snow depth measurements. Here, hfi represents the sea ice freeboard, hf is the total (snow) freeboard and SD is snow depth. The ~7 cm uncertainty caused by the difference in snow salinity is shown in yellow.

## 2.10 Uncertainties in Snow Depth estimation from Coincident Radar and Laser Altimetry

Kwok et al., (2020) proposed using the combination of laser altimeter (ICESat-2) and radar altimeter (Cryosat-2) for simultaneously retrieving snow depth and sea ice thickness. Kwok et al (2020) assumes that at temperatures below freezing, the laser (ICESat-2) and radar (Cryosat-2) returns are from the air-snow and snow-ice interface, respectively. However, there are several sources of uncertainties in the process of using coincident Cryosat-2 and ICESat-2 for estimating snow depth. One vital uncertainty lies in using the Ku-band radar altimeter Cryosat-2 to estimate the ice freeboard. The assumption that Ku-band scatters off the ice surface is based on laboratory observations for dry and cold snow packs (Beaven et al., 1995). However, (Nandan et al., 2017) argues that if a snowpack contains brine, which is more common over first-year ice, the scattering horizon at Ku-band is shifted by approximately 0.07 meters. Therefore, freeboard values derived from Cryosat-2 would be biased (Nandan et al. 2017). Based on field observations collected in 2008 in the Antarctic, (Willatt et al., 2011) also showed that when the temperature was below freezing, around 80% of the dominant scattering horizons from the radar signals came closer to the air-snow interface rather than the snow-ice interface. (Ricker et al., 2014) demonstrates that the choice of retracker thresholds used on the Ku-band radar waveform significantly impacts the sea ice freeboard retrievals from Cryosat-2. The differences in the nature of scattering depending on varying snow grain size has also been identified as a critical uncertainty in the Cryosat-2 freeboard calculations (Larue et al., 2021). ( Landy et al., 2020) also demonstrated that the impact of sea ice surface roughness is a critical uncertainty in freeboards estimated from Cryosat-2.

Additionally, the conventional procedure for estimating snow depth proposed by (Kwok et al., 2020) uses snow density values from Warren's climatology. However, (Lawrence et al., 2018) asserts that such estimations are not based on the precipitation differences and therefore cannot be used to do any sort of time series analysis. ( Kwok et al 2020) uses a modified version of Warren's Climatology for snow bulk density estimates while accounting for reductions in Ku-band propagation speeds. (Mallett et al., 2020) shows that assumption of snow bulk density from Warren's climatology in the process of accounting for reduction in radar propagation speed can introduce significant uncertainties.

There are several critical challenges using satellite altimetry-based products specifically in the Canadian Arctic. Most of the satellite altimetry missions e.g. Cryosat-2 and ICESat-2 have better spatio-temporal coverage over the Central Arctic rather than the Canadian Arctic, and the coincidence of having both ICESat-2 and Cryosat-2 over the same area in the Canadian Arctic is rare. This lack of coincidence makes monitoring of sea ice using satellite altimetry in this region challenging. However, the recent CRYO2ICE mission has improved the coincidence of the altimeters and provides for an opportunity to validate retrievals during this phase of the mission for the Canadian Arctic. The application of land-masks and the uncertainties with land-contamination of sea ice products from both Cryosat-2 and ICESat-2 has been identified as a challenge to producing basin-scale outputs especially in the Canadian Arctic Archipelago. The general scarcity of leads in the landfast sea ice during winter in the Canadian Arctic Archipelago makes it difficult to ascertain the sea surface level, making it challenging to obtain snow depth differencing freeboards as suggested by (Kwok et al 2020). The narrow channels in the Canadian Arctic Archipelago make these two factors i.e. land contamination of the signals and lack of leads in the landfast ice a very common recurring challenge when trying to produce basin level sea ice products from CRYO2ICE.

## References

Andersen, O. B., Nilsen, K., Sørensen, L. S., Skourup, H., Andersen, N. H., Nagler, T., Wuite, J., Kouraev, A., Zakharova, E., & Fernandez, D. (2019). Arctic freshwater fluxes from earth observation data: International Review Workshop on Satellite Altimetry Cal/Val Activities and Applications. *Fiducial Reference Measurements for Altimetry*, 97–103. https://doi.org/10.1007/1345_2019_75

Andreas, E. L., Jordan, R. E., & Makshtas, A. P. (2005). Parameterizing turbulent exchange over sea ice: The ice station weddell results. *Boundary-Layer Meteorology*, *114*(2), 439–460. https://doi.org/10.1007/s10546-004-1414-7

Armitage, T. W. K., & Ridout, A. L. (2015). Arctic sea ice freeboard from AltiKa and comparison with CryoSat-2 and Operation IceBridge. *Geophysical Research Letters*, *42*(16), 6724–6731. https://doi.org/10.1002/2015GL064823

Barber, D. G., Fung, A. K., Grenfell, T. C., Nghiem, S. V., Onstott, R. G., Lytle, V. I., Perovich, D. K., & Gow, A. J. (1998). The role of snow on microwave emission and scattering over first-year sea ice. *IEEE Transactions on Geoscience and Remote Sensing*, *36*(5), 1750–1763. https://doi.org/10.1109/36.718643

BEAVEN, S. G., LOCKHART, G. L., GOGINENI, S. P., HOSSETNMOSTAFA, A. R., JEZEK, K., GOW, A. J., PEROVICH, D. K., FUNG, A. K., & TJUATJA, S. (1995). Laboratory measurements of radar backscatter from bare and snow-covered saline ice sheets. *International Journal of Remote Sensing*, *16*(5), 851–876. https://doi.org/10.1080/01431169508954448

Cavalieri, D. J., Markus, T., Ivanoff, A., Miller, J. A., Brucker, L., Sturm, M., Maslanik, J. A., Heinrichs, J. F., Gasiewski, A. J., Leuschen, C., Krabill, W., & Sonntag, J. (2012). A

Comparison of Snow Depth on Sea Ice Retrievals Using Airborne Altimeters and an AMSR-E Simulator. *IEEE Transactions on Geoscience and Remote Sensing*, *50*(8), 3027–3040. https://doi.org/10.1109/TGRS.2011.2180535

Chelton, D. B., Ries, J. C., Haines, B. J., Fu, L.-L., & Callahan, P. S. (2001). Chapter 1 Satellite Altimetry. In L.-L. Fu & A. Cazenave (Eds.), *International Geophysics* (Vol. 69, pp. 1–ii). Academic Press. https://doi.org/10.1016/S0074-6142(01)80146-7

Comiso, J. C., Cavalieri, D. J., & Markus, T. (2003). Sea ice concentration, ice temperature, and snow depth using AMSR-E data. *IEEE Transactions on Geoscience and Remote Sensing*, *41*(2), 243–252. https://doi.org/10.1109/TGRS.2002.808317

Curry, J. A., Schramm, J. L., & Ebert, E. E. (1995). Sea Ice-Albedo Climate Feedback Mechanism. *Journal of Climate*, *8*(2), 240–247. https://doi.org/10.1175/1520-0442(1995)008<0240:SIACFM>2.0.CO;2

Drinkwater, M. R., & Crocker, G. B. (1988). Modelling Changes in Scattering Properties of the Dielectric and Young Snow-Covered Sea Ice at GHz Requencies. *Journal of Glaciology*, *34*(118), 274–282. https://doi.org/10.3189/S0022143000007012

ECCC. (2021). *Canadian environmental sustainability indicators: Sea ice in Canada*. Environment and Climate Change Canada = Environnement et changement climatique Canada.

Eicken, H., Grenfell, T. C., Perovich, D. K., Richter-Menge, J. A., & Frey, K. (2004). Hydraulic controls of summer Arctic pack ice albedo. *Journal of Geophysical Research: Oceans*, *109*(C8). https://doi.org/10.1029/2003JC001989

Forsström, S., Gerland, S., & Pedersen, C. A. (2011). Thickness and density of snow-covered sea ice and hydrostatic equilibrium assumption from in situ measurements in Fram Strait, the

Barents Sea and the Svalbard coast. *Annals of Glaciology*, *52*(57), 261–270. https://doi.org/10.3189/172756411795931598

Garnier, F., Fleury, S., Garric, G., Bouffard, J., Tsamados, M., Laforge, A., Bocquet, M., Fredensborg Hansen, R. M., & Remy, F. (2021). Advances in altimetric snow depth estimates using bi-frequency SARAL and CryoSat-2 Ka–Ku measurements. *The Cryosphere*, *15*(12), 5483–5512. https://doi.org/10.5194/tc-15-5483-2021

Geldsetzer, T., Langlois, A., & Yackel, J. (2009). Dielectric properties of brine-wetted snow on first-year sea ice. *Cold Regions Science and Technology*, *58*(1), 47–56. https://doi.org/10.1016/j.coldregions.2009.03.009

Giles, K. A., Laxon, S. W., Wingham, D. J., Wallis, D. W., Krabill, W. B., Leuschen, C. J., McAdoo, D., Manizade, S. S., & Raney, R. K. (2007). Combined airborne laser and radar altimeter measurements over the Fram Strait in May 2002. *Remote Sensing of Environment*, *111*(2), 182–194. https://doi.org/10.1016/j.rse.2007.02.037

Gommenginger, C., Thibaut, P., Fenoglio-Marc, L., Quartly, G., Deng, X., Gómez-Enri, J., Challenor, P., & Gao, Y. (2011). Retracking Altimeter Waveforms Near the Coasts. In S. Vignudelli, A. G. Kostianoy, P. Cipollini, & J. Benveniste (Eds.), *Coastal Altimetry* (pp. 61–101). Springer. https://doi.org/10.1007/978-3-642-12796-0_4

Granskog, M. A., Rösel, A., Dodd, P. A., Divine, D., Gerland, S., Martma, T., & Leng, M. J. (2017). Snow contribution to first-year and second-year Arctic sea ice mass balance north of Svalbard. *Journal of Geophysical Research: Oceans*, *122*(3), 2539–2549. https://doi.org/10.1002/2016JC012398

Guerreiro, K., Fleury, S., Zakharova, E., Kouraev, A., Rémy, F., & Maisongrande, P. (2017). Comparison of CryoSat-2 and ENVISAT radar freeboard over Arctic sea ice: Toward an improved Envisat freeboard retrieval. *The Cryosphere*, *11*(5), 2059–2073. https://doi.org/10.5194/tc-11-2059-2017

Guerreiro, K., Fleury, S., Zakharova, E., Rémy, F., & Kouraev, A. (2016). Potential for estimation of snow depth on Arctic sea ice from CryoSat-2 and SARAL/AltiKa missions. *Remote Sensing of Environment*, *186*, 339–349. https://doi.org/10.1016/j.rse.2016.07.013

Huang, L., Fischer, G., & Hajnsek, I. (2021). Antarctic snow-covered sea ice topography derivation from TanDEM-X using polarimetric SAR interferometry. *The Cryosphere*, *15*(12), 5323–5344. https://doi.org/10.5194/tc-15-5323-2021

Kern, S., Khvorostovsky, K., Skourup, H., Rinne, E., Parsakhoo, Z. S., Djepa, V., Wadhams, P., & Sandven, S. (2015). The impact of snow depth, snow density and ice density on sea ice thickness retrieval from satellite radar altimetry: Results from the ESA-CCI Sea Ice ECV Project Round Robin Exercise. *The Cryosphere*, *9*(1), 37–52. https://doi.org/10.5194/tc-9-37-2015

Kurtz, N. T., & Farrell, S. L. (2011). Large-scale surveys of snow depth on Arctic sea ice from Operation IceBridge. *Geophysical Research Letters*, *38*(20). https://doi.org/10.1029/2011GL049216

Kurtz, N. T., Markus, T., Cavalieri, D. J., Sparling, L. C., Krabill, W. B., Gasiewski, A. J., & Sonntag, J. G. (2009). Estimation of sea ice thickness distributions through the combination of snow depth and satellite laser altimetry data. *Journal of Geophysical Research*, *114*(C10), C10007. https://doi.org/10.1029/2009JC005292

Kwok, R., Cunningham, G. F., Wensnahan, M., Rigor, I., Zwally, H. J., & Yi, D. (2009). Thinning and volume loss of the Arctic Ocean sea ice cover: 2003–2008. *Journal of Geophysical Research: Oceans*, *114*(C7). https://doi.org/10.1029/2009JC005312

Kwok, R., Kacimi, S., Webster, M. a., Kurtz, N. t., & Petty, A. a. (2020). Arctic Snow Depth and Sea Ice Thickness From ICESat-2 and CryoSat-2 Freeboards: A First Examination. *Journal of Geophysical Research: Oceans*, *125*(3), e2019JC016008. https://doi.org/10.1029/2019JC016008

Kwok, R., & Markus, T. (2018). Potential basin-scale estimates of Arctic snow depth with sea ice freeboards from CryoSat-2 and ICESat-2: An exploratory analysis. *Advances in Space Research*, *62*(6), 1243–1250. https://doi.org/10.1016/j.asr.2017.09.007

Landy, J. C., Dawson, G. J., Tsamados, M., Bushuk, M., Stroeve, J. C., Howell, S. E. L., Krumpen, T., Babb, D. G., Komarov, A. S., Heorton, H. D. B. S., Belter, H. J., & Aksenov, Y. (2022). A year-round satellite sea-ice thickness record from CryoSat-2. *Nature*, *609*(7927), Art. 7927. https://doi.org/10.1038/s41586-022-05058-5

Landy, J. C., Petty, A. A., Tsamados, M., & Stroeve, J. C. (2020). Sea Ice Roughness Overlooked as a Key Source of Uncertainty in CryoSat-2 Ice Freeboard Retrievals. *Journal of Geophysical Research: Oceans*, *125*(5), e2019JC015820. https://doi.org/10.1029/2019JC015820

Larue, F., Picard, G., Aublanc, J., Arnaud, L., Robledano-Perez, A., LE Meur, E., Favier, V., Jourdain, B., Savarino, J., & Thibaut, P. (2021). Radar altimeter waveform simulations in Antarctica with the Snow Microwave Radiative Transfer Model (SMRT). *Remote Sensing of Environment*, *263*, 112534. https://doi.org/10.1016/j.rse.2021.112534

Lawrence, I. R., Tsamados, M. C., Stroeve, J. C., Armitage, T. W. K., & Ridout, A. L. (2018). Estimating snow depth over Arctic sea ice from calibrated dual-frequency radar freeboards. *The Cryosphere*, *12*(11), 3551–3564. https://doi.org/10.5194/tc-12-3551-2018

Laxon, S., Peacock, N., & Smith, D. M. (2003). High interannual variability of sea ice thickness in the Arctic region. *Nature*. https://doi.org/10.1038/nature02050

Laxon, S. W., Giles, K. A., Ridout, A. L., Wingham, D. J., Willatt, R., Cullen, R., Kwok, R., Schweiger, A., Zhang, J., Haas, C., Hendricks, S., Krishfield, R., Kurtz, N., Farrell, S., & Davidson, M. (2013). CryoSat-2 estimates of Arctic sea ice thickness and volume. *Geophysical Research Letters*, *40*(4), 732–737. https://doi.org/10.1002/grl.50193

Leuschen, C. J., Swift, R. N., Comiso, J. C., Raney, R. K., Chapman, R. D., Krabill, W. B., & Sonntag, J. G. (2008). Combination of laser and radar altimeter height measurements to estimate snow depth during the 2004 Antarctic AMSR-E Sea Ice field campaign. *Journal of Geophysical Research: Oceans*, *113*(C4). https://doi.org/10.1029/2007JC004285

Liston, G. E., Itkin, P., Stroeve, J., Tschudi, M., Stewart, J. S., Pedersen, S. H., Reinking, A. K., & Elder, K. (2020). A Lagrangian Snow-Evolution System for Sea-Ice Applications (SnowModel-LG): Part I—Model Description. *Journal of Geophysical Research: Oceans*, *125*(10), e2019JC015913. https://doi.org/10.1029/2019JC015913

Maaß, N., Kaleschke, L., Tian-Kunze, X., & Drusch, M. (2013). Snow thickness retrieval over thick Arctic sea ice using SMOS satellite data. *The Cryosphere*, *7*(6), 1971–1989. https://doi.org/10.5194/tc-7-1971-2013

Mallett, R. D. C., Lawrence, I. R., Stroeve, J. C., Landy, J. C., & Tsamados, M. (2020). Brief communication: Conventional assumptions involving the speed of radar waves in snow introduce systematic underestimates to sea ice thickness and seasonal growth rate estimates. *The Cryosphere*, *14*(1), 251–260. https://doi.org/10.5194/tc-14-251-2020

Markus, T., & Cavalieri, D. J. (1998). Snow Depth Distribution Over Sea Ice in the Southern Ocean from Satellite Passive Microwave Data. In *Antarctic Sea Ice: Physical Processes,* *Interactions and Variability* (pp. 19–39). American Geophysical Union (AGU). https://doi.org/10.1029/AR074p0019

Maslanik, J., Stroeve, J., Fowler, C., & Emery, W. (2011). Distribution and trends in Arctic sea ice age through spring 2011. *Geophysical Research Letters*, *38*(13). https://doi.org/10.1029/2011GL047735

Maykut, G. A., & Untersteiner, N. (1971). Some results from a time-dependent thermodynamic model of sea ice. *Journal of Geophysical Research (1896-1977)*, *76*(6), 1550–1575. https://doi.org/10.1029/JC076i006p01550

McCrystall, M. R., Stroeve, J., Serreze, M., Forbes, B. C., & Screen, J. A. (2021). New climate models reveal faster and larger increases in Arctic precipitation than previously projected. *Nature Communications*, *12*(1), Art. 1. https://doi.org/10.1038/s41467-021-27031-y

Meier, W., & Stroeve, J. (2022). An Updated Assessment of the Changing Arctic Sea Ice Cover. *Oceanography*. https://doi.org/10.5670/oceanog.2022.114

Mundy, C. J., Barber, D. G., & Michel, C. (2005). Variability of snow and ice thermal, physical and optical properties pertinent to sea ice algae biomass during spring. *Journal of Marine Systems*, *58*(3), 107–120. https://doi.org/10.1016/j.jmarsys.2005.07.003

Nandan, V., Geldsetzer, T., Yackel, J., Mahmud, M., Scharien, R., Howell, S., King, J., Ricker, R., & Else, B. (2017). Effect of Snow Salinity on CryoSat-2 Arctic First-Year Sea Ice Freeboard Measurements. *Geophysical Research Letters*, *44*(20), 10,419-10,426. https://doi.org/10.1002/2017GL074506

Petty, A. A., Webster, M., Boisvert, L., & Markus, T. (2018). The NASA Eulerian Snow on Sea Ice Model (NESOSIM) v1.0: Initial model development and analysis. *Geoscientific Model Development*, *11*(11), 4577–4602. https://doi.org/10.5194/gmd-11-4577-2018

Pouw, A. F., Kheyrollah Pour, H., & MacLean, A. (2023). Mapping snow depth on Canadian sub-arctic lakes using ground-penetrating radar. *The Cryosphere*, *17*(6), 2367–2385. https://doi.org/10.5194/tc-17-2367-2023

Raney, R. K., & Leuschen, C. (2003). Technical Support for the Deployment Of Radar and Laser Altimeters during LaRA 2002. *Final Report*, 21.

Ricker, R., Hendricks, S., Helm, V., Skourup, H., & Davidson, M. (2014). Sensitivity of CryoSat-2 Arctic sea-ice freeboard and thickness on radar-waveform interpretation. *The Cryosphere*, *8*(4), 1607–1622. https://doi.org/10.5194/tc-8-1607-2014

Rostosky, P., Spreen, G., Farrell, S. L., Frost, T., Heygster, G., & Melsheimer, C. (2018). Snow Depth Retrieval on Arctic Sea Ice From Passive Microwave Radiometers—Improvements and Extensions to Multiyear Ice Using Lower Frequencies. *Journal of Geophysical Research: Oceans*, *123*(10), 7120–7138. https://doi.org/10.1029/2018JC014028

Screen, J. A., & Simmonds, I. (2012). Declining summer snowfall in the Arctic: Causes, impacts and feedbacks. *Climate Dynamics*, *38*(11), 2243–2256. https://doi.org/10.1007/s00382-011-1105-2

Semmler, T., Cheng, B., Yang, Y., & Rontu, L. (2012). Snow and ice on Bear Lake (Alaska) – sensitivity experiments with two lake ice models. *Tellus A: Dynamic Meteorology and Oceanography*, *64*(1), 17339. https://doi.org/10.3402/tellusa.v64i0.17339

Shalina, E. V., & Sandven, S. (2018). Snow depth on Arctic sea ice from historical in situ data. *The Cryosphere*, *12*(6), 1867–1886. https://doi.org/10.5194/tc-12-1867-2018

Shupe, M. D., Rex, M., Dethloff, K., Damm, E., Fong, A. A., Gradinger, R., Heuzé, C., Loose, B., Makarov, A., Maslowski, W., Nicolaus, M., Perovich, D., Rabe, B., Rinke, A., Sokolov, V., & Sommerfeld, A. (2020). *Arctic Report Card 2020: The MOSAiC Expedition: A Year Drifting with the Arctic Sea Ice*. https://doi.org/10.25923/9G3V-XH92

Stroeve, J. C., Markus, T., Maslanik, J. A., Cavalieri, D. J., Gasiewski, A. J., Heinrichs, J. F., Holmgren, J., Perovich, D. K., & Sturm, M. (2006). Impact of Surface Roughness on AMSR-E Sea Ice Products. *IEEE Transactions on Geoscience and Remote Sensing*, *44*(11), 3103–3117. https://doi.org/10.1109/TGRS.2006.880619

Stroeve, J., Liston, G. E., Buzzard, S., Zhou, L., Mallett, R., Barrett, A., Tschudi, M., Tsamados, M., Itkin, P., & Stewart, J. S. (2020). A Lagrangian Snow Evolution System for Sea Ice Applications (SnowModel-LG): Part II—Analyses. *Journal of Geophysical Research: Oceans*, *125*(10), e2019JC015900. https://doi.org/10.1029/2019JC015900

Stroeve, J., Nandan, V., Willatt, R., Tonboe, R., Hendricks, S., Ricker, R., Mead, J., Mallett, R., Huntemann, M., Itkin, P., Schneebeli, M., Krampe, D., Spreen, G., Wilkinson, J., Matero, I., Hoppmann, M., & Tsamados, M. (2020). Surface-based Ku- and Ka-band polarimetric radar for sea ice studies. *The Cryosphere*, *14*(12), 4405–4426. https://doi.org/10.5194/tc-14-4405-2020

Sturm, M., & Massom, R. A. (2017). Snow in the sea ice system: Friend or foe? In *Sea Ice* (Third). Wiley Blackwell.

Tilling, R. L., Ridout, A., & Shepherd, A. (2018). Estimating Arctic sea ice thickness and volume using CryoSat-2 radar altimeter data. *Advances in Space Research*, *62*(6), 1203–1225. https://doi.org/10.1016/j.asr.2017.10.051

Ullaby, F. T., Moore, R. K., & Fung, A. K. (1987). Microwave Remote Sensing. Active and Passive. *Geological Magazine*, *124*(1), 88–88. https://doi.org/10.1017/S0016756800015831

Vancoppenolle, M., Fichefet, T., & Bitz, C. M. (2006). Modeling the salinity profile of undeformed Arctic sea ice. *Geophysical Research Letters*, *33*(21). https://doi.org/10.1029/2006GL028342

Warren, S. G., Rigor, I. G., Untersteiner, N., Radionov, V. F., Bryazgin, N. N., Aleksandrov, Y. I., & Colony, R. (1999). Snow Depth on Arctic Sea Ice. *Journal of Climate*, *12*(6), 1814–1829. https://doi.org/10.1175/1520-0442(1999)012<1814:SDOASI>2.0.CO;2

Webster, M. A., Rigor, I. G., Nghiem, S. V., Kurtz, N. T., Farrell, S. L., Perovich, D. K., & Sturm, M. (2014). Interdecadal changes in snow depth on Arctic sea ice. *Journal of Geophysical Research: Oceans*, *119*(8), 5395–5406. https://doi.org/10.1002/2014JC009985

Weeks, W. F., & Ackley, S. F. (1986). The Growth, Structure, and Properties of Sea Ice. In N. Untersteiner (Ed.), *The Geophysics of Sea Ice* (pp. 9–164). Springer US. https://doi.org/10.1007/978-1-4899-5352-0_2

Willatt, R., Laxon, S., Giles, K., Cullen, R., Haas, C., & Helm, V. (2011). Ku-band radar penetration into snow cover on Arctic sea ice using airborne data. *Annals of Glaciology*, *52*(57), 197–205. https://doi.org/10.3189/172756411795931589

Yackel, J. (2001). *On the Use of Synthetic Aperture Radar (SAR) for Estimating the Thermodynamic Evolution of Snow Covered First Year Sea Ice*. Department of Geography, University of Manitoba.

Zhou, L., Stroeve, J., Xu, S., Petty, A., Tilling, R., Winstrup, M., Rostosky, P., Lawrence, I. R., Liston, G. E., Ridout, A., Tsamados, M., & Nandan, V. (2021). Inter-comparison of snow depth over Arctic sea ice from reanalysis reconstructions and satellite retrieval. *The Cryosphere*, *15*(1), 345–367. https://doi.org/10.5194/tc-15-345-2021

# Chapter 3 Surface-Based Fully Polarized Dual-Frequency Altimeter Retrievals Over Snow On First-Year Sea Ice and Lake Ice

## 3.1 Introduction

In this chapter, I aim to improve my understanding of the interaction of microwave radar with brine-wetted first-year sea ice close to the freeze-up season as well as fresh snow on lake ice. The interaction of both co-polarized(HH) and cross-polarized(VH) Ku and Ka band microwave over snow on sea ice and lake ice is presented. As mentioned in Section 2.9 and 2.12, previous studies utilizing both dual frequency radar and coincident laser and radar approaches assumes the Ku-band dominant scattering horizon is the snow-ice interface. However, the brine content of snow on sea ice seems to play a critical role in the nature of interaction of Ku band shifting the dominant scattering horizon closer to the air-snow interface (Nandan et al., 2017,2020). It is important to understand the impact of the presence or absence of brine in the snow pack and how this impacts Ku and Ka band main scattering horizons in different polarizations. Therefore, this study compares the Ku and Ka band co-polarized and cross-polarized waveform over brine-wetted snow on first-year landfast sea ice with fresh snow on top of lake ice under the same meteorological conditions. The objectives of this chapter are to:

- Identify and compare the positions of the main scattering horizons of Ku and Ka band waveforms for snow on sea ice and lake ice.
- Assess the impact of snow geophysical properties on the position of the main scattering horizon of sea ice using snow on lake ice as a control
- Assess the potential of estimating snow depth on sea ice using the main scattering horizons considering both the cross-polarized and co-polarized Ku and Ka band waveforms

## 3.2 Methods

### 3.2.1 Study Area

The field sampling was performed over sea ice and lake ice near Churchill which is a community located along the West Coast of Hudson Bay. The study area was about 25 km away from the Churchill River Estuary. The sea ice in this region of Hudson Bay is usually a mixture of landfast and floating ice (Kuzyk et al., 2008). However, the sea ice sampling in this study is limited to landfast ice only. The sea ice was ~50 cm thick between December 2nd and 13th 2021 when the sampling was conducted. Sentinel-1 SAR imagery was used to identify the presence of landfast sea ice. The sea ice sampling was conducted ~ 1km from the coast on landfast sea ice and therefore there was no drifting of the sea ice floe during sampling. While sampling was conducted throughout December 2nd and 13th (Figure 4,5), this study focuses on the sampling done on December 11th over sea ice and December 4th over lake ice. The sampling on lake ice was conducted at the Malcolm Ramsay Lake on December 4th, 2021 which is about 7 km away from the coastline.

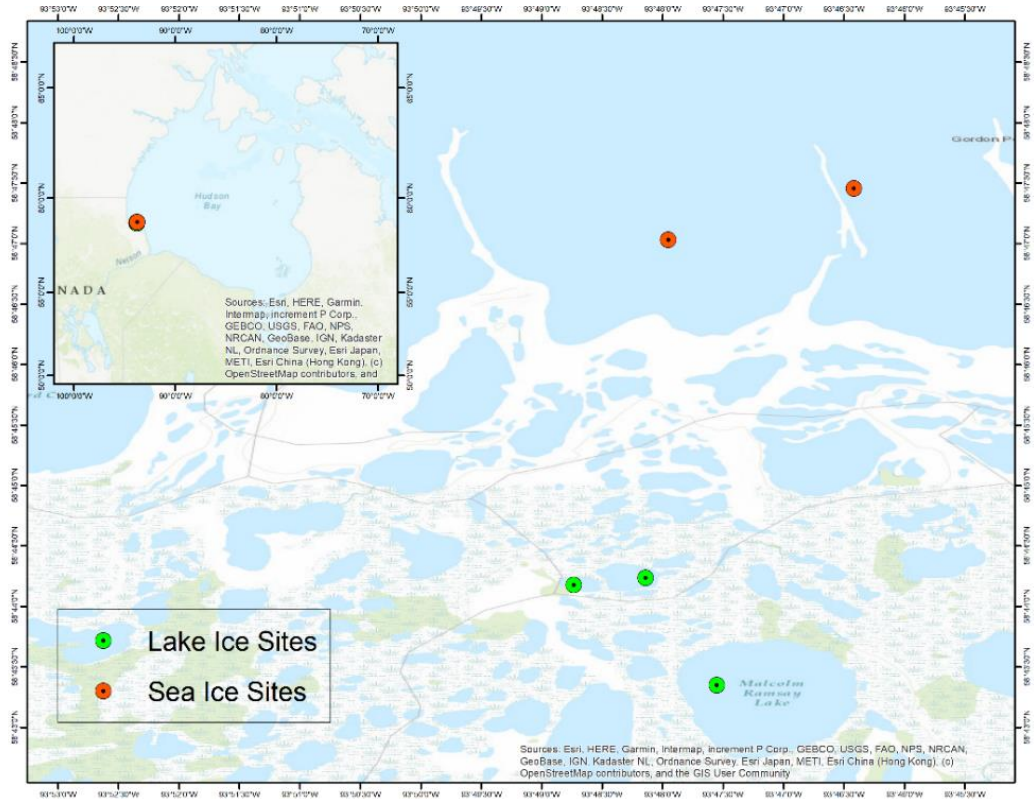

Sources: Esri, HERE, Garmin, Intermap, increment P Corp., GEBCO, USGS, FAO, NPS, NRCAN, GeoBase, IGN, Kadaster NL, Ordnance Survey, Esri Japan, METI, Esri China (Hong Kong), (c) OpenStreetMap contributors, and

Sources: Esri, HERE, Garmin, Intermap, increment P Corp., GEBCO, USGS, FAO, NPS, NRCAN, GeoBase, IGN, Kadaster NL, Ordnance Survey, Esri Japan, METI, Esri China (Hong Kong), (c) OpenStreetMap contributors, and the GIS User Community

Figure 4 Map showing the locations of the Sea Ice and Lake ice sampling sites visited between December 2nd and 13th.

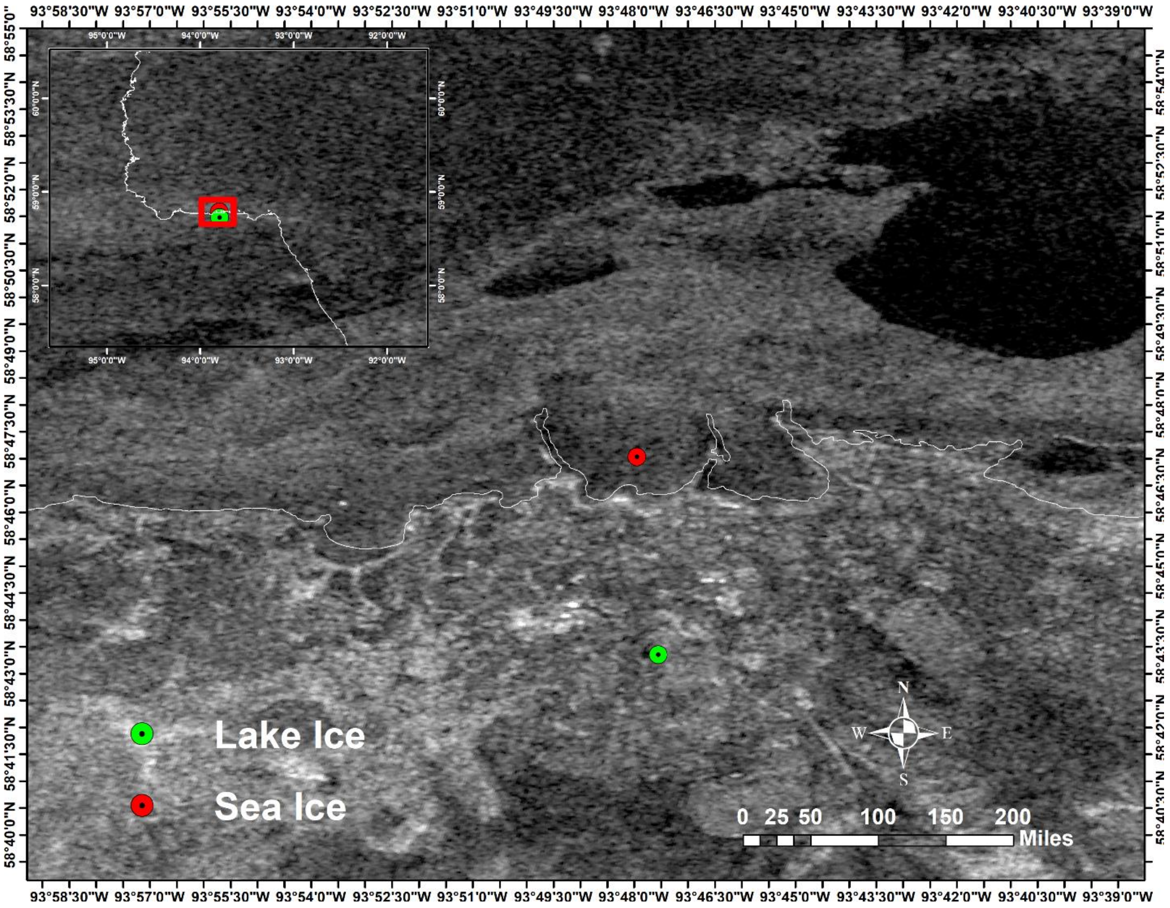

Figure 5 Sentinel-1 Map from 11th December, 2021 showing the condition of sea ice and lake ice during the sampling. The red dot represents the location of the sampling snow pits on December 11th, 2021 while the green dot shows the lake ice sampling site

### 3.2.2 Snow Geophysical Properties

Snow geophysical properties were recorded from both lake ice and sea ice between December $2^{nd}$ and $13^{th}$, 2021. Snow density, salinity and temperatures were recorded from 23 snow pits conducted throughout the study areas. The snow pits were located in order to take snow samples representative of the spatial heterogeneity along different parts of KuKa and magnaprobe transects. The temperature of the air, snow layers and sea ice interface were recorded using a Digi-Sense RTD thermometer probe, with a resolution of 0.1°C and an accuracy ±0.2°C. The temperature measurements with the probe were taken in the shade ensuring that the readings were stable before recording.

Snow density samples were acquired using a 66 $cm^3$ (2 x 5.5 x 6 cm) density cutter at 2-cm vertical intervals. The samples were collected in Whirl-Pack sterile sampling bags for laboratory analysis. The snow samples along with the sampling bag were weighed after adjusting for the mass of the whirl-pack sample bags. The volume of snow was assumed to be the same as the density cutter (66 $cm^3$).

Snow samples were permitted to melt and salinity measurements were performed using a Cole-Parmer C100 Conductivity Meter. The measurements are taken within 6 hours of sampling to prevent changes due to evaporation.

### 3.2.3 KuKa Radar Instrument Specifications

The KuKa radar was developed to operate in similar frequencies to Ka-band AltiKa (30 to 40 GHz) and Ku-band Cryosat-2 (12 to 18 GHz). Both the Ka and Ku band units are Frequency Modulated Continuous Wave (FMCW) radars which utilize linear frequency modulation. Given the radar is fully polarimetric, this gives us the opportunity to retrieve radar signals both in co-polarization and cross-polarization for both Ku and Ka band microwaves. Additionally, the instrument runs in both nadir and scan mode where the antenna can be steered at different angles allowing the retrieval of further vital information including interaction of the microwave at different incidence angles with the snow surface (Stroeve et al., 2020). The central radar chirp frequencies are set to 35 GHz which is closer to AltiKa (Ka-band satellite altimeter) and 13.575 GHz for Ku-band close to Cryosat-2 (Ku-band altimeter) (Nandan et al. 2022). The instrument has very high bandwidth which allows for a range-resolution of 1.5 cm for Ka-band and 2.5cm for Ku-band. The Kuka radar transmits with very low power and is therefore suitable for short ranges typically less than 30 meters (Stroeve et al., 2020). The radar system is bistatic, with separate transmit and receive antennas in both Ku- and Ka-band. The Ku- band antennas have a 16.5° beamwidth and 11.9° at Ka-band. The two antennas are not scanning the same surface, however spatio-temporal averaging is done in the data possessing. In the altimeter mode, the RF units are powered by two 12V DC batteries.

Table 1 Specifications of the Ku-Ka Radar (Adapted from Stroeve et al., 2020)

| | Ku-band | Ka-band |
|---|---|---|
| RF output frequency | 12-17 GHz | 30-40 GHz |
| Transmit power | 10dBm | 6 dBm |
| Transmit bandwidth | 6 GHz | 10 GHz |
| Range resolution | 2.5 cm | 1.5 cm |
| Transmit-Receive Polarization | VV,HH, HV,VH | VV,HH,HV,VH |
| Noise Floor | -70 dB (VV,HH)<br>-80 dB(HV,HH) | -90 dB(VV,HH,HV,VH) |

### 3.2.4 KuKa Radar Deployment

The Kuka Instrument was deployed over both sea ice and lake ice at Churchill, Manitoba between 2-13 December, 2021 (Figure 6). The Kuka instrument was mounted on a sledge and pulled at a fairly steady speed between 1 and 3 m/s. Radar pulses were transmitted every 0.33 seconds for Ka band and 0.5 seconds for Ku-band. The radar returns are independently geo-located using GPS data. It is important to ensure that radar returns from when the instrument is moving are considered to avoid oversampling in particular regions where the instrument is stationary or moving slowly. To verify instrument calibration, an experiment using a metal plate which demonstrates the response of the system to a flat and highly scattering surface was conducted. The data from the metal plate were then compared with the calibration loop to ensure there was good agreement. This calibration was repeated each day before recording the data from the transects. The measured peak range which corresponds with the distance from the antenna to the air-snow interface is about 1.55 m for both antennas. Additionally, the data where Kuka was tilted more than 10° were ignored from the analysis (Willatt et al., 2023).

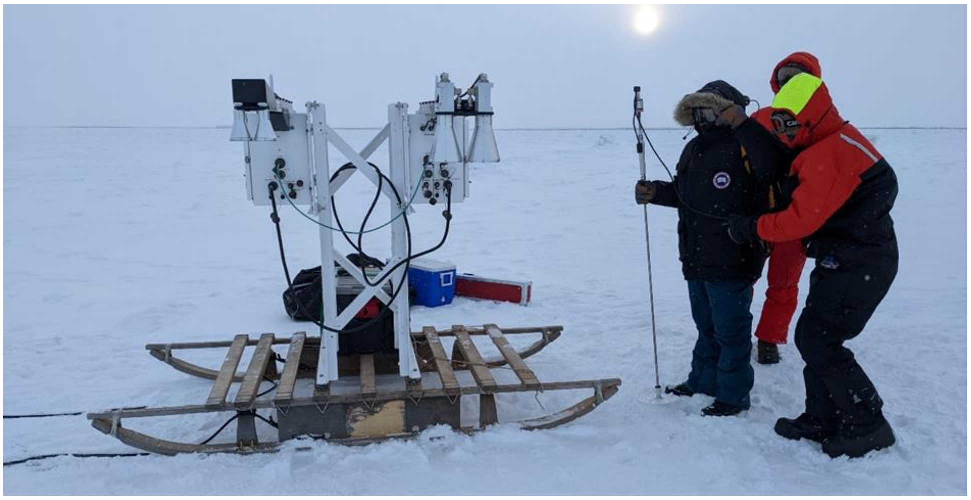

Figure 6 The KuKa radar deployment on a sledge on the sea ice at Churchill, Manitoba

### 3.2.5 Magnaprobe Snow Depths

An automated snow depth probe (magnaprobe) from Snow Hydro was used to collect coincident snow depth measurements along the KuKa transects that were conducted on both sea ice and lake ice (Figure 7). The magnaprobe measures snow on level sea ice with an accuracy of ±0.3 cm (Webster et al., 2014; Strum and Holmgren, 2018). The probe is inserted into the snow until the user hits the sea ice and the basket floats on the surface of the snow (Strum and Holmgren, 2018). The user then presses a switch to trigger the measurement. The time of travel for the sonic pulse to travel back to the head of the rod is then converted to a distance which is then adjusted to snow depth measurements.

Figure 7 Snow Hydro Magnaprobe for measuring snow depth on sea ice

In order to assess the accuracy of the magnaprobe to measure snow depth, we to cross-compared with coincident metre rule. Comparing the magnaprobe derived snow depth with the metre rule derived snow depths, we found very good correlation (R Squared- 0.90) (Figure 9). Therefore, we can confidently say that the magnaprobe snow depths are reliable in these conditions.

The magnaprobe data were sampled within 15 metres of the Kuka tracks in order to ensure that there was spatial correspondence. The sampling interval for taking magnaprobe measurements were taken approximately every 3 metres. The magnaprobe data were also collected within 30 minutes of the Kuka transects in order to ensure there wasn't any major snow drift between the

Kuka tracks and magnaprobe sampling.

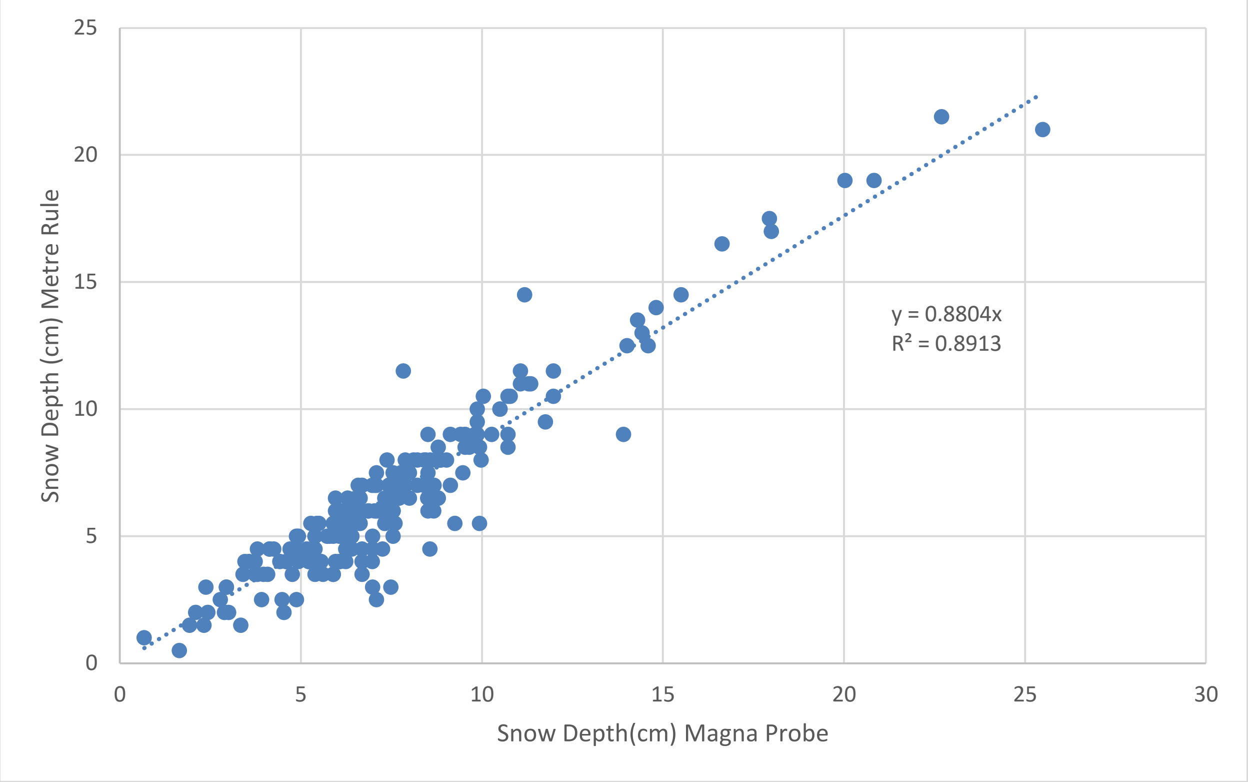

Figure 8 Snow depths retrieved from metre rule versus magnaprobe derived snow depths

### 3.2.6 KuKa Radar Data Processing

The KuKa data processing was done following Willatt et al., (2023) with some adaptations for the Churchill dataset. In the altimeter mode, the radar measures the backscatter at nadir as a function of time. The instrument generated a separated file every 5 min. The waveform data were generated following the software developed by Mead et al., (2023). However, the minimum along-track velocity was set to 0.4 m/s in order to ensure that only true motion is considered for processing. This minimum speed was set to ensure that the drifting GPS location does not appear as true motion. This ensures that the number of independent samples sufficiently represent the spatial variability of snow. Each data block consists of six signal states: data from the four different polarizations (HH, HV, VV, VH), a calibration loop signal and a noise signal. A Fourier transform

(FFT) is used to convert the complex received voltage into range profiles (Stroeve et al., 2020). In order to reduce the variance, the range profiles are spatially averaged every 20 independent records. Based on the averaged power profiles, the Normalized Radar Cross Section (NRCS) is calculated using the following equation:

$$NRCS\ \sigma° = \frac{8ln\ (2)\ h^2 \sigma_c}{\pi {R_C}^4 {\theta_{3dB}}^2 cos\theta} \left(\frac{P_r}{P_{rc}}\right) \text{(ix)}$$

Where, $R_C$ is the range to the corner reflector (in metres), $h$ is the antenna height (in metres), $\theta_{3dB}$ is the antenna's one-way half-power beamwidth (in degrees), $P_r$ is the recorded power from the illuminating scene and $P_{rc}$ is the power recorded from the corner reflector (in Watts). The process is same for both Ku and Ka band frequencies. The NRCS $\sigma°$is then used to compute the co-polarized and cross-polarized backscatter cross-sections. Uncertainties in the NRCS arises from calibration error due to the use of a metal plate as a calibration target, standard deviation in estimated signal power, finite signal-to-noise ratio, and errors due to approximations of the sensor and target geometry (Stroeve et al., 2020).

One of the central problems in FMCW systems is the presence of chirp non-linearity (Ayhan et al., 2016). This leads to an overall degradation of the system's performance and can cause range side lobes in the measurements (Stroeve et al., 2016). Both amplitude and phase non-linearities need to be addressed. Therefore, the presence of radar side lobes need to be considered while interpreting the waveforms.

The radar propagation speed is reduced from the speed of light in air *c* due to the change in medium (snow). Therefore, the speed of the radar waveforms (c´) under the air-snow interface is adjusted assuming a dry snowpack according to the following Halikainen et al.,(1986):

$$c' = \frac{c}{\sqrt{1+1.9\rho}} \quad \text{(x)}$$

The snow bulk snow density (ρ) in g/cm$^3$is estimated from the snow samples collected from the field as explain in Section 2.2. This methodology is valid for snow densities less than 0.5 g/cm$^3$.

### 3.2.7 KuKa Main Scattering Horizon

The main scattering horizon is the range corresponding to the maximum peak power of Ku and Ka band at specified ranges. For this study, the range bin for snow on sea ice was set between 1 metre and 3 metres for identifying the main scattering horizon. This is to ensure that both the air-snow and the snow-ice interfaces fall within the specified range window. The distance from the antenna to the air-snow interface was approximately 1.55 metre. The range to the air snow interface was assumed to be greater than 1 metre while the maximum snow depth recorded from the magnaprobe was ~0.45 metre. Therefore, we can expect the snow-ice interface within the 1 metre to 3 metre range.

The data processing steps were adapted using the software developed by Willatt et al., (2023). The main scattering horizon for both the co-polarized (HH) and cross-polarized (VH) radar signals in the snow was determined considering the range of the maximum power signals from each polarization. In order to determine the air-snow interface (AS), the range (starting from 1 m) was searched until the power exceeded a set threshold for both Ku and Ka band at the HH polarization waveform (Willatt et al., 2023). This threshold was determined by analyzing the waveforms from each transect day. The air snow interface was determined by selecting the range (starting from 1 m) at which the power exceeded a set threshold for the Ku and Ka band waveforms. The highest amplitude peak was then searched within the next 10 cm (Ku) and 6 cm (Ka) considering 4 times the range resolution of each sensor. The range corresponding to the maximum peak of both the co-polarized HH ($P_{HH}$) and cross-polarization VH ($P_{VH}$) waveforms were also determined considering the highest power within a 1 to 3 metre range window.

The main scattering horizon at both the HH ($R_{HH}$) and VH ($R_{VH}$) polarization for both Ku and Ka band was determined taking the difference in range of the maximum peak and the identified air-snow interface.

Therefore,

$$R_{HH} = P_{HH} - AS \quad \text{(xi)}$$

$$R_{VH} = P_{VH} - AS \quad \text{(xii)}$$

Where, $R_{HH}$ and $R_{VH}$ are the main scattering horizon in metres at the HH and VH polarization for both Ku and Ka band respectively, $P_{HH}$ and $P_{VH}$ is the range corresponding to the maximum power within 1 to 3 metre range window at the HH and VH polarization and AS is the range at which the air-snow interface is identified.

### 3.2.8 KuKa Snow Depth Estimation

Snow depth on sea ice was retrieved from the surface based fully polarimetric KuKa radar following Willatt et al, (2023) utilizing both co-polarized (HH) and cross-polarized (VH) Ku and Ka signals. Willatt et al., (2023) observed that the Ku and Ka band co-polarized HH scattering mostly occurs in the range between 1.5 to 1.6 metres. This corresponds with the air-snow interface, which lies approximately at that same distance from the antenna phase centers (The phase center of an antennae is point from which the electromagnetic radiation spreads spherically outward). Additionally, the magnaprobe snow depth data corresponds well with the range to the maximum peak of the cross-polarized VH signals at both frequencies (Ku and Ka). Therefore, Willatt et al., (2023) suggests that maximum peak of the co-polarized (HH) Ku and Ka band signals come off the air-snow interface whereas the maximum peak of the cross-polarized (VH) signal corresponds with the snow-ice interface. In order to test this assumption on first-year landfast sea ice, this study computes snow depths as the difference between the range corresponding to the maximum peak of the cross-polarized (VH) and co-polarzied (HH) signal for both Ku and Ka band. The snow depths  are also adjusted for the reduced speed of the radar by multiplying with $c'$ which is calculated using Equation (ii) as mentioned in section 3.5.1. Snow depths which are less than 2.5 cm (mimumum resolvable distance based on the range resolution of Ku) are discarded from the analysis. The snow depth (SD) is therefore computed as the difference between the range corresponding to the HH maximum peak ($P_{HH}$) and the VH maximum peak ($P_{VH}$) for both Ku and Ka band:

$$SD = (P_{HH} - P_{VH})^* c' \quad \text{(xiii)}$$

### 3.2.9 Modelling the Main Scattering Horizon from Snow-Geophysical properties

The Ku and Ka band interaction with the snow pack based on the snow-geophysical data is conducted following the procedure proposed in Nandan et al., (2017, 2020). The main scattering horizon ($S_H$) was modelled considering a multi-layered snow-covered first-year sea ice system (Figure 9). Therefore, $S_H$ is considered to be a function of the snow geophysical properties throughout the different layers of the snow pack. The changes in the Ku-band microwave interaction (which is mostly surface scattering at the Cryosat-2 incidence angle (up to 0.76°) with the different layers of snow is modelled considering the changes in snow geophysical properties in the different snow layers. Both the reflection and two-way loss of the Ku-band microwave is considered to simulate the normalized echo power ($P_T$) at each layer (Figure 9). The layer-wise snow salinity, density and temperature data are considered to estimate the $P_T$ at each layer using the following equation:

$$P_{T(n\geq 2)} = (1 - P_{n-1})^*[\prod_{k=2}^{n-1}[\{T_k(\theta')^* \prod(1 - \prod_{k=2}^{n-1} L_k(\theta')\}] * R_n(\theta') \qquad (xiv)$$

Where, $\theta'$ is the refracted incidence angle, $T_k(\theta')$ is the transmission coefficient and $R_n(\theta')$ is the reflection coefficient at the top-surface of each snow layer. The snow layer having the maximum $P_T$ is identified as the main scattering horizon and the distance from the air-snow interface to that layer is identified as the $S_H$.

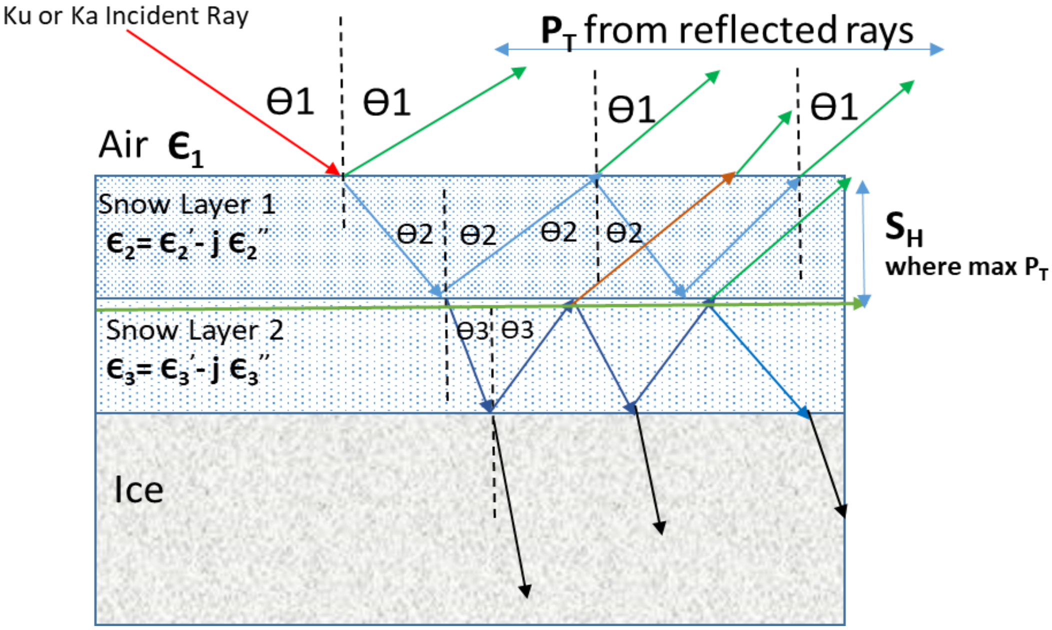

Figure 9 Simplified schematic showing a hypothetical interaction of the Ku and Ka band incident ray across the multi-layered snow model. Diagram adapted after Ulaby and Long (2014)

## 3.3 Results

### 3.3.1 Meteorological Conditions

The meteorological conditions at which the snow sampling is conducted are very important for interpreting Ku and Ka band interaction with the air and snow pack. The variation in weather during the days of sampling was monitored using data from the nearest Environment and Climate Change Canada's (ECCC) weather station, located at the Churchill Airport. The air temperature ranged between -10 °C and -30 °C and therefore can be considered to be typical winter temperatures at Churchill (Figure 10). There was a sharp increase in temperature from -30 °C to -15 °C between December 9th and 10th. There was a lot of variation in the wind-speed (5 to 40 km/h) but the wind was relatively calmer between December 5th and 13th with exception of a sharp rise on December 9th. The snow thickness remained constant during each day of sampling with the exception of some snow fall recorded on December 7$^{th}$. This added an extra 3 cm of snow on ground (Figure 11).

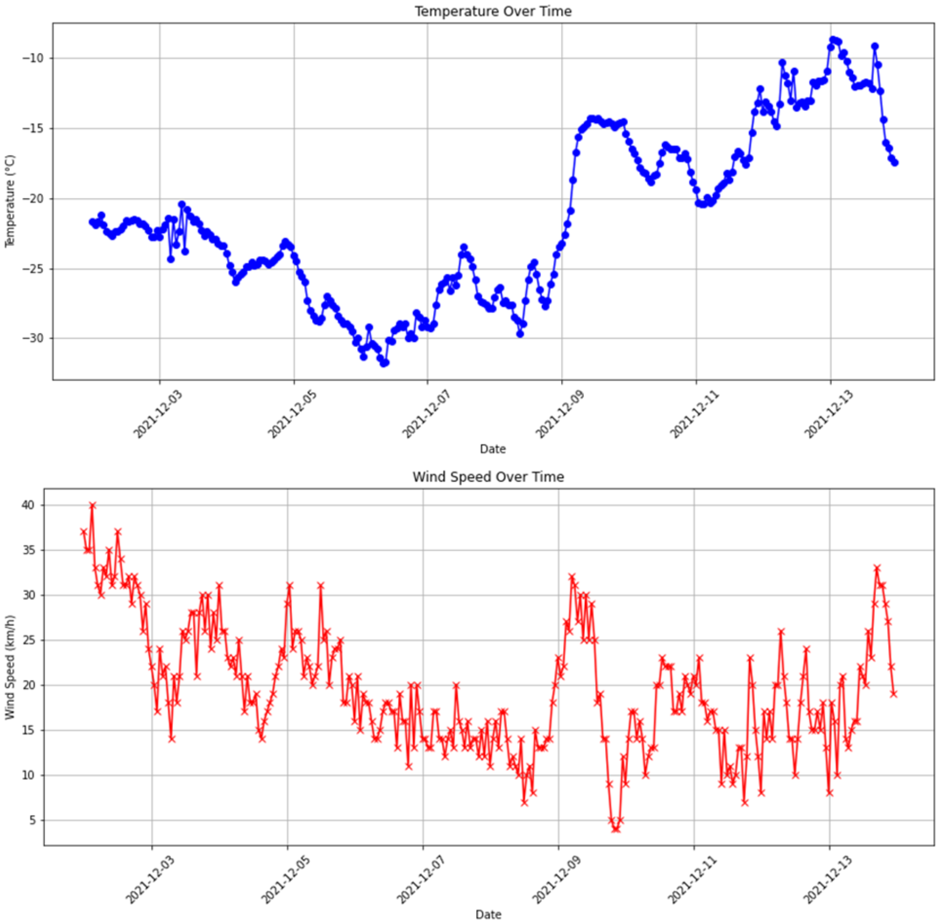

Figure 10 Hourly variation in air temperature and wind speed between December 2nd and 13th during the days of sampling at the Environment and Climate Change Canada’s (ECCC) weather station at the Churchill Airport, Manitoba.

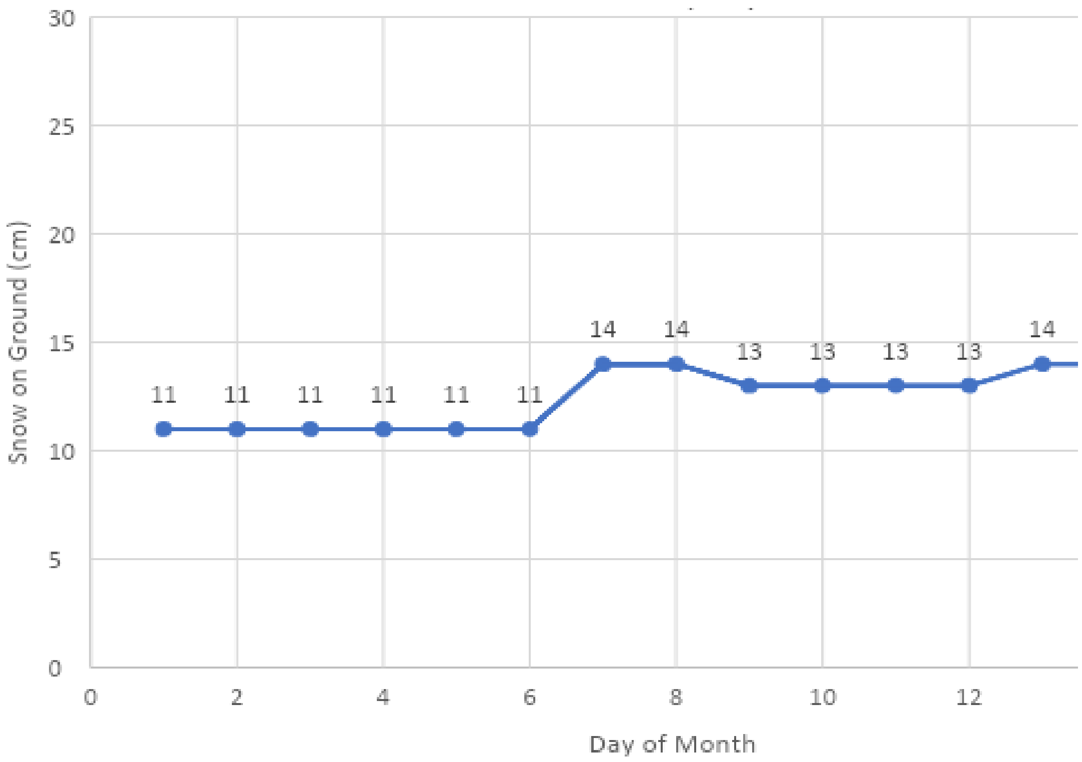

Figure 11 Snow on ground measurements from ECCC Churchill Airport Station during the days of Sampling

### 3.3.2 Lake Ice

#### 3.3.2.1 Snow on Lake Ice Geophysical Properties

As expected, the snow salinity measured on lake ice was negligible and therefore the snow was considered to be fresh. The snow density ranged between 320 and 400 kg/m$^3$ for the snow pit on December 4th conducted on Malcolm Ramsay Lake (Figure 12). There is a relatively high snow density layer around 6 cm from the snow-ice interface with densities up to 400 kg/m$^3$.

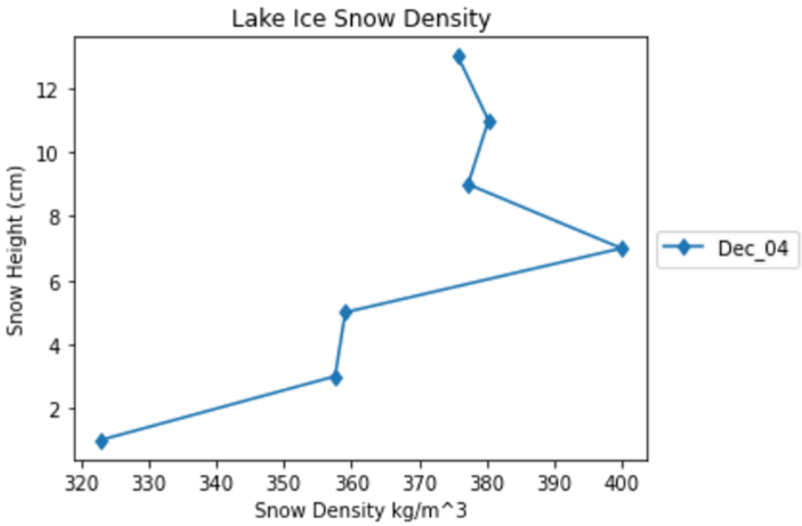

Figure 12 Snow density over lake ice on December 4th, 2021

Figure 13 Photograph showing the snow pit on lake ice taken on December 4th, 2021 (Photo: Rosemary Willatt)

### 3.3.2.2 Kuka Radar Echogram over Lake Ice

The KuKa Radar echogram over lake ice demonstrates the interaction of both the co-polarized (HH) and cross-polarized (VH) Ku and Ka band waveforms over lake ice on December 4th, 2021 (Figure 14). Both the Ku and Ka band interacted significantly with the snow on lake ice compared to snow on sea ice. Given the average snow depth measured using magnaprobe was ~8 cm, there was significant scattering from the snowpack, lake ice and the ice-water interface. As shown in Figure 14, Ka band dominant scattering occurred at the snowpack which corresponded with the range of 1 to 2 metres.  The Ka co-polarized (HH) dominant scattering horizon occurred at lower ranges (closer to the air-snow interface) compared to the Ka VH main scattering horizons. However, while most of the maximum peaks come from either the air-snow interface or the snow-ice interface, there is a significant portion of the Ka HH and VH main scattering horizons corresponding to the 2.25 to 2.50-metre range, which may be the ice-water interface.

The Ku-band dominant scattering horizon mostly corresponds with the ice-water or the ice ground interface. While there is significant scattering from the snowpack (1.5 to 2.0 metre range), both the Ku HH and VH scattering seems to occur at the 2.25 to 2.50 metre range. While Ku HH waveforms seems to have significant peaks at the 1.5 to 2.0 metre ranges, the Ku VH scattering mostly occurs at the 2.25 to 2.50 metre range.

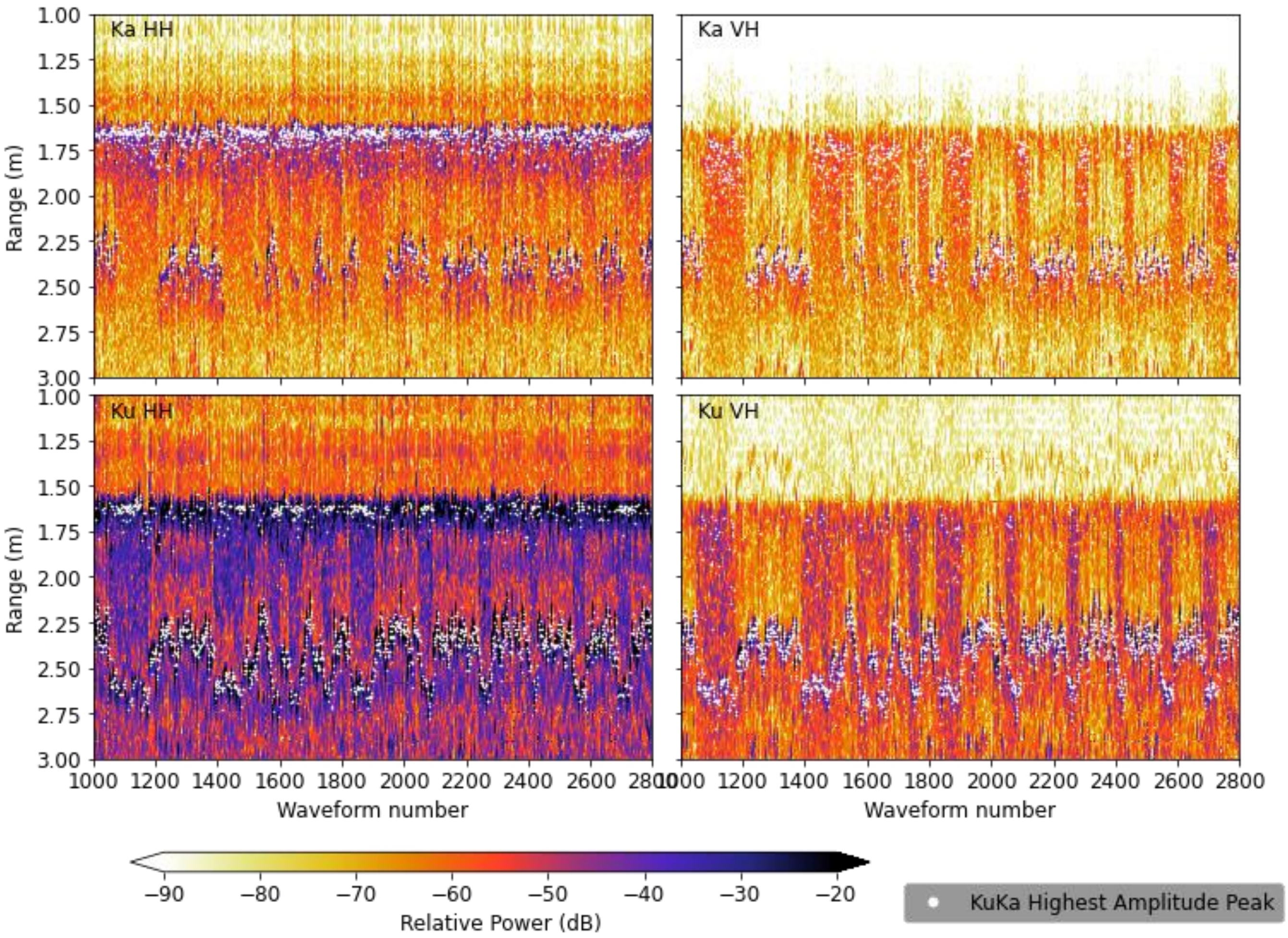

Figure 14 KuKa radar echogram over lake ice on December 4th, 2021. The white dots represent the maximum peaks for both the co-polarized and cross-polarized Ka and Ku waveforms. The range is the distance from the antenna to the surface. The distance between the antenna to the surface. The distance between the antenna to the air-snow interface is approximately 1.55 m.

### 3.2.4 KuKa Main Scattering Horizons over Lake Ice

As mentioned in Section 3.3.3, there are significant differences in Ku and Ka HH and VV interactions. In order to understand spatial variations among individual waveforms, 6 different sites (LI 1, LI 2, LI 3, LI 4, LI 5 and LI 6) are selected, and the closest Ku and Ka band echo is analyzed (Figure 15). The individual waveforms along with the Ku and Ka HH and HV maximum peaks between 1.00 to 3.00-metre range are presented in Appendix 5 to 10. We notice that the Ka and Ku waveforms have significantly different waveforms throughout the different sites (LI 1 to LI 2). Peaks have relative power greater than -50dB corresponds to the 1.00 to 1.75-metre range for Ka while for Ku there are two main peaks one corresponding to the 1.00 to 1.50-metre range and the other to the 2.25 to 2.50-metre range (Figure 16 and Appendix 5 to 10 ). However, the Ku main scattering horizon in the 2.25 to 2.50-metre range has slightly higher power. Therefore, Ku HH and VH maximum peaks correspond to the 2.25 to 2.50-metre range while the Ka HH and VH main scattering horizons are confined to the 1 to 1.75-metre range. However, an exception is for the waveform corresponding to the LI 5 site where the Ku band HH and VH main scattering horizon corresponds to the 1.75 to 2.00-metre range. We also notice that the Ku HH main scattering horizon is at a lower range (closer to the air-snow interface) compared to Ku VH. Similarly, Ka band HH maximum peaks are also at a lower range corresponding to Ka band VH maximum peak.

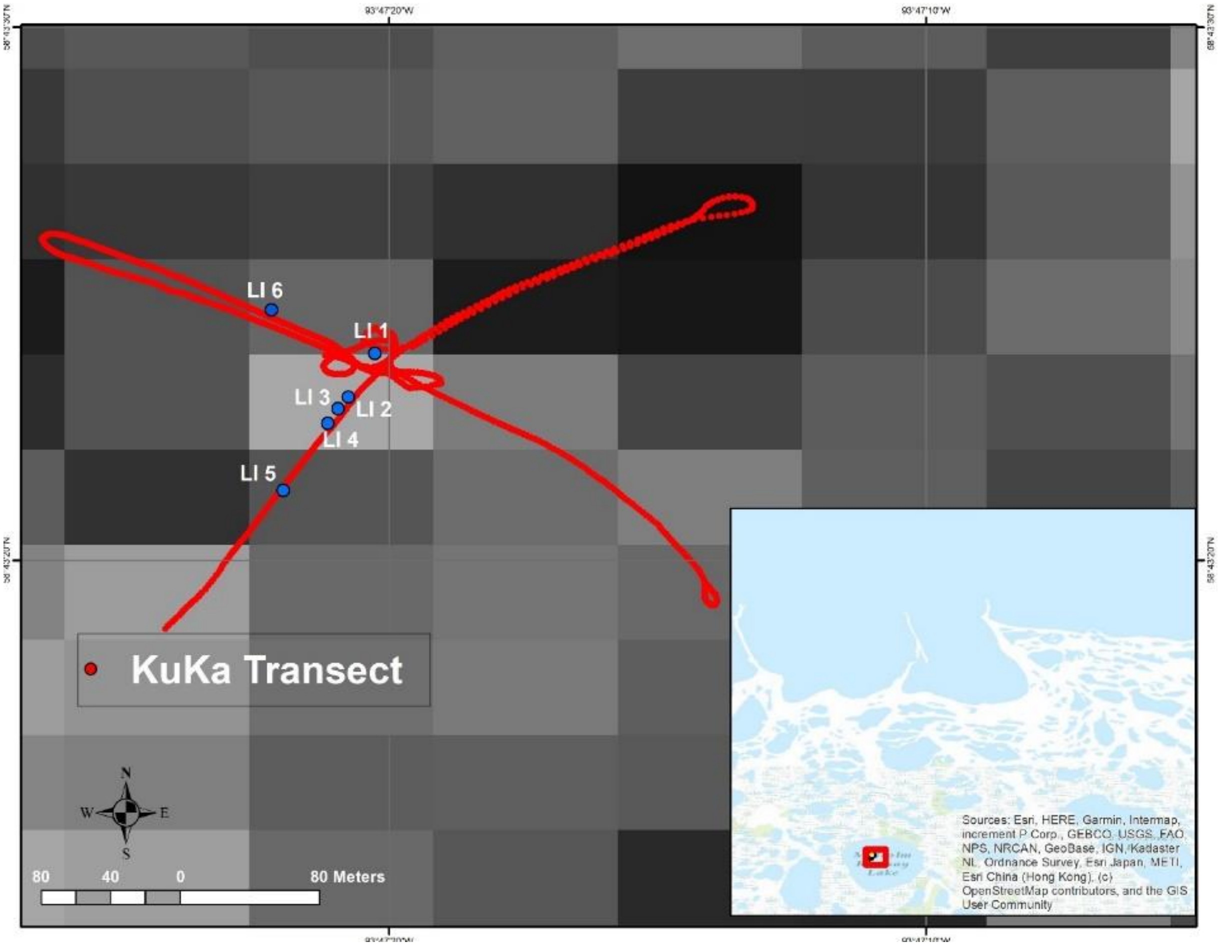

Figure 15 KuKa transect conducted over snow on lake ice at the Malcolm Ramsay Lake with the positions of the specific sites (L1 to L6) used for analyzing the waveforms

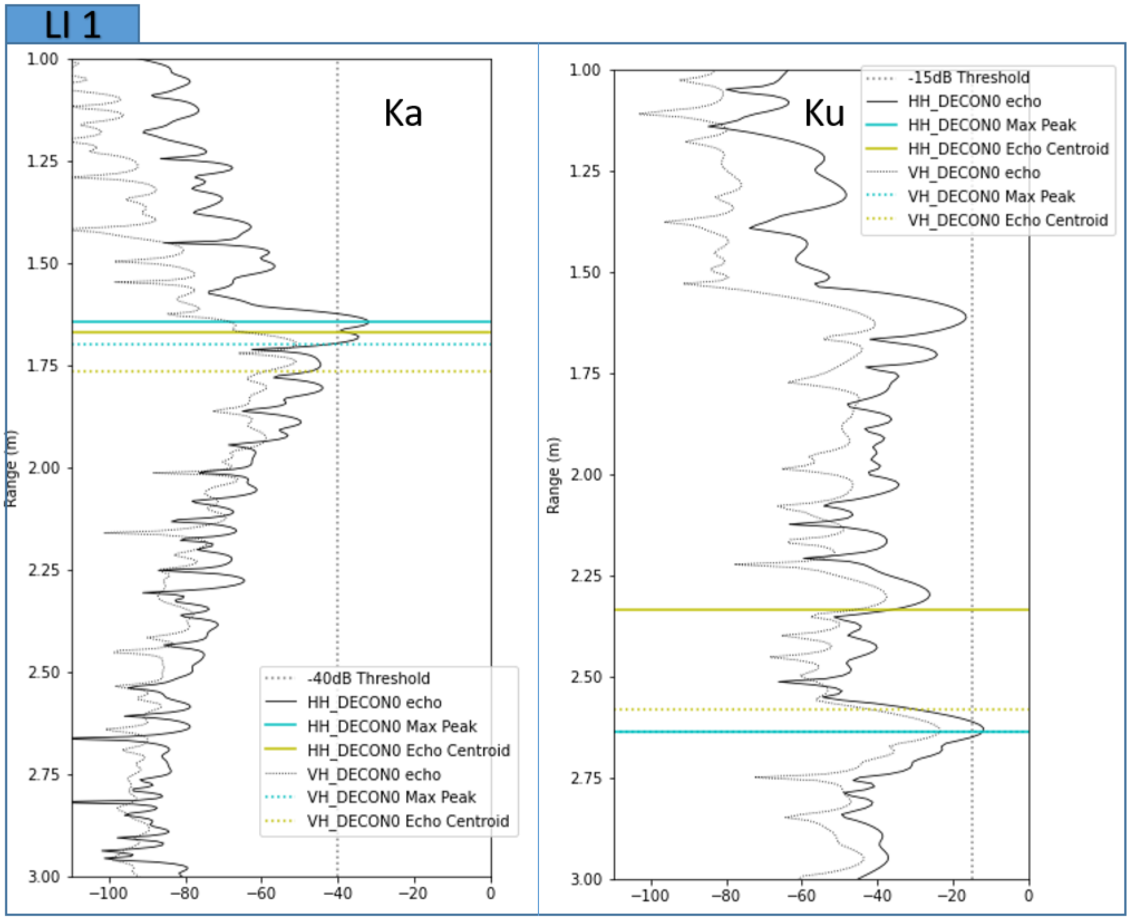

Figure 16 Ka and Ku waveforms from the closest echo from lake ice LI1 magnaprobe location

### 3.3.3 Sea Ice

#### 3.3.3.1 Snow on Sea Ice Geophysical Properties

Snow geophysical properties from the four snow pits (TP1, TP2, TP3, TP4) conducted on December 11th are presented in Figure 17. The snow salinity varied throughout the snowpack with values close to zero in the layers near the air-snow interface while basal snow salinity reached up to 9 ppt (Figure 18). TP4 had the highest basal salinity whereas TP3 had the highest salinity throughout the snowpack. There was a sharp increase in the snow salinity for TP4 with the first 4 cm of the snow pack being relatively fresh with the layer closest to the snow-interface have a salinity of 9 ppt. The snow density varied between the sites but ranged between 175 and 375 kg/m$^3$.

There was no discernable pattern in the snow density layer structure and there were no excessively high snow density layers identified. The snow density was significantly higher at TP3 compared to the other snow pits. The temperature profiles of the snow pits were comparable and ranged between -16 ℃ and -8 ℃. The coldest temperatures were closer to the air-snow interface and there was a gradual rise in temperature throughout the snowpack.

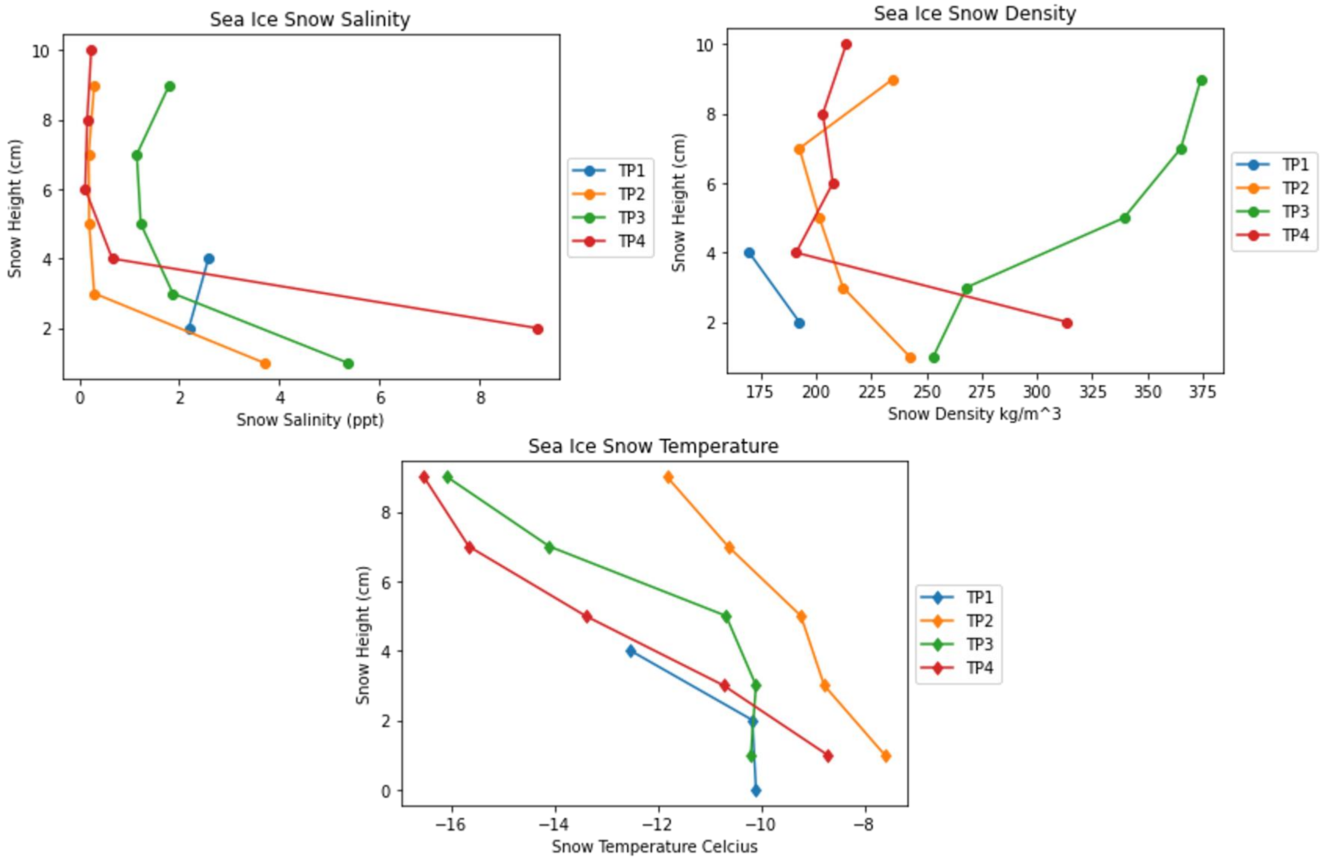

Figure 17 Snow Salinity, Density and Temperatures from the snow pits on sea ice conducted on December 11th, 2021. The snow heights are measured as the height from the snow-ice interface.

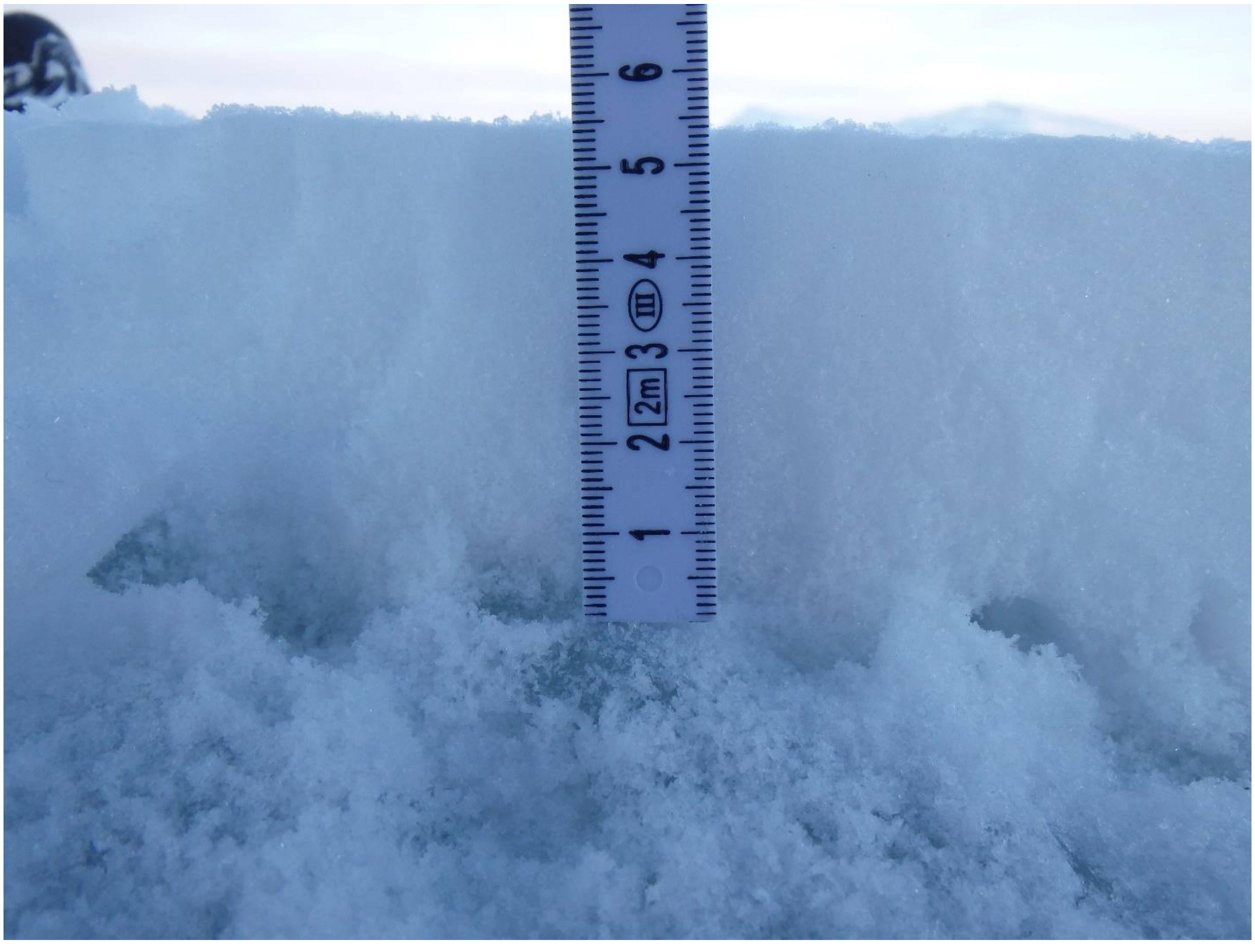

Figure 18 Photograph showing snow on sea ice taken on December 11th, 2021 (Photo: Rosemary Willatt)

### 3.3.3.2 Snow Depth on Sea Ice from Magnaprobe

In-situ snow depths were retrieved using magnaprobe according to the procedure explained in Section 2.4. The mean snow depth retrieved from the transects conducted on December 11 was 7.7 cm. The mean difference in snow depth between the sites are less than 1cm. However, the distribution of snow depths across the four transects (TP1, TP2, TP3 and TP4) are different (Figure 19,20). All of the transects had a positively skewed snow depth distribution with the majority of the snow depths between 4 and 8 cm (Figure 20,21). TP1 had the highest mean snow depth and this was apparent with a smaller second peak in the distribution for snow depths between 20 and

22 cm (Figure 20,21). TP2 had the longest tail among the distributions with some snow depths greater than 40 cm.

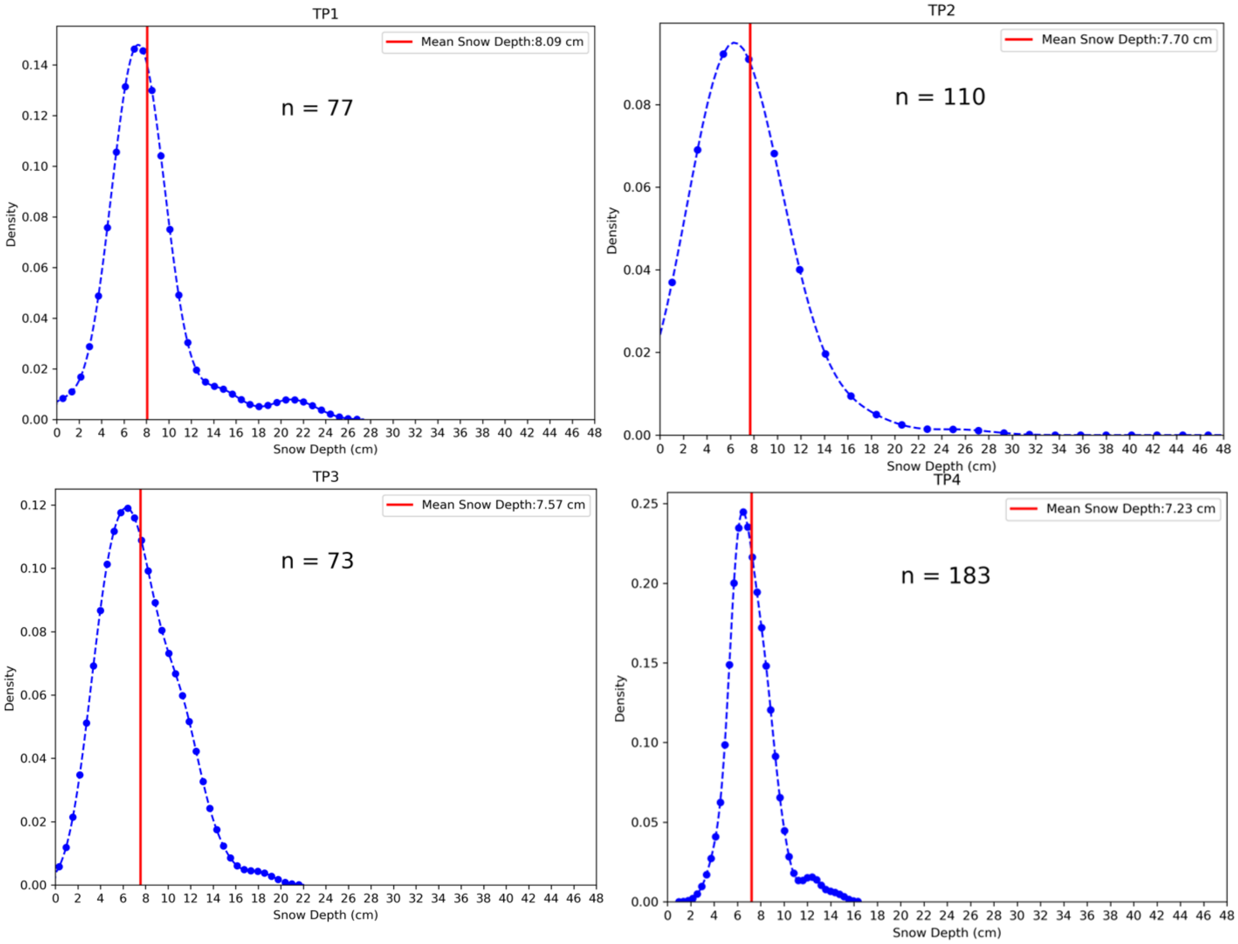

Figure 19 Distribution of snow depth on sea ice collected from the four different transects (TP1, TP2, TP3 and TP4) on December 11th, 2021. The number of snow depth samples are indicated by n.

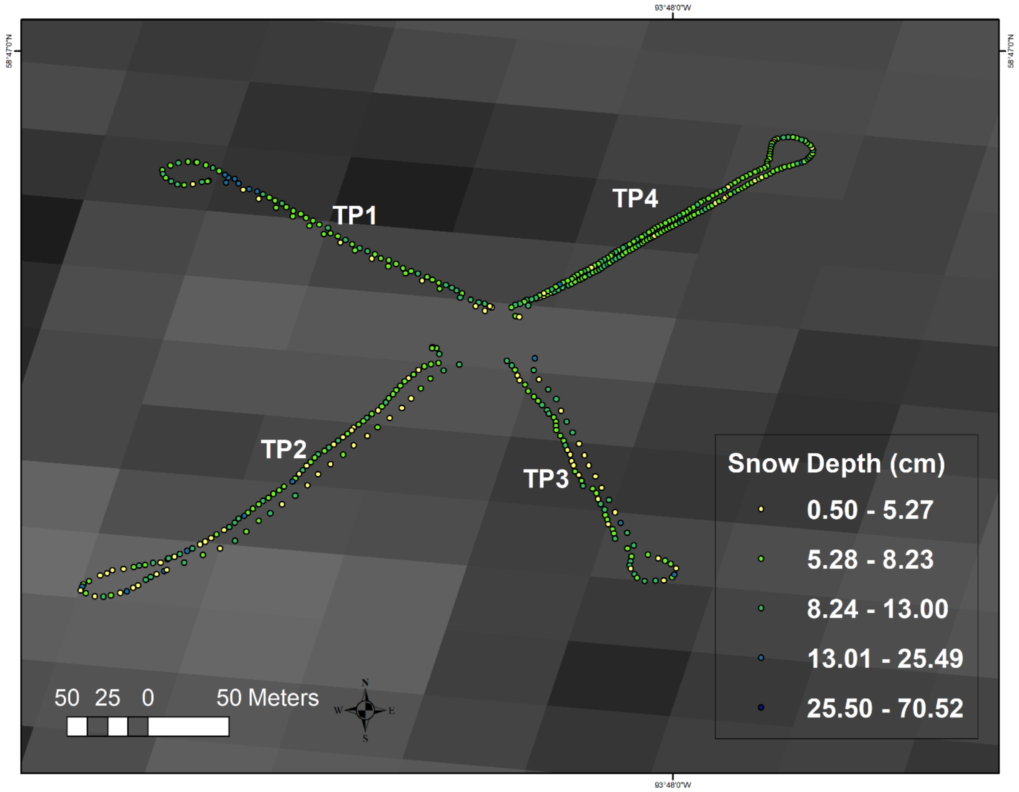

Figure 20 Spatial Distribution of snow depths across the four transects surveyed with magnaprobe on December 11th, 2021. The background imagery is a sentinel-1 HH backscatter image from December-11, 2021.

### 3.3.3.3 KuKa Radar Echograms over Sea Ice

The KuKa radar echograms over sea ice showed distinctive trends both Ka and Ku band over different polarizations. As shown in Figure 21, the dominant scattering (indicated in blue) for Ku band was coming from deeper ranges when compared to Ka band. We noticed that the co-polarized (HH) power was generally higher for both Ka and Ku band compared to the cross-polarized waveforms between 1.5 and 2.0 metre ranges. The cross-polarized (VH) Ku and Ka had dominant scattering from deeper into the snow pack. The maximum peaks of the co-polarized (HH) Ka band returns are mostly located closer to the air-snow interface whereas the Ku-band maximum peaks seem to be coming from both the air-snow interface and deeper into the snowpack. However, we notice that for both Ka and Ku, the maximum peaks of the cross-polarized VH returns are coming from greater ranges compared to range of the air-snow interface (Figure 22).

Further analysis of the transects (TP1, TP2, TP3, TP4) (Figure 20) surveyed on December 11th (Figure 25 and Appendix 1,2,3,4) showed that the Ku and Ka radar waveforms interact differently with the spatially heterogeneous snow at the different transects. We noticed that the HH waveforms have generally higher relative power when compared to the VH waveforms for both Ku and Ka band (Figure 25 and Appedix 1, 2, 3, 4). As mentioned in Section 3.5.2, a threshold power is set on the Ku and Ka HH waveform to pick up the air-snow interface. This threshold at -30 dB for Ku band sufficiently captures the highest HH peak but we notice the presence of radar sidelobe for the Ku waveform at TP2. This ultimately leads to the air-snow interface being identified at a lower range than the HH max peak. However, we noticed that the threshold set for the Ka band varied between -30 dB (TP2, TP3) and -45 dB (TP1, TP4) The Ku VH max peak is at a higher range (deeper into the snowpack) compared to the Ku HH max peak at all sites. However, we notice that the Ka band VH max peak is slightly lower than the HH max peak at sites TP3 and TP4.

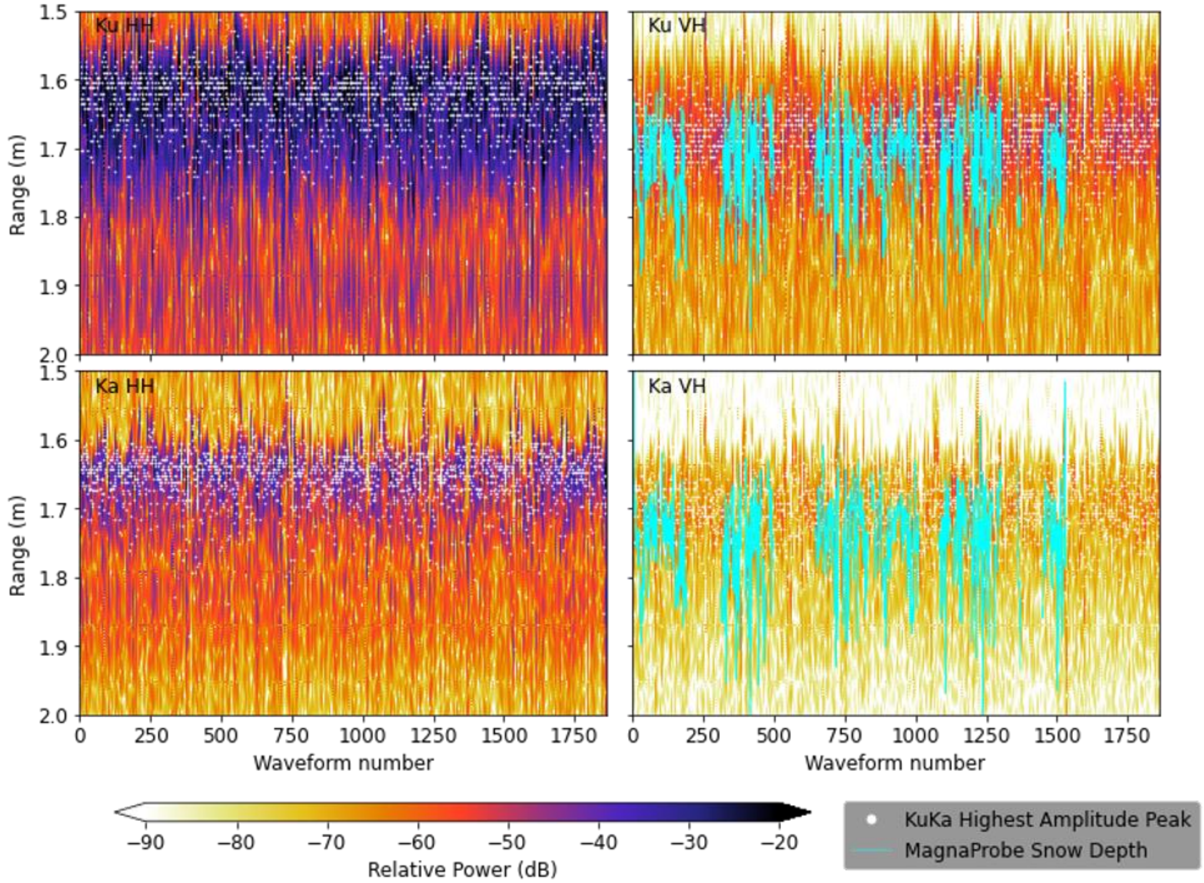

Figure 21 KuKa Radar Echograms demonstrating the relative power at specific range section (1.5 to 2 metre) from December 11th. The magnaprobe snow depths are scaled by c´ which adjusts for the reduced propagation speed within the snow pack. The magnaprobe snow depths are presented in cyan.

#### 3.3.3.4 KuKa Main Scattering Horizons over Sea Ice

As mentioned in Section 3.4, the Ku and Ka waveforms corresponding to the four different transects (TP1, TP2, TP3, TP4) are shown in the Appendix 1,2,3 and 4. The main scattering horizons ($R_{HH}$ and $R_{VH}$) was calculated for the HH and VH max peaks for both the Ku and Ka band waveforms according to Equation iii and iv. Table 2 shows the main scattering horizons ($R_{HH}$ and $R_{VH}$) for both HH and VH polarization for both Ka and Ku band. The $R_{HH}$ for both Ku and Ka band corresponded with the air-snow interface (Table 2). The $R_{VH}$ is at a greater range (deeper into the snowpack) for all four transects at the Ku band. However, the $R_{VH}$ at the Ka band is at the AS for TP3 and TP4 while it is deeper into the snow pack at TP1 and TP2. However, we noticed that the $R_{VH}$ at the Ku band is generally deeper into the snow pack when compared to $R_{VH}$ at the Ka band.

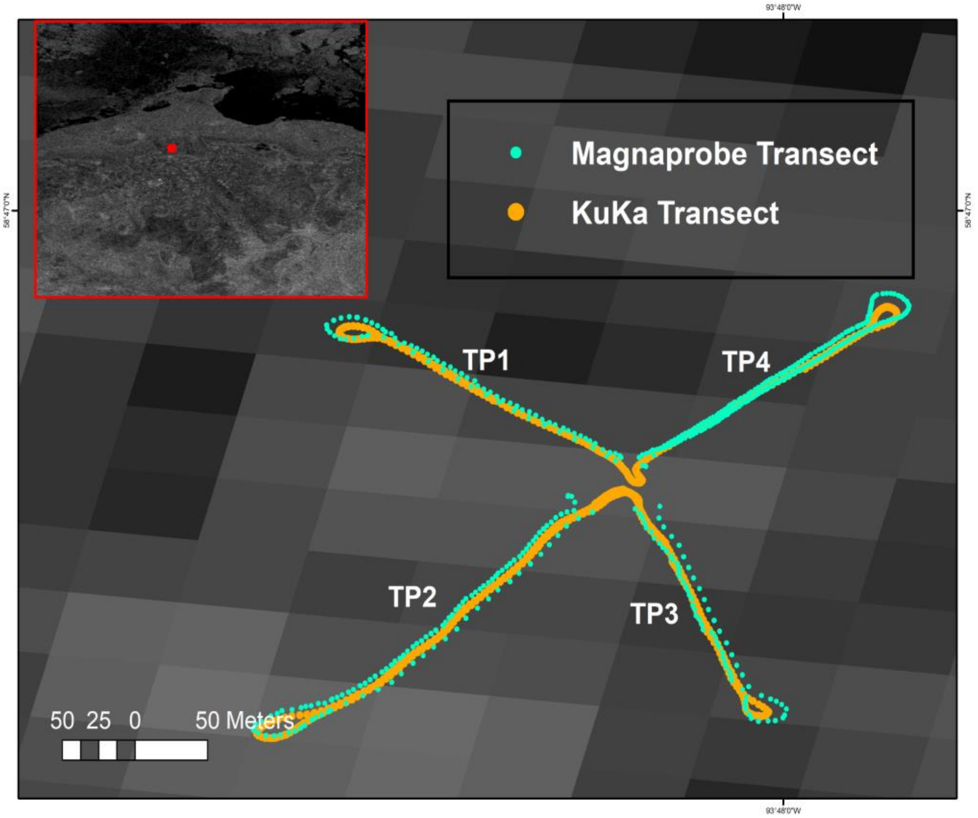

Figure 22 Map showing the KuKa and magnaprobe transect from the survey on December 11th, 2021. Location of the snow pits corresponding to each transect is labelled TP1, TP2, TP3 and TP4.

Table 2 Ku and Ka Main Scattering Horizons measured from the air-snow interface along the different snow pit sites (TP1 to TP4)

| Snow Pit | | Ka (cm) | Ku (cm) |
|---|---|---|---|
| TP1 | $R_{HH}$ (cm) | 0.00 (AS) | 0.00 (AS) |
| | $R_{VH}$ (cm) | 6.41 | 8.39 |
| TP2 | $R_{HH}$ (cm) | 0.00 (AS) | 14.49 |
| | $R_{VH}$ (cm) | 7.32 | 10.68 |
| TP3 | $R_{HH}$ (cm) | 0.00 (AS) | 0.00 (AS) |
| | $R_{VH}$ (cm) | -0.45(AS) | 6.10 |
| TP4 | $R_{HH}$ (cm) | 0.00 (AS) | 0.00 (AS) |
| | $R_{VH}$ (cm) | -0.45(AS) | 7.63 |

#### 3.3.3.5 KuKa Snow Depth on Sea Ice

Snow depths were retrieved following the the polarization based method proposed by Willatt et al., (2023) as explain in Section 2.5.3. The snow depths retrieved from the difference in VH and HH max peaks of Ku band were generally higher when compared to snow depth retrieved using Ka band (Figure 23). The mean snow depth retrieved from Ka band was underestimated by ~1.26 cm compared to the Ku band retrieval. The distribution of snow depths retrieved using the Ka band and Ku band are similar (Figure 23). However, the Ku band distribution has a slightly longer tail compared to the Ka band snow depths.

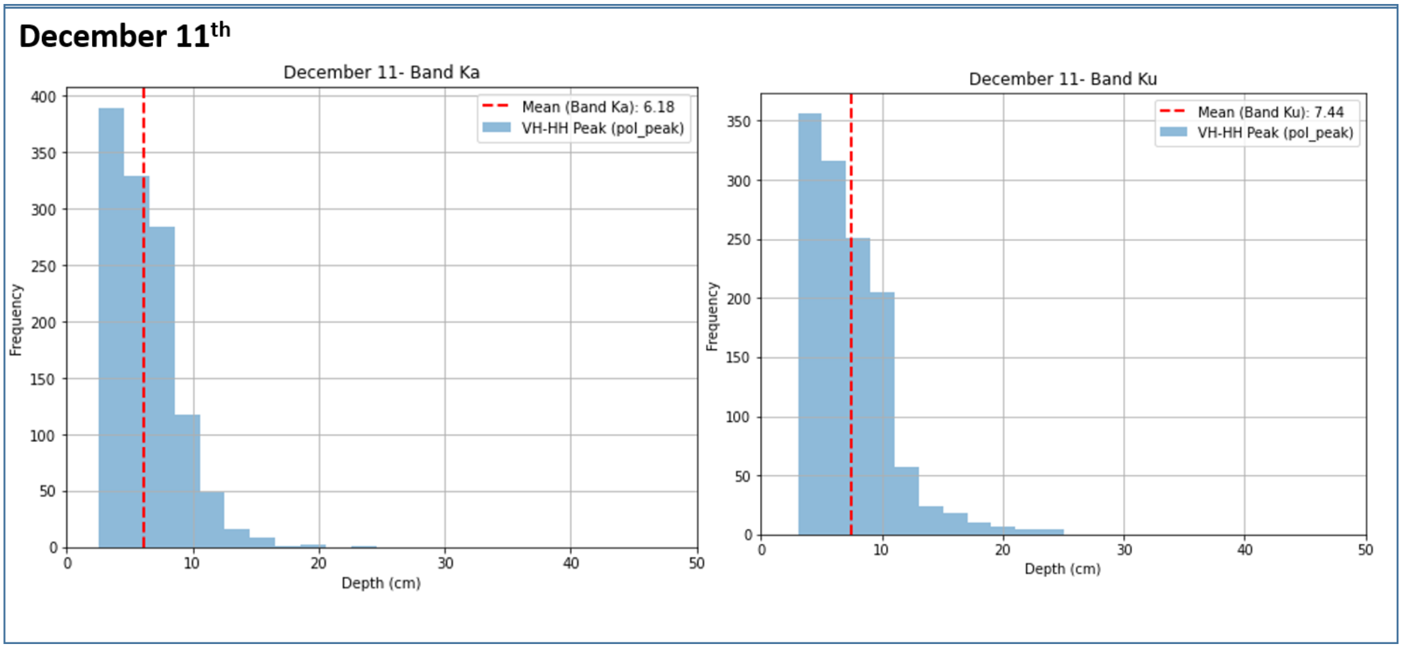

Figure 23 Snow depth distribution calculated as the difference between VH and HH max peaks for both Ka and Ku band. The data was collected over Sea Ice December 11th.

## 3.4 Discussions

### 3.4.1 Sea Ice Main Scattering Horizons

The main scattering horizon ($S_H$) was modelled for the Ku and Ka band using the snow geophsycial data as mentioned in Section 2.5.4 while the main scattering horizons ($R_{VH}$ and $R_{HH}$) for the Ku and Ka returns from the KuKa radar was retrieved using the procedure mentioned in Section 2.5.2. Table 3 shows the modelled main scattering horizons for the snow pits conducted at each site. Majority of the snow pits had $S_H$ deeper into the snow pack for both Ku and Ka band. However, 3 out of the 10 snow pits on sea ice had the main scattering horizon for both Ku and Ka band at the air-snow interface (AS) (Table 3). This implied that there was insignificant penetration of Ku and Ka band beyond the AS for these snow pits.

The $S_H$ for each snow pit (Table 3) are compared to the main scattering horizons for both the Ku and Ka co-polarized (HH) and cross-polarized (VH) waveforms(Table 2). The Ku and

Ka $S_H$ was modelled at the air-snow interface based on the snow geophysical data for the TP1 and TP3 snow pits (Table 3). This is also apparent in the HH main scattering horizon $R_{HH}$ from the KuKa radar at TP1 and TP3 (Table 2). However, the KuKa radar derived VH main scattering horizon $R_{VH}$ is at 6 cm for Ka and 8 cm for Ku band respectively for snow pit TP1. Therefore, we observe that while there is apparently no penetration in to the snowpack at the Ku and Ka HH polarization, there was significant penetration of Ku and Ka VH polarization. For the snow pit at TP4, the modelled Ku $S_H$ is at 7 cm (Table 3) which corresponded exactly with the Ku $R_{VH}$ retrieved from the radar (Table 2). However, although the modelled data showed the Ka $S_H$ to be atleast 3 cm at TP4, the corresponding Ka $R_{VH}$ is at the air-snow interface. Although Ku $R_{VH}$ TP2 showed a ~10 cm penetration, upon further inspection of the waveform (Appendix 1), this is considered anomalous because of the mis-classification of the air-snow interface due to the presence of a radar side lobe. Therefore, the corresponding modelled penetration of 4 cm is more realistic for Ku band at TP2. We notice that while there is some correspondence of the Ku and Ka main scattering horizons at both polarizations with the modelled $S_H$ especially at TP2 and TP4, the cross-polarized Ku $R_{VH}$ shows relatively better correspondence.

Table 3 Modelled main scattering horizon based on snow geophysical data from snow pits. AS is the air-snow interface and SI being the snow-ice interface.

| | **Date** | **Snow pit (Date_Snow Pit Number)** | **$S_H$ Ka Main Scattering Horizon** | **$S_H$ Ku Main Scattering Horizon (Distance from the AS)** | **Snow Depth(cm)** |
|---|---|---|---|---|---|
| **Sea Ice Site 1 (SI_1)** | 11/12/2021 | Dec11_TP1 | AS | AS | 5 |
| | 11/12/2021 | Dec11_TP2 | 1 | 4 | 10 |
| | 11/12/2021 | Dec11_TP3 | AS | AS | 10 |
| | 11/12/2021 | Dec11_TP4 | 3 | 7 | 11 |

### 3.4.2 Sea Ice Snow Geophysical Properties and KuKa Main Scattering Horizons

The impact of snow geophysical properties on the interaction of Ku and Ka band is assessed by comparing the December 11 snow pit data (TP1, TP2, TP3 and TP4) to the main scattering horizons ($R_{HH}$ & $R_{VH}$) retrieved from the KuKa radar. The HH main scattering horizon $R_{HH}$ for both Ku and Ka was at the air-snow interface irrespective of the difference in snow geophysical properties between the snow pits. However, the VH main scattering horizon for both the Ka and Ku band was impacted by the difference in snow density and salinity. TP1 and TP3 have relatively saline (> 2 ppt) snow packs but the snow bulk density at the first 4 cm of the snow pack is relatively higher for TP3 (~370~170 kgm$^3$) compared to TP1(~170 kgm$^3$ ) (Figure 17). Therefore, while Ku band $R_{VH}$ is deeper into the snow pack for both TP1 and TP3, the Ka band $R_{VH}$ at TP3 is at the air-snow interface. Therefore, the highly dense snow pack may have hindered the Ka band waveforms from penetrating the snow pack.

The salinity in first few centimetres from the air-snow interface has impacts on both Ku and Ka band VH main scattering horizons ($R_{VH}$). The Ku $R_{VH}$ at TP3 (6 cm) is lowest when compared to snow pits which have similar snow depths (TP2, TP4) (Table 2). The relatively high salinity (< 1 ppt) throughout the snowpack may have caused the Ku $R_{VH}$ to be shifted up the snowpack. Although the basal snow salinity at TP4 was very high (9ppt) compared to TP3 (3 ppt), which had relatively higher salinity (>1 ppt) throughout the snowpack, the Ku band $R_{VH}$ was closer to the snow-ice interface. Therefore, the impact of brine wicking up the snow pack (making the snow closer to the air-interface more saline) seems impact the Ku-band main scattering horizon.

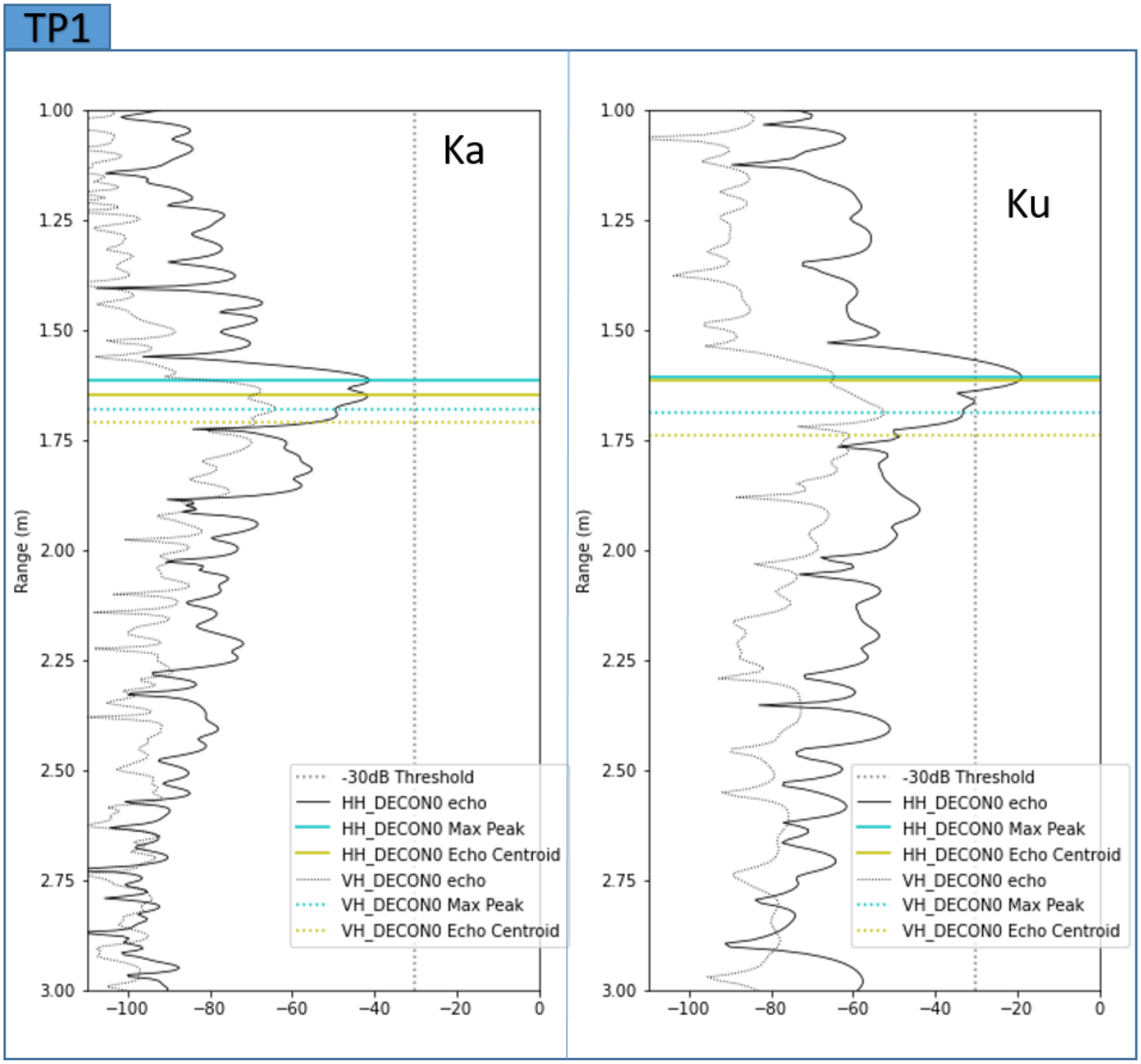

Figure 24 Ku and Ka band HH and VH echos along with the HH and VH max peaks and echo centroids at site TP1 on December 11.

### 3.4.3 Sea Ice KuKa vs Magnaprobe Snow Depth

Snow depth was retrieved based on the difference between the range corresponding to the VH and HH maximum peaks as described in Section 2.5.3 while the magnaprobe snow depth retrieval process was described in Section 2.4. The snow depths measured using the Ku band maximum peaks compared better with the magnaprobe snow depths (Figure 25). However, both the Ku and

Ka band retrievals had a mean bias of less than 2 cm. The underestimation of the Ka band snow depth could be a result of the position of the Ka band main scattering horizons generally being closer to the air-snow interface (Table 2). Comparing the snow depth distributions, the snow depths less than 10 cm are general underestimated by the Ku band retrievals while greater snow depths are well represented (Figure 25).

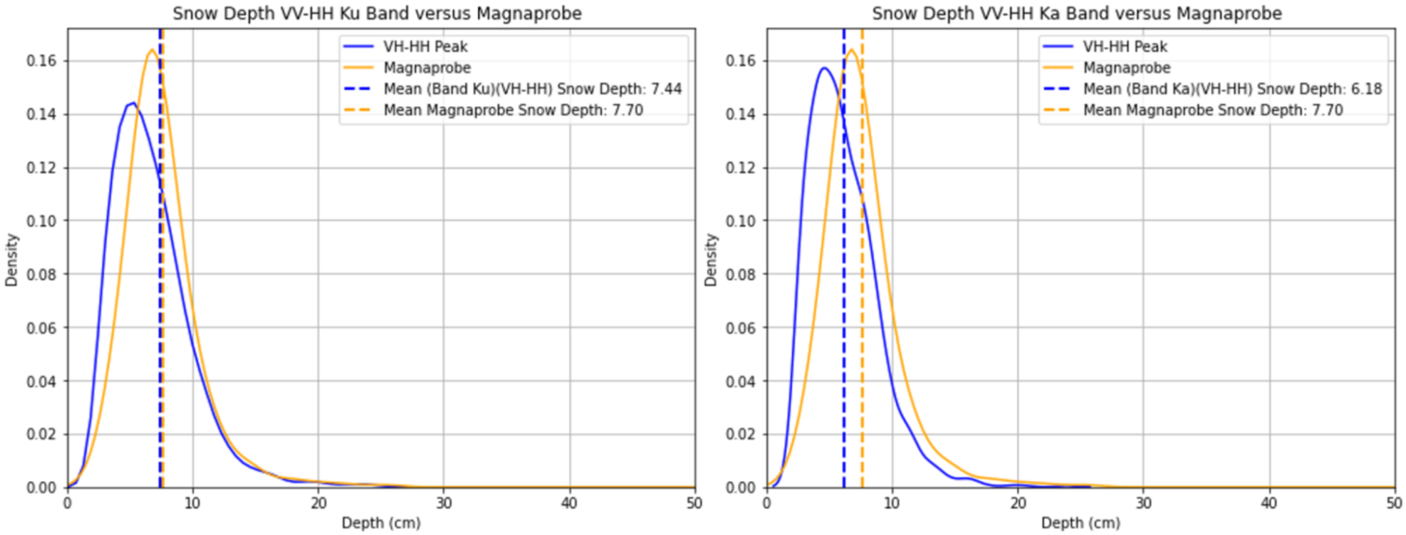

Figure 25 Comparing snow depths retrieved from KuKa radar with the magnaprobe snow depths. The data was collected on December 11th, 2021.

### 3.4.4 Lake Ice KuKa vs Magnaprobe Snow Depth

Figure 26 shows the distributions of snow depths retrieved using the polarization-based technique explained in Section 2.5. The snow density from the lake ice snow pit is used to estimate *c´* which is then used to scale the difference between the VH and HH max peaks. The range bin was set to 1 to 2 metres to ensure that the peaks corresponding solely to the snowpack was considered. The Ka band HH and VH combination seems to outperform Ku band which overestimates the snow depths compared to the magnaprobe snow depths (Figure 26). This corresponds with the observations made regarding the maximum peaks in Section 3.3.4. Therefore, the mean value of the magnaprobe does not agree well with the VH-HH peak. However, the VH-HH Peak agrees well with the distribution.

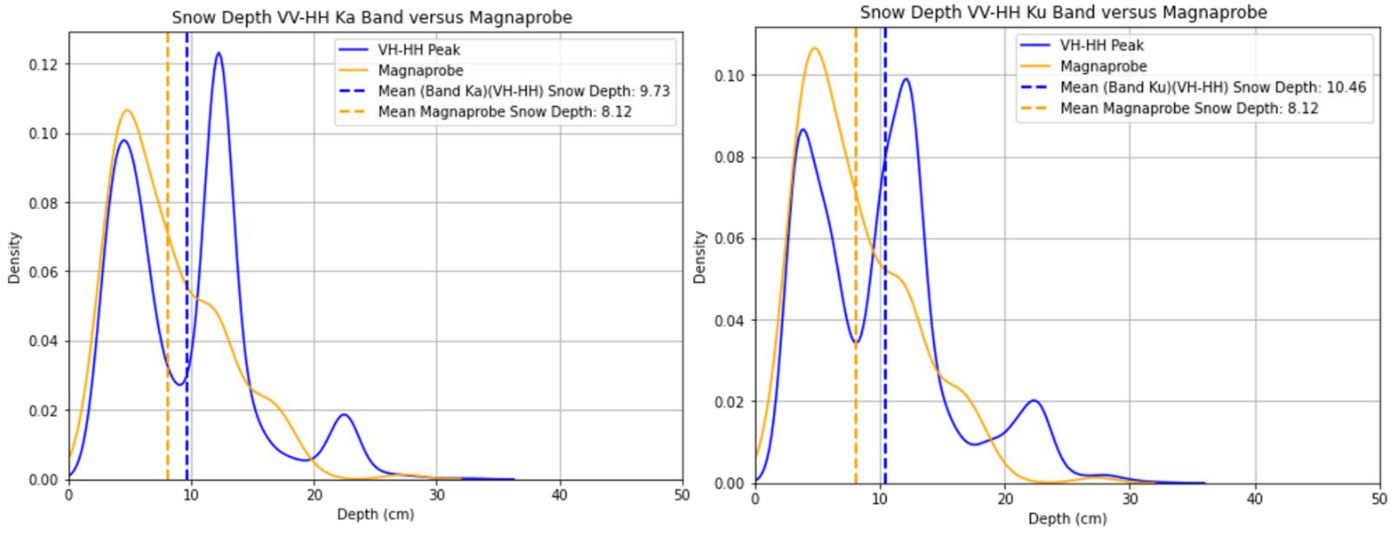

Figure 26 Snow depth retrieved over snow on lake ice using the difference between difference in co-polarized(HH) and cross-polarized(VH) maximum peaks

### 3.4.5 KuKa Main Scattering Horizons over Snow on Sea Ice and Lake Ice

The distance between the snow on lake ice and sea ice was ~7 kilometres which meant that the two sites have similar atmospheric temperature, pressure and snow fall. The results demonstrate that despite having snowpacks of the similar depth (Sea ice- 7.70 cm, Lake ice-8.12 cm), snow density (300 to 400 kg/m$^3$) and atmospheric temperature, the Ku and Ka band interact very differently with the snowpacks on sea ice and lake ice. For snow on sea ice, almost all maximum peaks for Ku and Ka band come off from within the snowpack either dominantly from the air-snow interface or closer to the snow-ice interface. However, we notice that significant portions of both the Ku and Ka maximum peaks for the snow on lake ice come off higher ranges beyond the snow-ice interface. The average ice thickness reported in Murfitt et al., (2022) ranges between 0.4

to 0.8 metres in between December 2009 and January 2010 at the Malcolm Ramsay Lake. This thickness roughly corresponds with the range between 2.25 to 2.50 metre (Figure 14). Therefore, we can assume that the Ku maximum peaks in the range between 2.25 to 2.50 metre corresponds roughly with the ice-water interface. However, it is to be noted that the presence of ice bubbles, which has not been verified in this study may significantly impact the dominant scattering from inside the lake ice (Atwood et al., 2015).

We observe that the interactions of Ku and Ka band vary widely depending on the polarization of the waveforms. The Ka and Ku co-polarized HH waveforms corresponds with the air-snow interface for sea ice but for the lake ice appears to come from deeper into the snowpack. Therefore, the determination of the air-snow interface is difficult to ascertain with the co-polarized data from Ka and Ku band for lake ice and requires further investigation.

The most significant difference between the snowpack on sea ice and lake ice is in the snow salinity. While snow on sea ice was significantly saline (5 to 9 ppt) especially in the basal snow layers, the snow on lake ice was fresh. Therefore, as demonstrated in the snow on sea ice modelling study (Section 4.1) and in the KuKa data (Section 3.2.3), snow pits having relatively high salinity throughout the snow pack limits the main scattering horizons within the snow pack. However, the fresh snow pack on lake ice leads to Ku and Ka band waveforms to have main scattering horizons beyond the snow pack. Therefore, we notice that the different polarizations of Ku and Ka band maximum peaks are significantly different for lake ice. We notice that while Ka band HH and VH maximum peaks are limited to the snow pack, Ku band maximum peaks arise beyond the snow pack and possibly from the ice-water interface.

## 3.5 Conclusion

This study presents insights into the interaction of Ku and Ka band co-polarized and cross-polarized radar waveforms with snow on first-year landfast sea ice and lake ice at Churchill, Manitoba. For snow on sea ice, the main scattering horizons of both the Ku and Ka co-polarization HH waveforms are observed to be at the air-snow interface which was also observed by Willatt et al., (2023) analyzing the MOSAiC snow packs. Both the Ka band and Ku band VH main scattering horizons arise from deeper in the snow pack than the air-snow interface. Therefore, although co-polarized (HH) Ka-band scatters mostly off the air-snow interace, cross-polarized (VH) Ka band waveforms scatters from deeper into the snowpack. This observation is further supported by the relative position of the Ku and Ka HH maximum peaks at ranges corresponding to the position of the air-snow interface (Appendix 1,2,3,4). The modelled main scattering horizons are compared to the Ku and Ka main scattering horizons however, the modelled horizons do not correspond with the Ka amd Ka HH main scattering horizons retrieved by the radar (Table 2). This observation is also supported by the fact that the HH main scattering horizon at the Ku and Ka-band (Table 2) remains at the air-snow interface even for snow pits where the modelled data predicted scatters beyond the air-snow interface. While this observation corroborates with the general assumption made at the satellite level (which uses HH co-polarized Ka and Ku band microwaves) that Ka-band does not scatter beyond the top of the snow pack, it contradicts the assumption of Ku band main scattering horizon coming off from the snow-sea ice interface. However, KuKa radar has a much finer footprint size (31cm (Ka) and 44 (Ku)) compared to the satellites, which have footprints hundreds of metre wide. Therefore, caution needs to be exercised while comparing the main scattering horizons at such different scales. Snow geophysical properties especially snow density and salinity in the top few layers of the snowpack may impact the position of the main VH scattering horizon at both the Ka and Ku band. Comparing the snow pit data with the closest Ku and Ka waveforms, we see that if snow salinity greater than 1 ppt occurs in the first ~4 cm of the snow pack, neither the VH Ku or Ka waveforms penetrates the snowpack. The impact of snow salinity is further realized comparing the interaction of Ku and Ka band with fresh snow on lake ice. The snow dielectrics are significantly different for a saline and a non-saline snow pack with similar snow densities. As presented in the results, both Ka and Ku band interacts significantly differently with a completely fresh and a saline snow pack. While the co-polarized (HH) and cross-polarized (VH) Ka band waveforms are mostly confined closer to the snow pack, Ku band dominant scattering horizons are identified beyond the snow pack closer to the ice-water interface. Therefore, the role of snow salinity in terms of setting the dielectrics and overall behavior of Ku and Ka band at different polarizations is significant and needs to be further investigated. Observations made on the Ku and Ka band maximum peaks are further investigated by testing the potential of retrieving snow depth on sea ice and lake ice based on differencing the co-polarized (HH) and cross-polarized (VH) maximum peaks proposed by Willatt et al., (2023). Based on the concept, snow depth on sea ice is retrieved with an accuracy of ~2 cm compared to magnaprobe retrieved snow depths. However, difference in Ku band VH and HH maximum peaks can be used to estimate the snow depth on sea ice while Ka band VH and HH does a better job at estimating snow depth on lake ice. Although beyond the scope of this study, observations made from KuKa on lake ice may have the potential to estimate both the snow on sea ice and lake ice and possibly the lake ice thickness. Preliminary results from this study show Ku band HH and VH main scattering horizon corresponds with the ice-water interface while Ka band HH and VH corresponds with the air-snow and snow-ice interfaces respectively. However, further investigation is required. This chapter helps us better understand how snow geophysical properties can significantly alter interaction of Ka and Ku microwaves. While the surface based observations cannot be translated directly to the satellite level due to the differences in footprint size, critical observations on the interaction of Ku and Ka in different snow geophysical conditions can be used to better interpret satellite level observations.

## References

Atwood, D. K., Gunn, G. E., Roussi, C., Wu, J., Duguay, C., & Sarabandi, K. (2015). Microwave Backscatter From Arctic Lake Ice and Polarimetric Implications. *IEEE Transactions on Geoscience and Remote Sensing*, *53*(11), 5972–5982. https://doi.org/10.1109/TGRS.2015.2429917

Hallikainen, M., Ulaby, F., & Abdelrazik, M. (1986). Dielectric properties of snow in the 3 to 37 GHz range. *IEEE Transactions on Antennas and Propagation*, *34*(11), 1329–1340. https://doi.org/10.1109/TAP.1986.1143757

Kuzyk, Z. A., Macdonald, R. W., Granskog, M. A., Scharien, R. K., Galley, R. J., Michel, C., Barber, D., & Stern, G. (2008). Sea ice, hydrological, and biological processes in the Churchill River estuary region, Hudson Bay. *Estuarine, Coastal and Shelf Science*, *77*(3), 369–384. https://doi.org/10.1016/j.ecss.2007.09.030

Nandan, V., Geldsetzer, T., Yackel, J., Mahmud, M., Scharien, R., Howell, S., King, J., Ricker, R., & Else, B. (2017). Effect of Snow Salinity on CryoSat-2 Arctic First-Year Sea Ice Freeboard Measurements. *Geophysical Research Letters*, *44*(20), 10,419-10,426. https://doi.org/10.1002/2017GL074506

Nandan, V., Scharien, R. K., Geldsetzer, T., Kwok, R., Yackel, J. J., Mahmud, M. S., Rösel, A., Tonboe, R., Granskog, M., Willatt, R., Stroeve, J., Nomura, D., & Frey, M. (2020). Snow Property Controls on Modeled Ku-Band Altimeter Estimates of First-Year Sea Ice

Thickness: Case Studies From the Canadian and Norwegian Arctic. *IEEE Journal of Selected Topics in Applied Earth Observations and Remote Sensing*, *13*, 1082–1096. https://doi.org/10.1109/JSTARS.2020.2966432

Nandan, V., Willatt, R., Mallett, R., Stroeve, J., Geldsetzer, T., Scharien, R., Tonboe, R., Landy, J., Clemens-Sewall, D., Jutila, A., Wagner, D. N., Krampe, D., Huntemann, M., Yackel, J., Mahmud, M., Jensen, D., Newman, T., Hendricks, S., Spreen, G., … Hoppman, M. (2022). *Wind Transport of Snow Impacts Ka- and Ku-band Radar Signatures on Arctic Sea Ice* [Preprint]. Sea ice/Remote Sensing. https://doi.org/10.5194/tc-2022-116

Stroeve, J., Nandan, V., Willatt, R., Tonboe, R., Hendricks, S., Ricker, R., Mead, J., Mallett, R., Huntemann, M., Itkin, P., Schneebeli, M., Krampe, D., Spreen, G., Wilkinson, J., Matero, I., Hoppmann, M., & Tsamados, M. (2020). Surface-based Ku- and Ka-band polarimetric radar for sea ice studies. *The Cryosphere*, *14*(12), 4405–4426. https://doi.org/10.5194/tc-14-4405-2020

Sturm, M., & Holmgren, J. (2018). An Automatic Snow Depth Probe for Field Validation Campaigns. *Water Resources Research*, *54*(11), 9695–9701. https://doi.org/10.1029/2018WR023559

Webster, M. A., Rigor, I. G., Nghiem, S. V., Kurtz, N. T., Farrell, S. L., Perovich, D. K., & Sturm, M. (2014). Interdecadal changes in snow depth on Arctic sea ice. *Journal of Geophysical Research: Oceans*, *119*(8), 5395–5406. https://doi.org/10.1002/2014JC009985

Willatt, R., Stroeve, J. C., Nandan, V., Newman, T., Mallett, R., Hendricks, S., Ricker, R., Mead, J., Itkin, P., Tonboe, R., Wagner, D. N., Spreen, G., Liston, G., Schneebeli, M., Krampe, D., Tsamados, M., Demir, O., Wilkinson, J., Jaggi, M., … Oggier, M. (2023). Retrieval of Snow Depth on Arctic Sea Ice From Surface-Based, Polarimetric, Dual-Frequency Radar

Altimetry. *Geophysical Research Letters*, *50*(20), e2023GL104461. https://doi.org/10.1029/2023GL104461

## Appendix

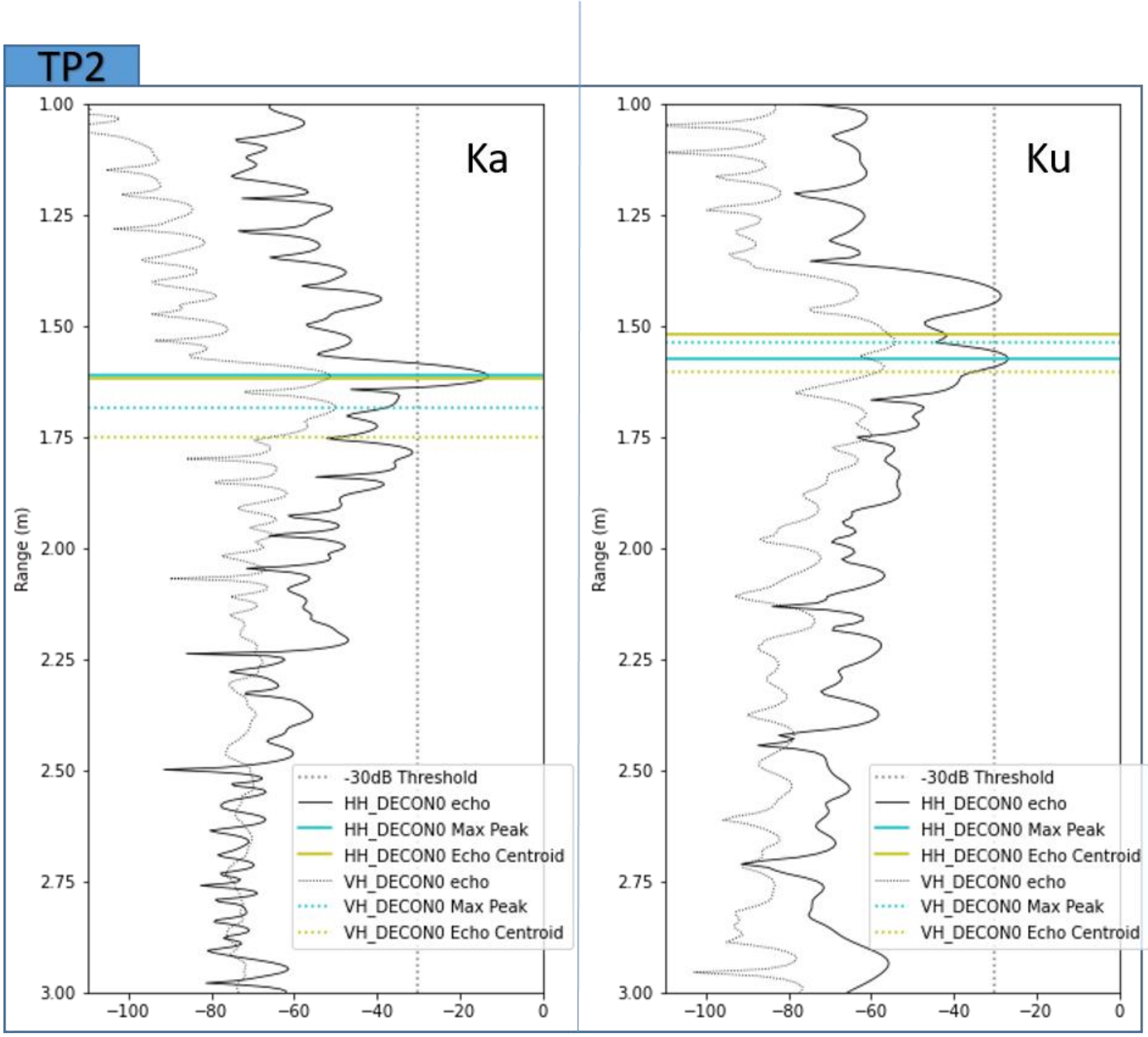

Appendix 1: Ku and Ka band HH and VH echos along with the HH and VH max peaks and echo centroids at site TP2 on December 11.

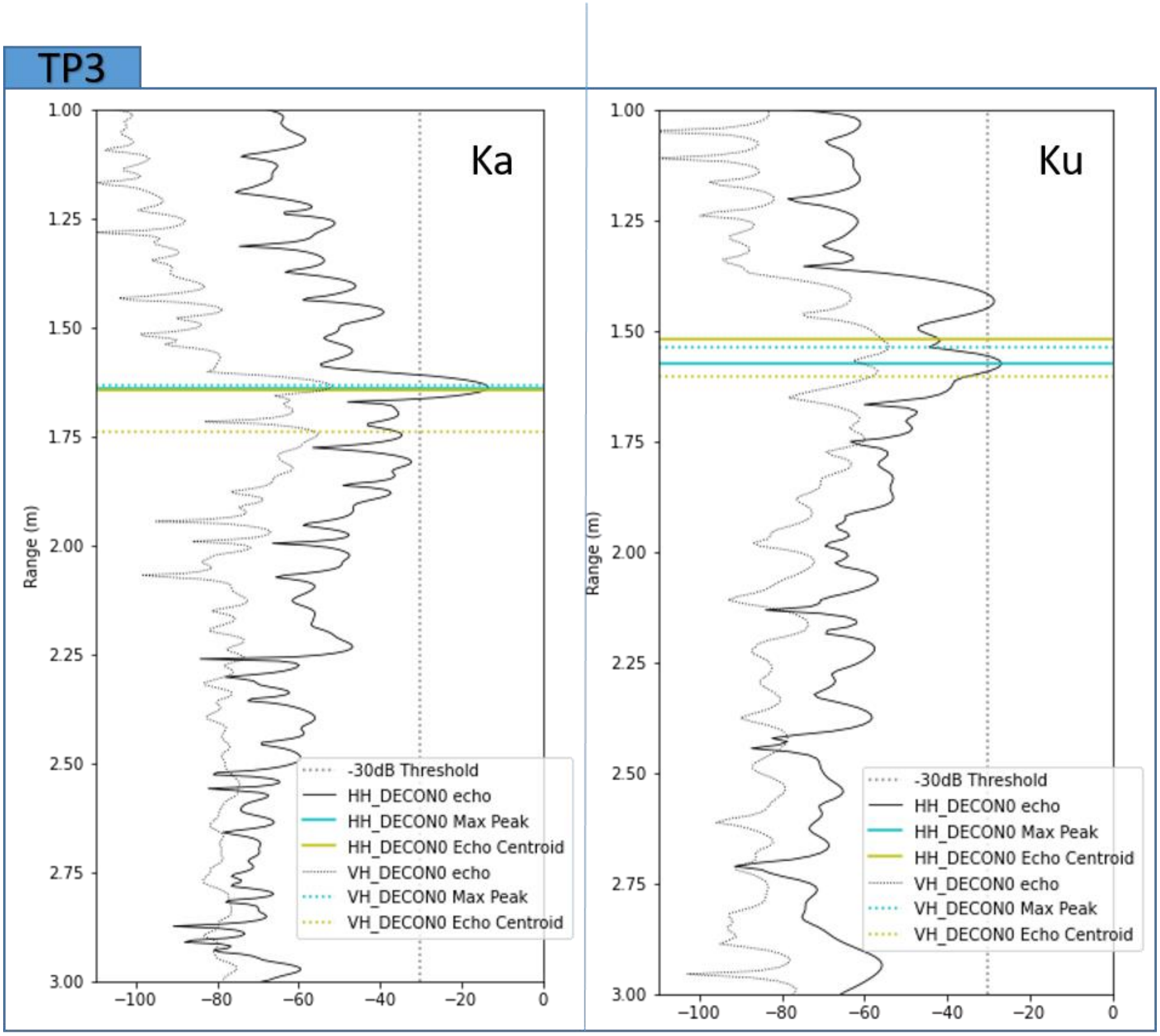

Appendix 2: Ku and Ka band HH and VH echos along with the HH and VH max peaks and echo centroids at site TP3 on December 11.

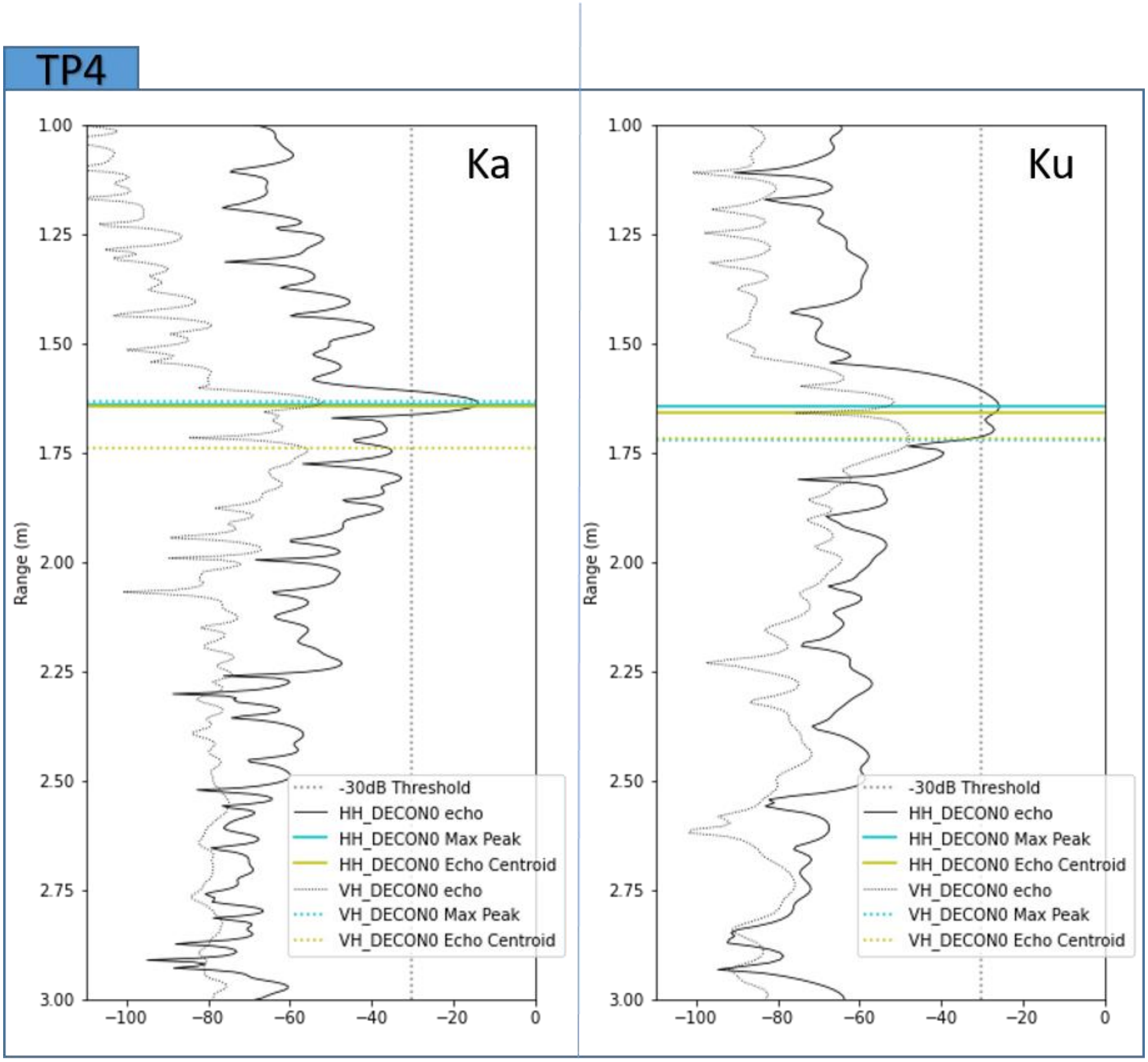

Appendix 3: Ku and Ka band HH and VH echos along with the HH and VH max peaks and echo centroids at site TP4 on December 11.

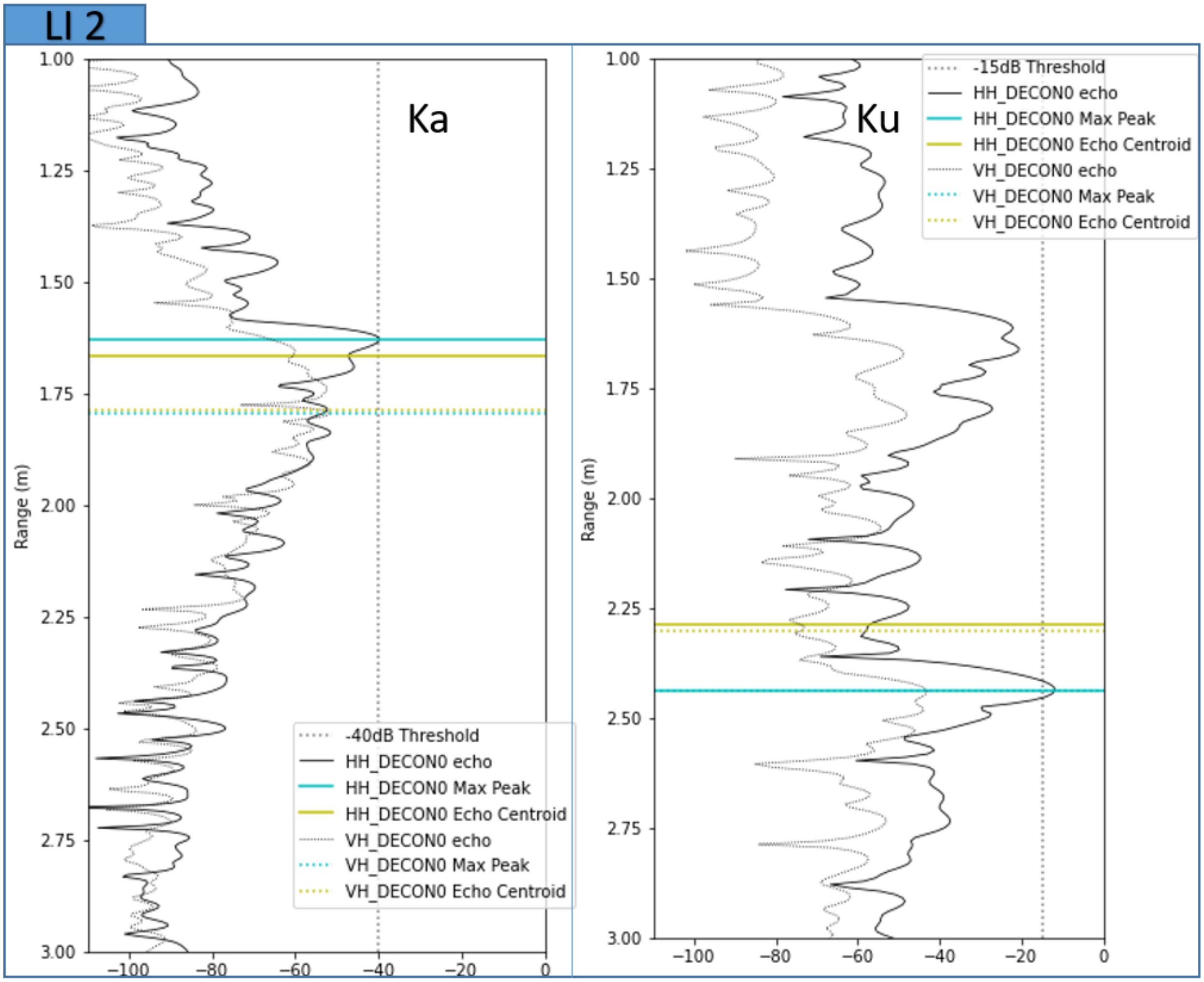

Appendix 4: Ka and Ku waveforms from the closest echo from lake ice LI2 magnaprobe location

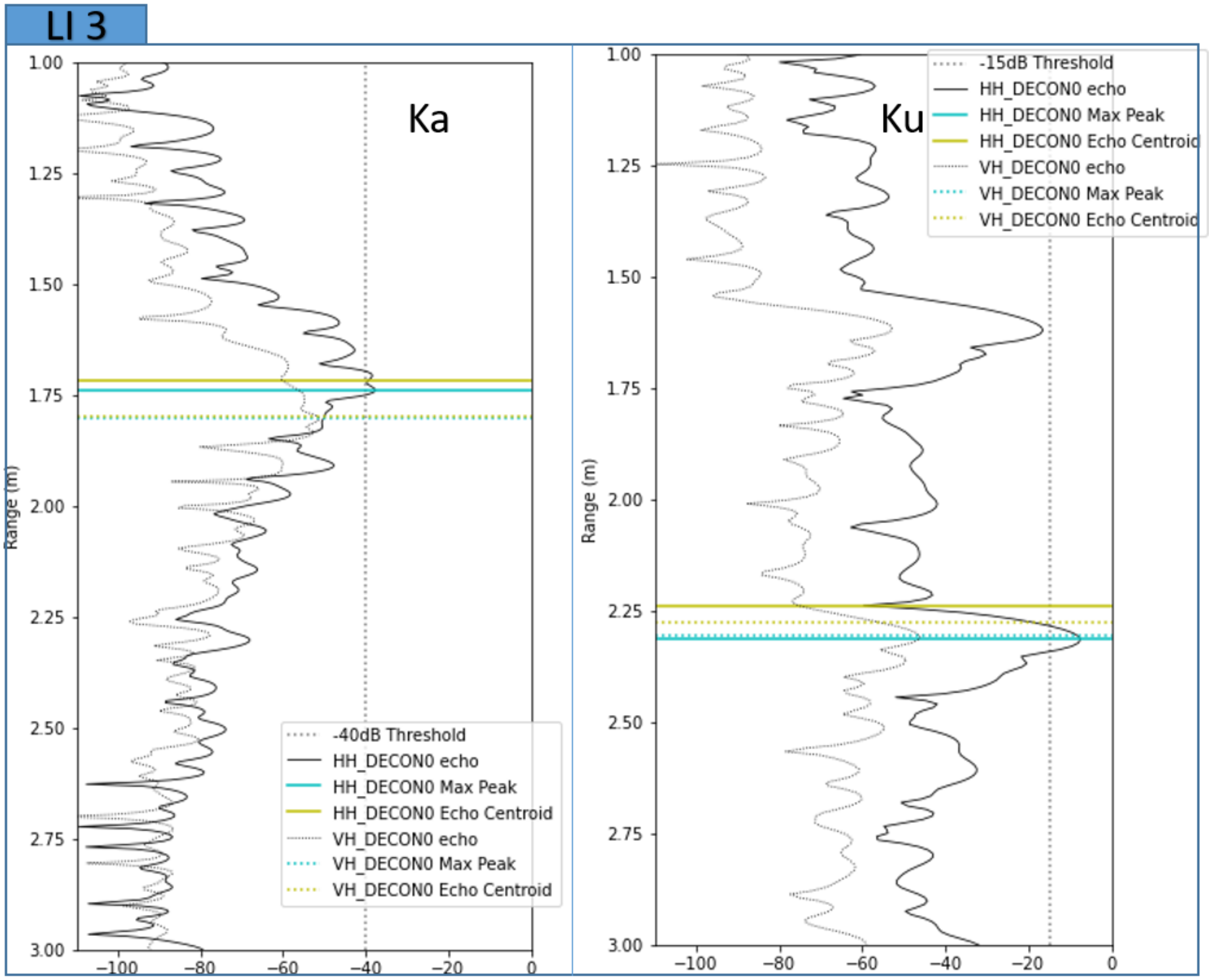

Appendix 5: Ka and Ku waveforms from the closest echo from lake ice LI3 magnaprobe location

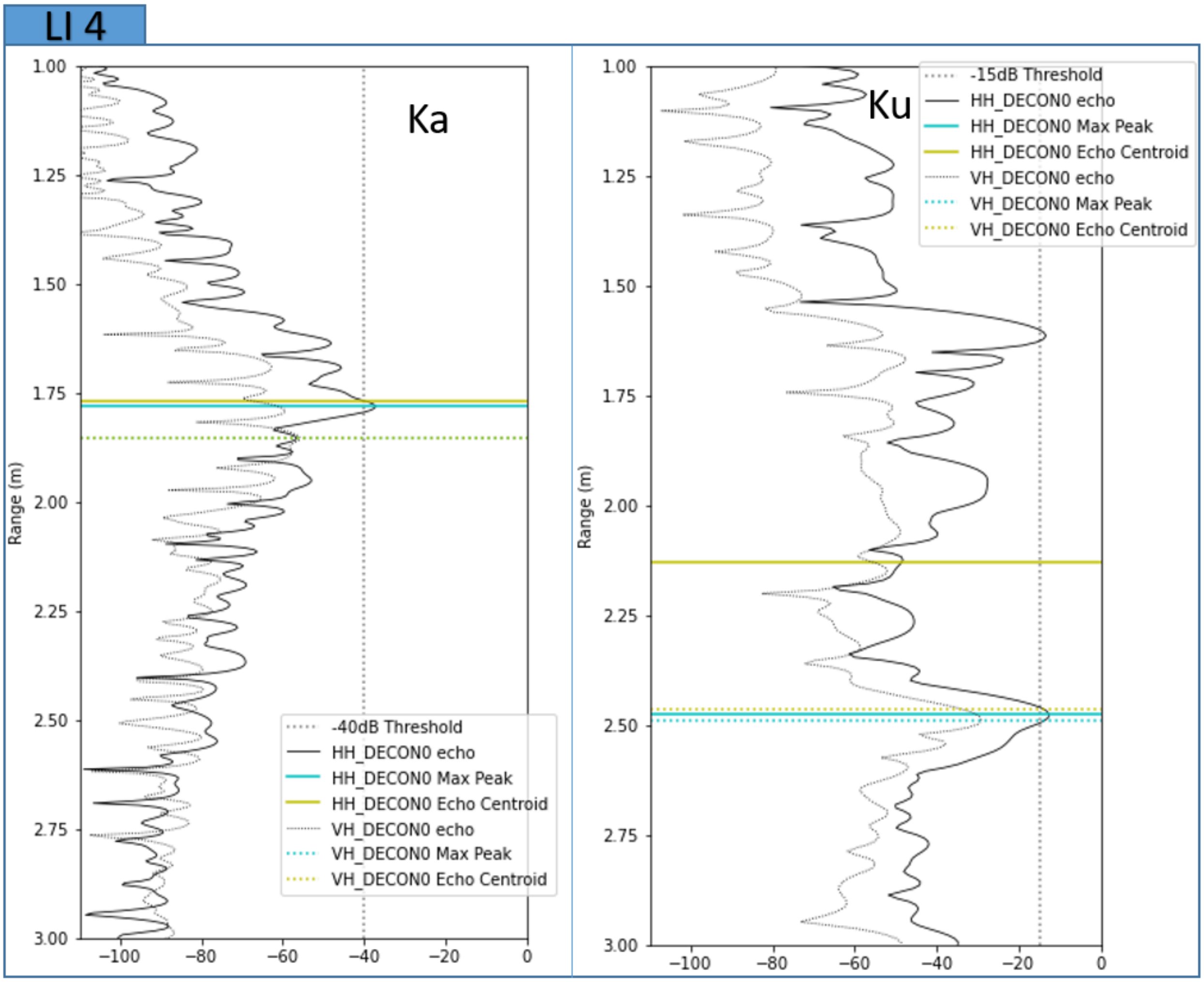

Appendix 6: Ka and Ku waveforms from the closest echo from lake ice LI4 magnaprobe location

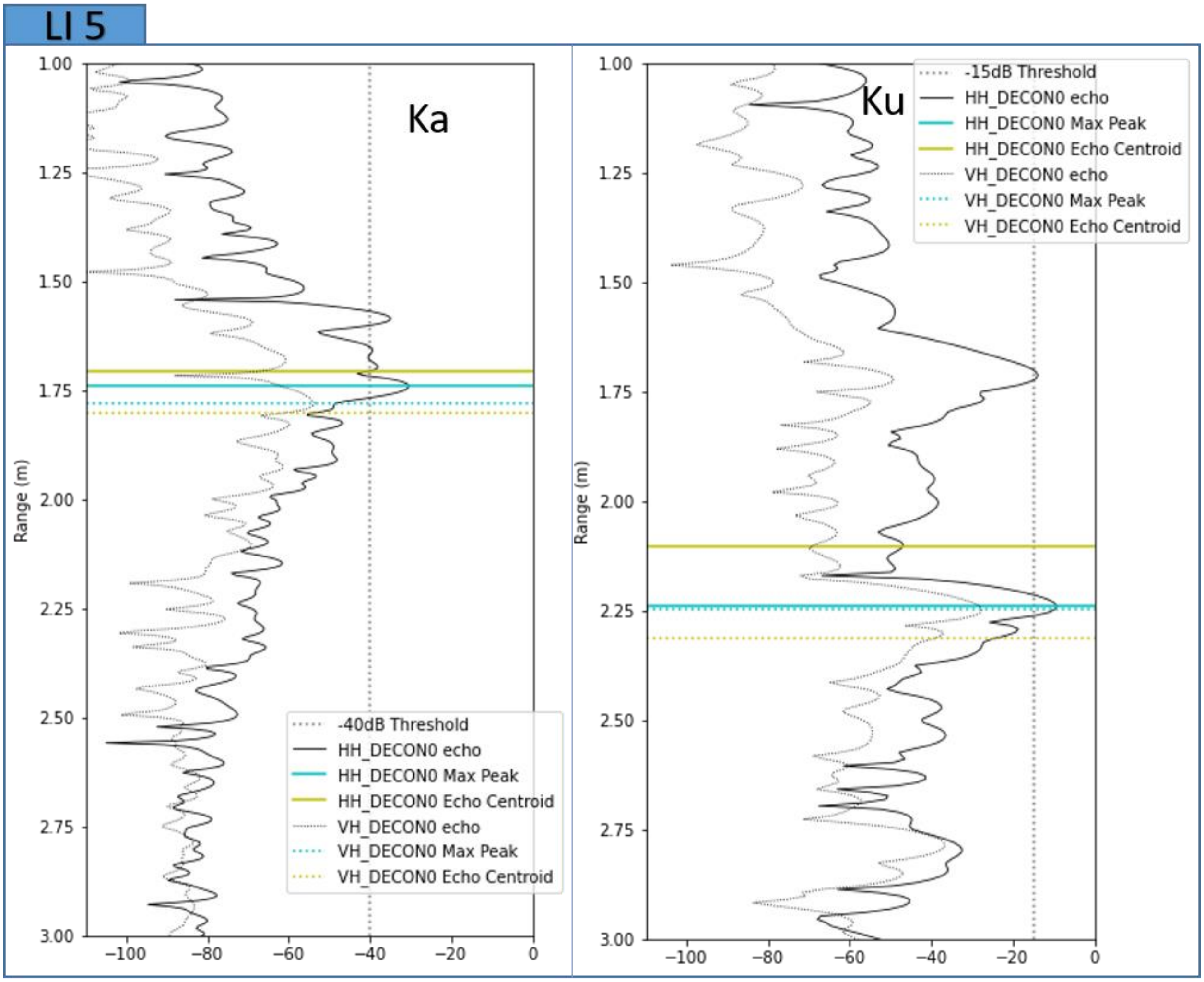

Appendix 7: Ka and Ku waveforms from the closest echo from lake ice LI5 magnaprobe location

LI 6

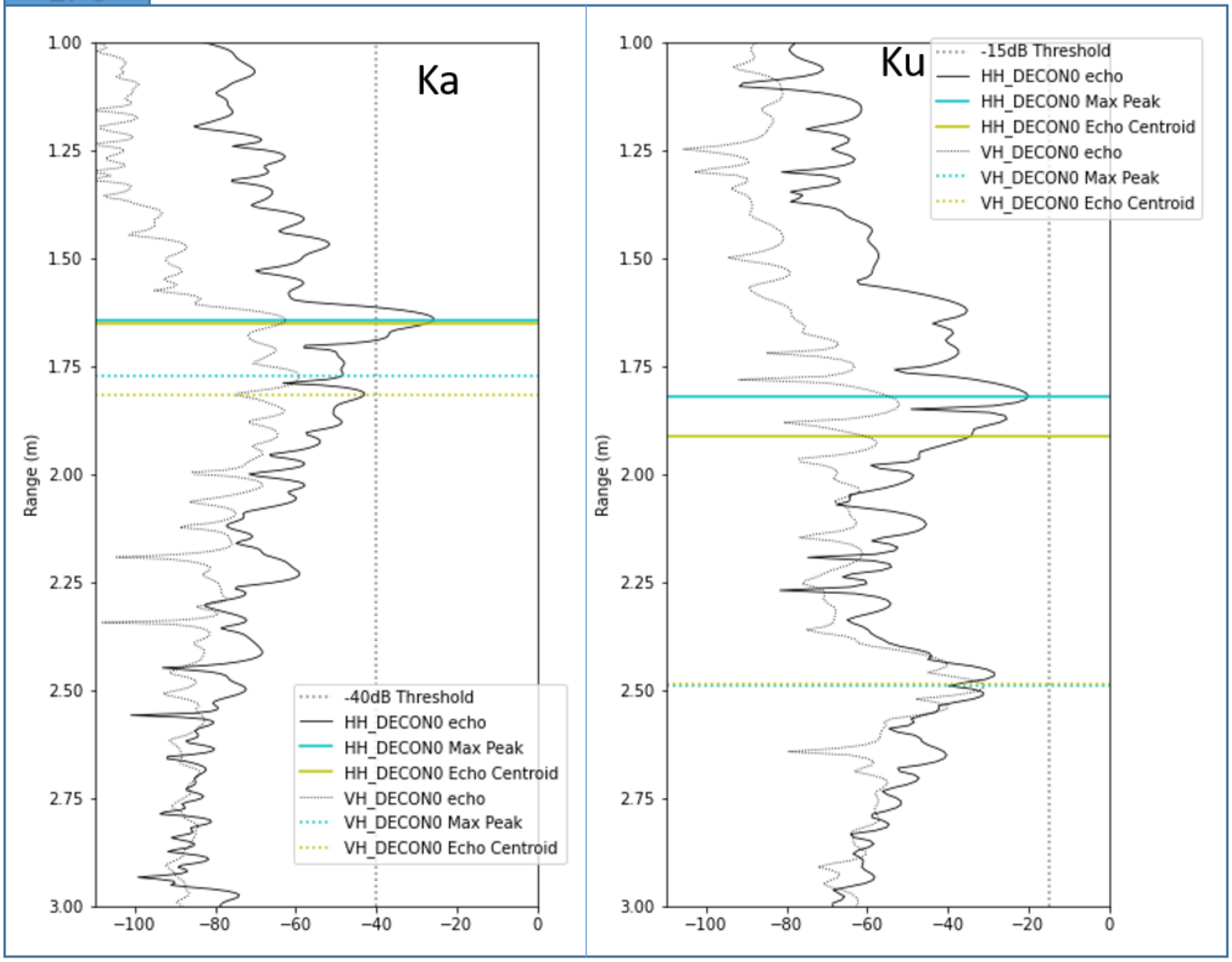

Appendix 8: Ka and Ku waveforms from the closest echo from lake ice LI6 magnaprobe location

# Chapter 4 Satellite Based Snow Depth on Sea Ice Retrievals from Cryo2Ice

The previous Chapter 3 was aimed towards improving our understanding of satellite microwave interactions with snow on sea ice from the surface level. Chapter 3 presented findings about the main-scattering horizons over snow on landfast sea ice in Churchill Manitoba over both the cross-polarized (HH) and co-polarized (VH) Ku and Ka band frequencies. We noted that the co-polarized frequencies (HH) Ku band frequencies have main-scattering horizons closer to the snow-ice interface. The control experiment with snow on lake ice corroborated that the presence of brine in the snow layer contributed to the shift of the main scattering surfaces closer to the air-snow interface for snow on sea ice. Next, we try to test these findings from a satellite level. In the following Chapter 4, frequency Ku-band microwave in Cryosat-2 is used along with coincident satellite laser (ICESat-2) to estimate snow depth on landfast sea ice.

This chapter has been submitted for publication at *The Cryosphere* as follows:

Saha,M., Stroeve,J., Isleifson,D., Yackel,J., Nandan,V., Landy,J., Lam,H.M., (2023) Snow Depth Estimation on Lead-less Landfast ice using Cryo2Ice satellite observations, *The Cryosphere* (Submitted)

## 4.1 Abstract

Observations of snow on Arctic sea ice are vitally important for sea ice thickness estimation as well as for understanding bio-physical processes and human-activities. This study is the first assessment of the potential for near-coincident ICESat-2 and Cryosat-2 (Cryo2Ice) snow depth retrievals in a lead-less region of the Canadian Arctic Archipelago. Snow depths are retrieved using the absolute difference in surface height from a near-coincident ICESat-2 and Cryosat-2 after applying an ocean tide correction between satellite passes 77 minutes apart. Both the absolute mean snow depths and snow depth distributions retrieved from Cryo2Ice compare favourably to

in-situ measurements. All four in-situ sites had snow with saline basal layers and different levels of roughness/ridging. The retrieved Cryo2Ice snow depths were underestimated by an average of 20.7 % which is slightly higher than the tidal adjustment applied. Differences in the Cryo2Ice and in-situ snow depth distributions reflected the different sampling resolutions between the sensors and the in-situ measurements, with more heavily ridged areas producing larger mean underestimation of the snow depth. Results suggest the possibility of estimating snow depth over lead-less landfast sea ice but attributing 2-3 cm biases to differences in sampling resolution, snow salinity, density, surface roughness and/or errors in altimeter's tidal corrections require further investigation.

## 4.2 Introduction

Changes in Arctic sea ice are affecting climate, ecosystems and traditional ways of living and harvesting (Meier and Stroeve, 2022). A critical component of the sea ice cover is its overlying snow cover, which has been challenging to accurately measure by satellites (Webster et al., 2018). Snow acts as an insulator, impacting both the growth and decay of sea ice (Maykut and Untersteiner, 1971). Snow also (1) limits the amount of light penetrating through the sea ice, affecting the timing of sea ice algae growth (Mundy et al., 2005); (2) contributes to the amount of freshwater discharged to the ocean, affecting its budget (Andersen et al., 2019); and (3) affects the heat exchange between the atmosphere and the sea ice (Andreas et al., 2005).

Using coincident airborne laser and radar altimeter data collected during the Laser-Radar Altimetry (LaRA) mission over sea ice around Svalbard, Leuschen et al., 2008, suggested snow depth could be retrieved by differencing freeboards, though there was a lack of in-situ ground truth to validate results. Following this, studies have differenced coincident satellite radar (CryoSat-2;

hereafter CS2) and laser (ICESat-2; hereafter IS2) altimeter freeboards to estimate pan-Arctic (e.g. Kwok and Markus, 2018; Kwok et al., 2020) and Antarctic snow depth (Kacimi and Kwok, 2020). However, significant uncertainties remain related to (1) differences in electromagnetic frequencies and spatial resolution (Fons et al., 2021), (2) whether or not the CS2 Ku-band radar returns originate from the snow/ice interface, which has been contested even for a dry and cold (below freezing) snow pack (Willatt et al., 2011; Nandan et al., 2017; de Rijke Thomas et al., 2023), (3) the influence of surface roughness over different length scales on the laser and radar waveforms (Landy et al., 2019) and (4) spatial heterogeneity of snow distributed over sea ice.

Earlier studies also faced challenges of having different orbits for CS2 and IS2, limiting the number of exact footprint crossovers (Kwok & Markus, 2018). Kwok and Markus (2018) made a case for adjusting the CS2 orbit to achieve more overlaps with IS2, thereby improving both spatial and temporal coincidence. As part of the Cryo2Ice campaign, the CS2 orbit was raised by ~ 900 meters in August 2020 to significantly increase the amount of IS2 crossovers (ESA, 2020). This realignment means that once in every 19 CS2 (20 IS2) cycles, the two ground track nearly align for a few hundred kilometres over the Arctic.

With the Cryo2Ice campaign, new opportunities are possible to improve and validate snow depths retrieved by combining laser and radar freeboards. This study provides the first high-resolution in-situ validation of snow depths retrieved along coincident Cryo2Ice tracks on the 29th of April 2022 (29-04-2022) near Cambridge Bay, Nunavut in the Canadian Arctic Archipelago (CAA). The CAA is a region with significantly different bathymetry and icescape than the Central Arctic (Galley et al., 2012). Sea ice in the CAA is landfast ice for the majority of the year (6 to 8 months) (Melling, 2002), and exhibits minimal ice drift (Galley et al., 2012). The tidal amplitudes within the shallow bathymetry of the CAA are also much larger than in the open ocean. This poses additional challenges compared to validation studies in the Central Arctic Ocean. The most prominent challenge is the lack of open water for estimating the local sea surface height (SSH) needed to reference the freeboards. Landfast ice grows along the narrow channels in the CAA and often lacks leads for several hundred kilometres (Galley et al., 2012). Therefore, assuming IS2 and CS2 are viewing the same landfast ice, the variation in SSH due to tidal variations must be known and corrected between the two sensors. Our objective is to develop an approach to combine IS2 and CS2 along-track data in regions where the local SSH estimate is not readily available from local observations.  The along-track CS2/IS2 retrieved snow depths are then validated using near-coincident in-situ snow depth observations. We further use in-situ snow property observations and satellite estimates of the surface roughness to examine the drivers of CS2 and IS2 height variability. Finally, the sources of bias in the retrieval process and major challenges are discussed.

## 4.3 Data and Methods

### 4.3.1 ICESat-2 (IS2)

The Advanced Topographic Laser Altimeter System (ATLAS) is the photon counting LiDAR system onboard ICESat-2. ATLAS emits low-energy 532 nm (green) pulses in three two-beam pairs which have a cross track spacing of 3.3 km between each pair with intra-pair spacing of 90 metres. The laser has a footprint size of 11 metres (Magruder et al., 2020). Detailed specifications can be found in Neumann et al., (2019).

In this study, the uncorrected ATL07 Sea Ice Height Release Version 6 available from the National Snow and Ice Data Centre (https://nsidc.org/data/atl07ql/versions/6#anchor-2) is used, which provides uncorrected sea ice heights computed directly from ATL03 photo heights. Sea ice heights within the 25 km land-buffer are included despite low confidence in the geophysical corrections close to land (Kwok et al., 2023). The strong beam (gt2l) from ATL07 is used based on proximity to the CS2 reference ground track and field sampling sites.

The ATL07 geophysical corrections are summarized in Appendix 1. Each correction is time-varying and has different impacts on the retrieved IS2 heights. The ocean tide corrections are provided every hour and can vary between ±62 cm which is the largest among the different geophysical corrections applied. The ocean tide corrections are obtained from the Global Ocean Tide Model 4.8 (GOT 4.8) (Kwok et al., 2021). GOT 4.8 model provides tide predictions for all regions of the globe based on the assimilation of data from satellite altimetry and tide gauge measurements into a tidal model. Since the tidal corrections originate from different models between the two sensors with varying spatio-temporal resolutions, the accuracy of these corrections varies regionally.

### 4.3.2 CryoSat-2 (CS2)

The SAR Interferometric Radar Altimeter (SIRAL) is the primary instrument on board CryoSat-2, which is a combination of a pulse-limited radar altimeter along with a Synthetic Aperture Radar (SAR) Interferometer system (SARIn). SIRAL operates at Ku-band (13.575 GHz) and in three different modes with along-track sampling resolution of around 300 m and across- track resolution of 1600 m (ESA, 2013). Cryosat-2 operated in the SARIn mode in the CAA during the study period. Here we use the CS2 Level 2 Baseline E products available through the European Space Agency's EO-CAT web explorer (https://eocat.esa.int/). The CS2 Level 2 sea ice heights are re-tracked using the University College London (UCL) retracker (Tilling et al., 2018) which assumes a threshold on the first peak for diffuse echoes representing the mean elevation of the snow/sea ice interface within the footprint.

Tidal corrections (ocean, long-period equilibrium, ocean loading, solid earth and geocentric polar) are included in the Level 2 Baseline E Cryosat-2 SAR/SARIn product (Appendix 2). The ocean tide, long-period equilibrium tide and ocean loading tide corrections used are retrieved from the Finite Element Solution 2004 Ocean Tide Model (FES 2004) (Cryosat-2 Product Handbook). The ocean tide corrections typically range from ± 50 cm.

### 4.3.3 Field Measurements

The study site comprised a 75 km long NNE-to-SSW transect across Dease Strait (69°26'58.02"N 106°41'57.25"W to 68°46'42.48"N 106°55'52.10"W) (Figure 28), ~70 km west of Cambridge Bay, NU. This region connects Coronation Gulf and Queen Maud Gulf of the Kitikmeot Sea and is a part of the southern route of the Northwest Passage (Xu et al., 2021). Dease Strait is relatively shallow (maximum depth ~ 100 metres), and its narrow channel is covered by landfast ice normally between November and mid-July (Galley et al., 2012). CS2 and IS2 coincident tracks were identified using the CS2 and IS2 Coincident Data Explorer (https://cs2eo.org/) (Ewart et al., 2022). The tracks were ~1.5 km apart and passing by within 77 minutes of each other (Figure 29).

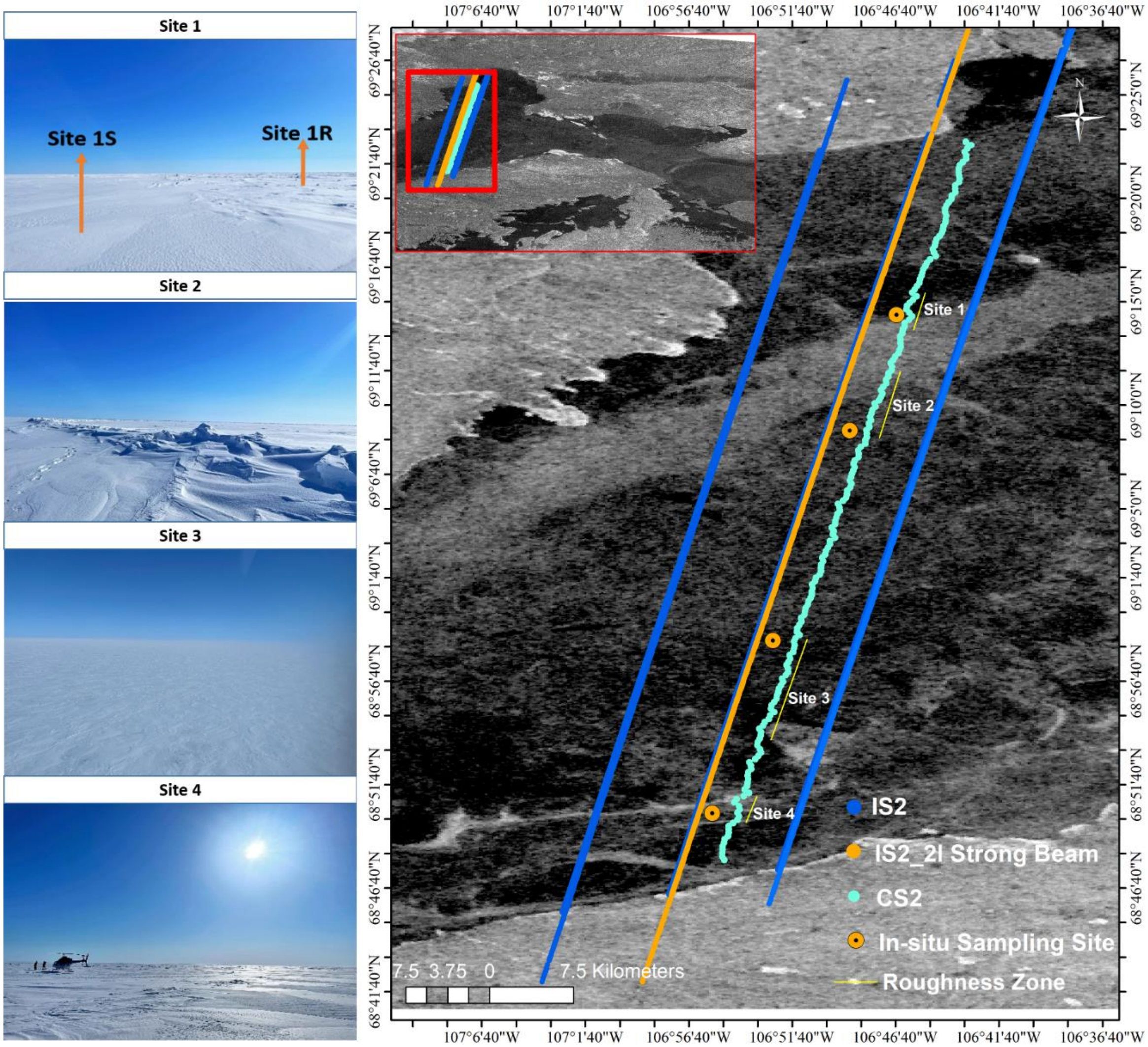

Figure 27 Map shows the Cryosat-2 Points of Closest Approach (POCA) locations, IS2 2l Strong Beam and other IS2 beam, in-situ sampling locations and identified roughness zones. The background contains Sentinel-1 HH-pol SAR imagery. Site photos show the variation in snow roughness.

In-situ snow depths were collected at four different sites (Sites 1-4) ranging from smooth, rough and mixed sea ice roughness zones. Based on Sentinel-1 SAR and field reconnaissance, Site 1 was classified as a rough and smooth sea ice transition zone; Site 2 was a thin snow zone with significant ridging; Site 3 was a smooth sea ice zone with extensive areas of thin snow; and Site 4 was a rough sea ice site with extensive areas of thick snow.  All sites were located equidistant between the IS2 strong beam and CS2 track to ensure the highest likelihood that snow depth sampling was representative of both sensors. The snow depth sampling direction was determined according to distinctive roughness features at individual sites, ensuring sufficient sampling distance in both the along- and across-track directions, representative of the prevailing east-southeast wind direction (ECCC, 2022) and snow dune pattern (Moon et al., 2019). Snow depth was surveyed using Snow-Hydro's automated snow depth magnaprobe, which has an accuracy of ±0.3 cm on level sea ice and snow (Strum and Holmgren, 2018). The magnaprobe was reassembled and re-calibrated before each sampling effort to avoid instrument bias. Sampling was conducted by a single person to avoid variations in instrument handling and to maintain constant intervals between samples.

All four sites were surveyed on 01-05-2022 within 48 hours of the ICESat-2 and Cryosat-2 pass on 29-04-2022. The sites were accessed via helicopter and no sampling was conducted within 200 metres of the helicopter landing zone to avoid snow redistribution during landing. The sampling interval was set at 5 m intervals to ensure spatial heterogeneity and avoid spatial autocorrelation of the sampled snow depth values following (Iacozza and Barber, 1999). There was no precipitation recorded during the sampling period, nor during the time interval between the CS2 and IS2 overpasses. Furthermore, high pressure dominated the region between 26-04-2022 and 04-05-2022 causing light surface winds. As such, snow redistribution between CS2 and IS2 overpasses and in-situ sampling was negligible. The air temperature varied between -11.7°C and -14.1°C during the sampling as measured at the Cambridge Bay, land-based meteorological station. Snow geophysical properties including snow salinity and density were sampled from all four sites. Snow temperature was not measured because the temperature probe would not calibrate quickly enough between the short helicopter landing durations. For Site 1, two pits were sampled, one for the rough sea ice (Site 1a) and one for the relatively smooth sea ice zone (Site 1b). Single pits were excavated at the other three sites. Snow density was measured using a 66 $cm^3$ (2 × 5.5 × 6 cm) density cutter at 2 cm intervals and weighed in the lab. Weighed samples were then melted at room temperature for snow salinity measurement using a Cole-Parmer C100 Conductivity Meter (accuracy of ± 0.5%). Sea ice thickness and freeboard at each site was measured using a freeboard tape to an accuracy of 0.5 cm.

### 4.3.4 Estimating Snow Depth from Cryosat-2 and ICESat-2

Kwok et al (2020) calculates snow depth (SD) as the difference between IS2-derived total freeboard (snow + ice) and CS2-derived sea ice freeboard (CS2), using the difference between the surface height and the instantaneous sea surface height interpolated from sea surface measurements from along-track leads to obtain the freeboards (Kwok et al., 2020; Ricker et al., 2014). However, reliable freeboard measurements from IS2 and CS2 are dependent on accurate estimation of the sea surface height which is dependent on the availability of leads within a reasonable distance (10's of km) along both the IS2 and CS2 track. No leads were detected along the portion of the IS2 and CS2 tracks in the study area and therefore the sea surface height could not be estimated. Therefore, we modified the approach used in Kwok et al., (2020). We used the absolute sea ice heights measured from IS2 ATL07 (hIS2) and CS2 (hCS2) referenced to the WGS84 ellipsoid to estimate SD (Figure 29). SD can be calculated as the freeboard differences under the assumption that Ku-band penetrates to the snow/ice interface according to Equation (viiii). Where ηs is the refractive index of Ku-band microwaves which compensates for the propagation delay through the snow pack (Kwok et al., 2020). The refractive index is calculated using (ηs=(1+0.51ρs)1.5 (Ulaby et al., 1986), where the in-situ bulk snow density (ρs) measured from the field is used. The average snow density from all four sites is used to compute snow depth for the entire track (Figure 35) while snow densities from each site are used to compute SD from corresponding portions of the Cryo2Ice track (Figure 37).

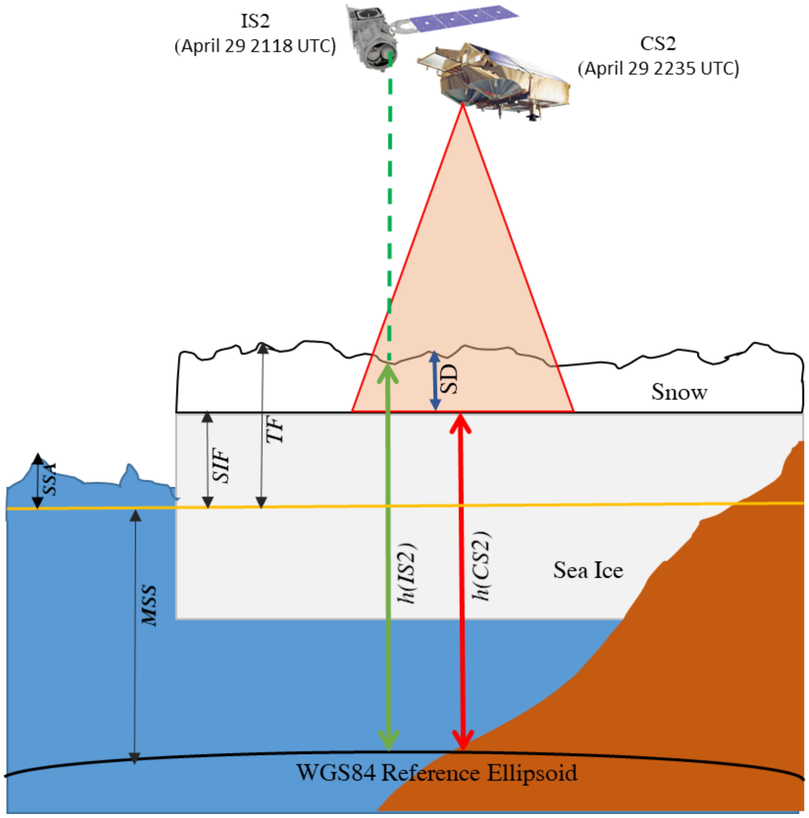

Figure 28 Schematic showing the calculation of snow depth (SD) from ICESat-2 and Cryosat-2 over sea ice. The diagram illustrates the representative heights for the sea surface anomaly (SSA), mean sea surface (MSS) in yellow, sea ice freeboard (SIF) and total freeboard (TF). SD is shown with the blue arrow, IS2 surface height (*hIS2*) is shown with the green arrow and CS2 surface height (*hCS2*) is represented by the red arrow. Land is orange.

### 4.3.5 Data Processing

The uncorrected IS2 ATL07 heights (*h (IS2))* are referenced to the WGS84 ellipsoid which is also consistent with the CS2 heights (Figure 29). The following geophysical corrections contained within the IS2 ATL07 product are applied to the ATL07 sea ice heights: ocean tide correction, long-period equilibrium tide and inverted barometer correction. However, the mean sea surface (MSS) is not added for reasons explained in Section 2.6. The same geophysical corrections included within the CS2 product are applied to the CS2 L2 sea ice heights. However, there is limited confidence in these individual geophysical corrections closer to land. Moreover, the tides varied over a range of ~ 6.0 cm in Dease Strait in between the two passes, so it was crucial to check if the tidal corrections contained within the products accurately accounted for tide differences in the ~77 minutes between passes. Therefore, after comparing the geophysical correction as explained in Section 2.6, an ocean tide correction factor is derived to account for the variation in SSH between the IS2 and CS2 acquisitions.

Both CS2 and IS2 have significantly different footprints (Section 2.1 and 2.2) and therefore the IS2 ATL07 geolocated heights need to be averaged to be spatially congruent with the CS2 footprint. IS2 photons are averaged over 300 m length segments to match the along-track CS2 footprint. Snow depths computed from the IS2 and CS2 height differences were estimated following Equation (1), and subsequently adjusted with the ocean tidal correction. To identify the extent of spatial heterogeneity in the retrieved snow depths from Cryo2Ice, the Moran's I test is performed to test the level of spatial autocorrelation. The semi variogram analysis of the in-situ snow distribution shows that the snow depth values are correlated within a lag distance of ~1 kilometre. Therefore, to compare snow distributions representative of each sampled field site (S1 to S4), snow depth is compared over similar roughness zones. Roughness zones corresponding to each Site are defined as a portion of the CS2/IS2 track which had IS2 surface roughness (Section 2.6) within one standard deviation of the IS2 derived surface roughness directly adjacent to the in-situ sampling site (Figure 29). The Cryo2Ice-derived snow depth corresponding to each roughness site was then compared against the in-situ snow distribution from the sampling sites.

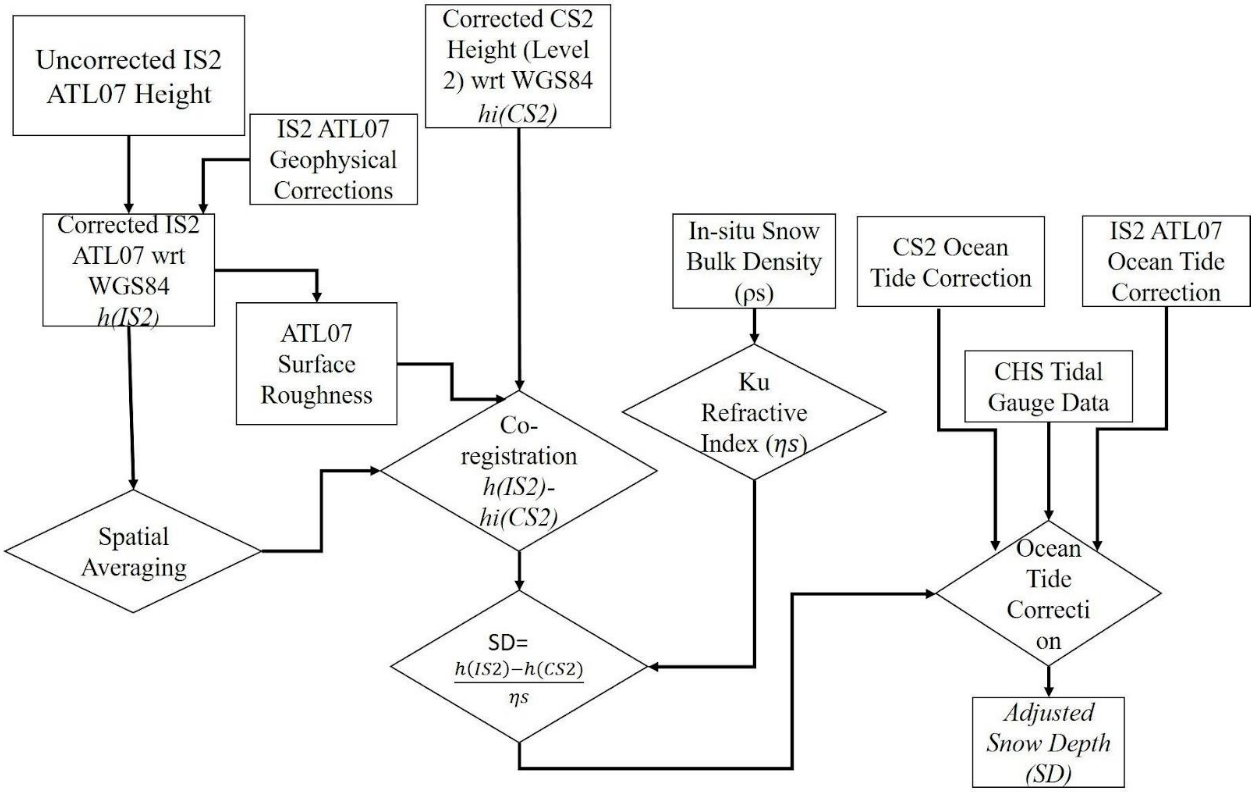

Figure 29 Methodological workflow for retrieving snow depth (SD) from CS2/IS2 co-registered averaged ATL07 (*h (IS2))* and Cryosat-2 heights (*h(CS2))* are subtracted following Equation 1. The differenced product is located at the Point of Closest Approach (POCA) of each CS2 footprint. The differenced product is then adjusted with the refractive index (ηs).

### 4.3.6 Adjusting for Sea Surface Height Variation

Assuming IS2 and CS2 are viewing the same landfast ice, any variation in sea surface height over the short 77 minute interval is assumed to be due to tidal variations. The long-period equilibrium tide and ocean-tide with the inverted barometer corrections were compared between the sensors to identify the difference between them. The ocean tide correction, which typically removes the impacts of local tides, had the most significant impact on the height retrievals (Appendix 3 See

Figure S1 in Bagnardi et al., 2021)), with values ranging between +/-50 cm in CS2 and +/-62 cm in IS2 (Kwok et al, 2021, Cryosat-2 Product Handbook). Ideally, the ocean tide correction applied to IS2 and CS2 should account for the variation in SSH due to local tides between passes. Although sea ice has been identified to significantly impact seasonal tidal dampening (Rotermund et al., 2021) it is considered negligible given the short time duration between the passes. Here we compare the average ocean tide corrections to local tidal gauge predictions from the Canadian Hydrographic Service (CHS) (https://tides.gc.ca) which are based on real-time and historical tidal gauge measurements from the Cambridge Bay station. The CHS dataset provides instantaneous tidal variations at the CB station every 15 minutes with six observations between the IS2 and CS2 passes. The difference in ocean tidal corrections between the IS2 and CS2 pass was 7.9 cm on average along the track whereas the difference in water level was 6.0 cm according to the CHS data. The difference in height between IS2 and CS2 was therefore adjusted by a single value of 1.9 cm before the snow depths were computed (Figure 30) and this value then represents a systematic uncertainty on the final snow depth estimates.

### 4.3.7 Evaluating Other Sources of Uncertainties

One of the critical assumptions is that IS2 and CS2 tracks are roughly coincident i.e. both tracks are measuring roughly the same snow despite their reference ground tracks being ~1.5 km apart. In order to test this assumption Sentinel-1 backscatter (which roughly indicates the snow distribution; Cafarella et al., 2019) was measured across both the IS2 and CS2 reference ground tracks. The SAR pixels intersecting with the IS2 and CS2 track were used to calculate the mean backscatter. The mean difference in backscatter (-0.3 dB) between IS2 (-17.82 dB) and CS2 (-18.11 dB) was less than 1 standard deviation of the backscatter of each track (Figure 31). Since both the tracks have similar backscatter, the assumption that they are coincident and observing snow packs with the same distribution is likely valid.

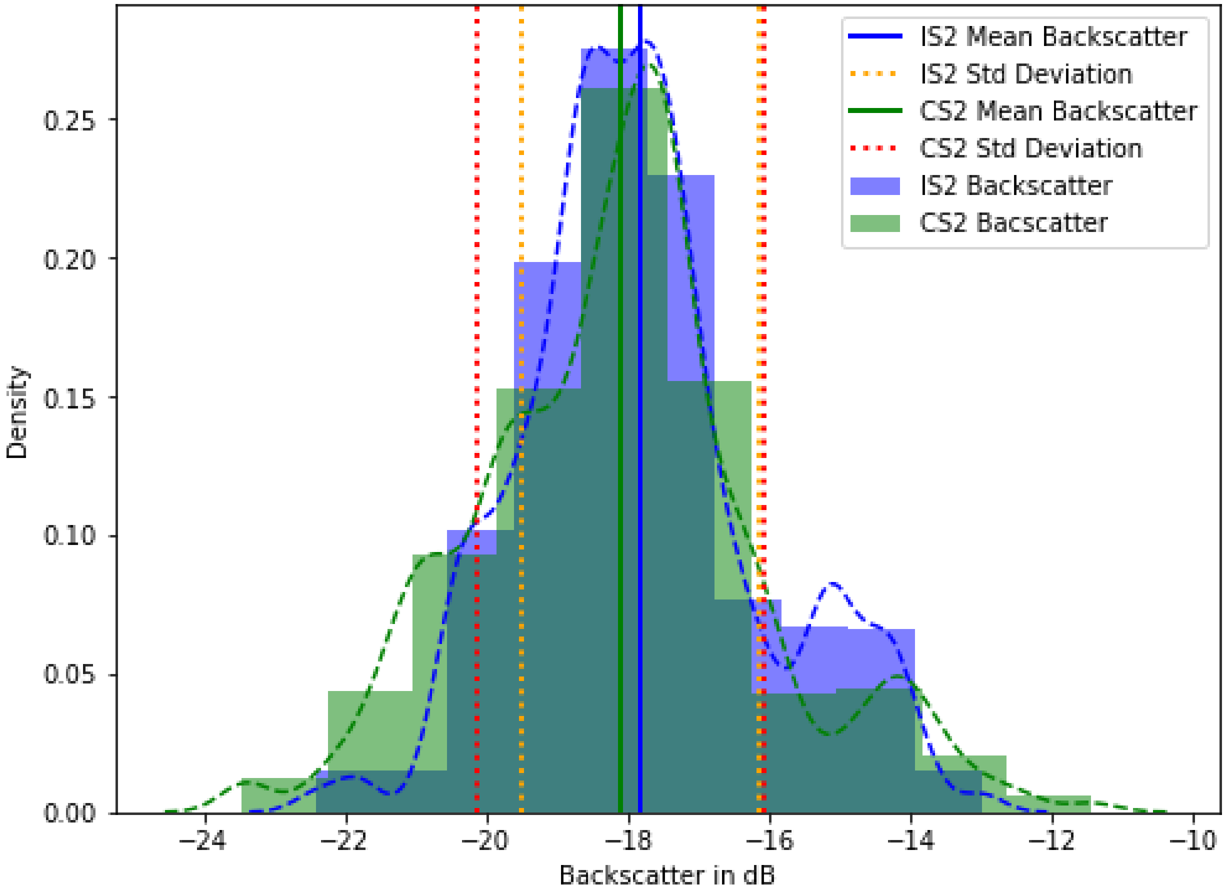

Figure 30 Sentinel-1 Backscatter in dB obtained from the IS2 and CS2 track locations. The Sentinel-1 VH backscatter from 05-05-2022 is used for extracting backscatter along both the tracks in order to assess whether the observed snow distribution is similar.

Landy et al (2019, 2020) demonstrated the importance of considering surface roughness in the radar data processing. Sea ice surface roughness was computed across the IS2 track using the ATL07 sea ice height product. Following Farrell et al (2020), surface roughness was calculated as the standard deviation of ATL07 sea ice height product calculated over 300-metre length segments to maintain consistency with the spatially averaged ATL07 heights.

Previous studies measured or modelled the dominant scattering surface over first-year sea ice

(FYI) at Ku-band several to many centimetres above the snow/sea ice interface even for cold snowpacks. Nandan et al. (2017, 2020) argue that when brine is present within the snowpack, the dominant scattering horizon at Ku-band is shifted by approximately 7 cm above the snow/sea ice interface. Mallett et al., (2020) further demonstrated that the use of fixed snow densities introduced significant biases in the snow depth retrievals. Provided snow salinity impacts the location of the Ku-band dominant scattering horizon (Nandan et al., 2017), an assessment was conducted to test the bias introduced by choosing different snow bulk densities (a) assuming Ku- band microwaves penetrate completely through the snow layers to the sea ice surface and (b) Ku-band microwaves penetrates through layers with snow salinity less than 1 ppt. The corresponding average in-situ snow bulk densities from (a) the complete snow layer (b) snow layers with less than salinity of 1 ppt were used to compute refractive indices followed by respective snow depth calculations. There was negligible difference in the refractive index (<0.05) considering the snow bulk densities with difference in salinity and therefore the average bulk densities from the complete snow pack was used in this study.

## 4.4 Results

### 4.4.1 In-Situ Snow Depths and Distributions

In-situ snow depths demonstrate significant spatial variability among the four sampled sites (Figure 32). The mean snow depth from the four different sites varies between 9 and 17 cm, and all sites have positively skewed distributions (Figure 32). Site 2 also has some exceptionally high snow depths (> 90 cm), corresponding to the ridged areas (Figure 32) and therefore show higher standard deviations (Figure 32). Sites 2 and 3 have similar snow distributions (Figure 32) but the presence of ridging in Site 2 results in a wider tail compared to Site 3. Site 4 has the highest mean snow depth (Figure 32) as well as the thickest tailed snow distribution (Figure 32).

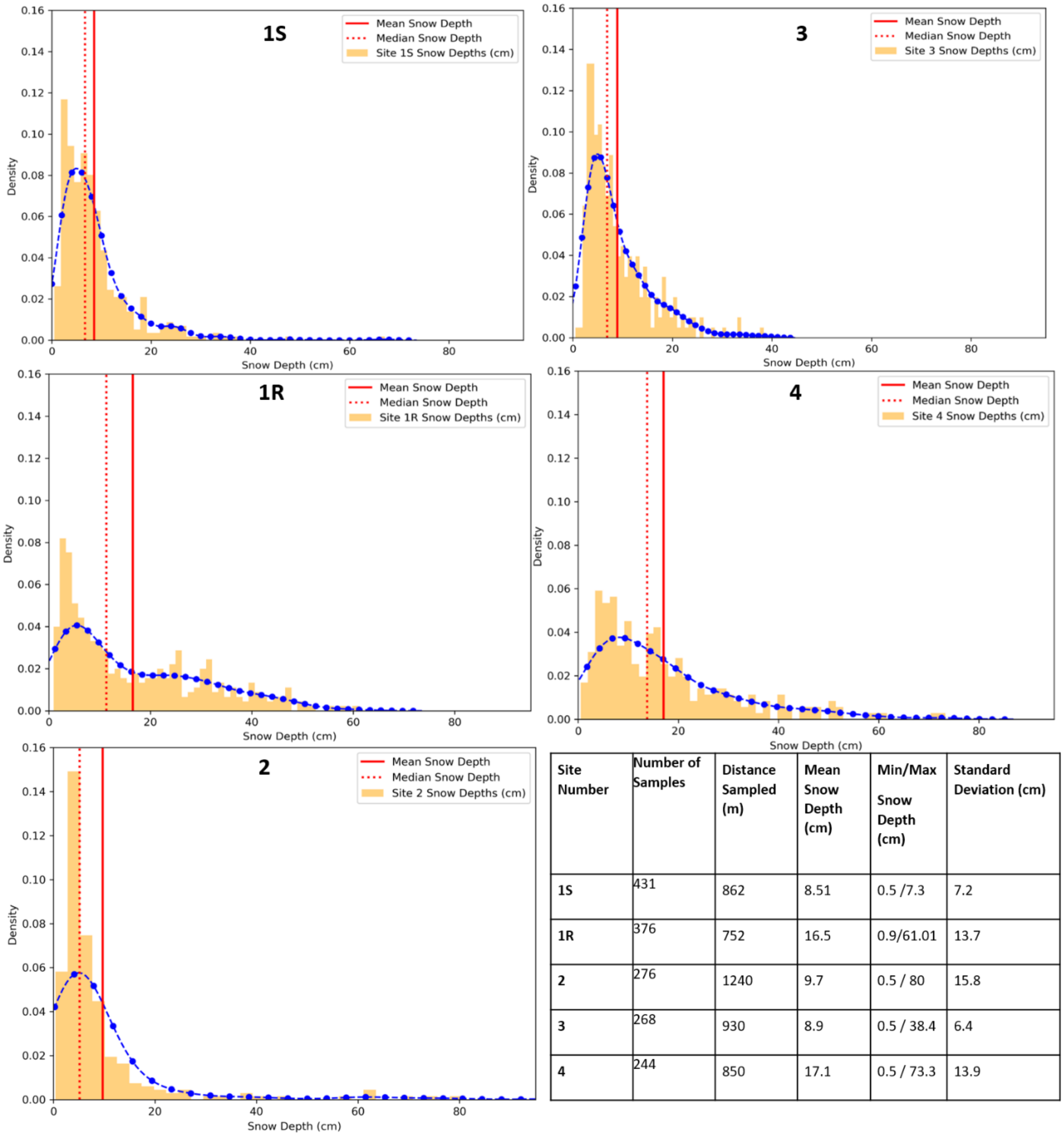

| Site Number | Number of Samples | Distance Sampled (m) | Mean Snow Depth (cm) | Min/Max Snow Depth (cm) | Standard Deviation (cm) |
|---|---|---|---|---|---|
| 1S | 431 | 862 | 8.51 | 0.5 /7.3 | 7.2 |
| 1R | 376 | 752 | 16.5 | 0.9/61.01 | 13.7 |
| 2 | 276 | 1240 | 9.7 | 0.5 / 80 | 15.8 |
| 3 | 268 | 930 | 8.9 | 0.5 / 38.4 | 6.4 |
| 4 | 244 | 850 | 17.1 | 0.5 / 73.3 | 13.9 |

Figure 31 Snow depth distributions from the four in-situ field measurement sites along the Cryo2Ice transect. The table presents descriptive statistics for the snow depth measurements.

### 4.4.2 Snow Geophysical Parameters

Mean snow salinity varies between 1.5 to 3.0 ppt for Sites 1S, 2, 3 and 4, whereas at Site 1S the snow salinity is 6.78 ppt (Figure 33). The mean snow bulk density varies between 0.358 and 0.374

g/cm$^3$ in all sites except Site 3 where the mean snow density is 0.248 g/cm$^3$.

Vertical profiles of snow salinity and bulk density present further insights. As shown in Figure 34, the snow density patterns are similar for Sites 1R, 1S, 2 and 4 with bulk density ranging between 0.260 to 0.420 g/cm$^3$ and lower at the base of the snowpack than the surface (Figure 33). The snow density varies in the different snow layers but there is a general trend towards higher densities at 4 to 7 cm above the snow-ice interface at all sites (Figure 33). This is attributed to the presence of a wind slab snow layer most prominent at Sites 1R, 2 and 4.

Snow salinity shows higher salinities closer to the snow-ice interface but decreasing with height up the interface (Figure 33 (a)). For snow pits greater than 7.5 cm thick, the salinity is less than 1 ppt closer to the air-snow interface. There is a spike in salinity between 5 to 3 cm from the snow-ice interface at Site 3 that corresponds to the high bulk density snow layer (Figure 33(b)).

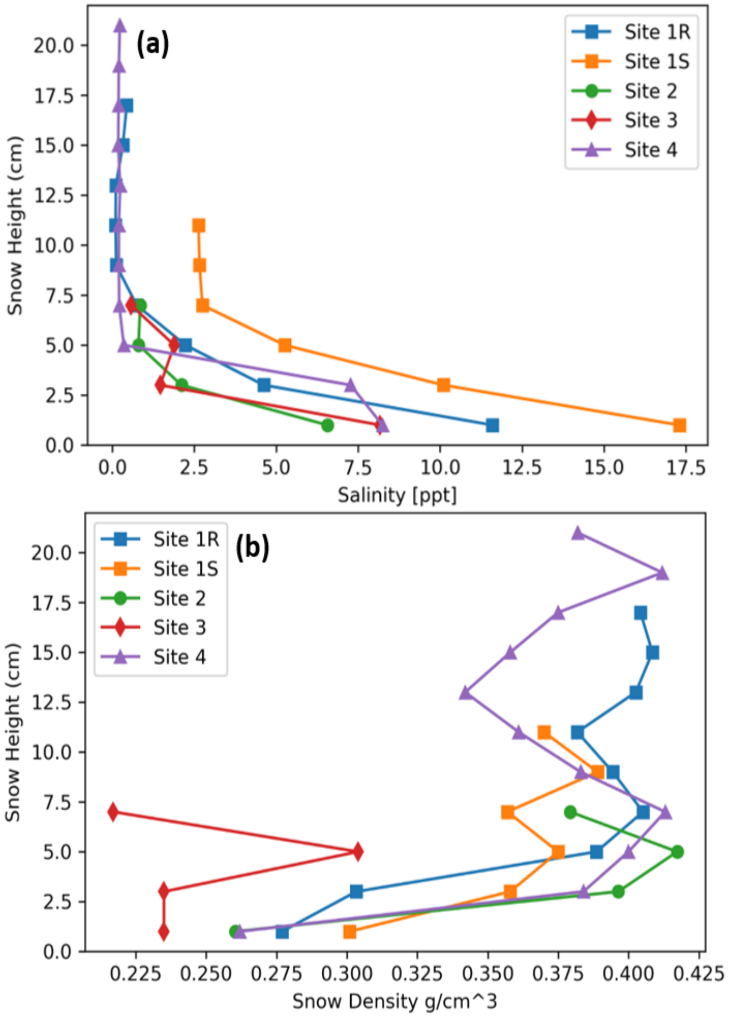

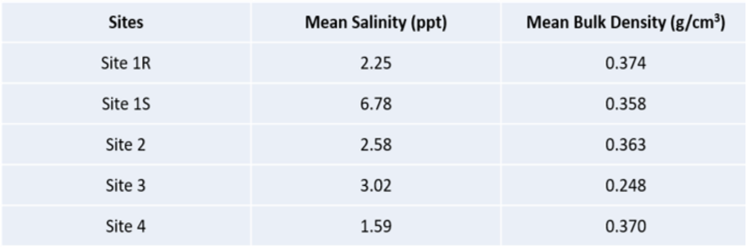

| Sites | Mean Salinity (ppt) | Mean Bulk Density (g/cm$^3$) |
|---|---|---|
| Site 1R | 2.25 | 0.374 |
| Site 1S | 6.78 | 0.358 |
| Site 2 | 2.58 | 0.363 |
| Site 3 | 3.02 | 0.248 |
| Site 4 | 1.59 | 0.370 |

Figure 32 (a) Snow salinity and (b) Snow density change by snow pack depth at the four snow sampling sites. Zero snow depth in both plots represents the snow-ice interface. The bottom table shows the variation in mean salinity and bulk density among the different sites.

### 4.4.3 ICESat-2/Cryosat-2 Derived Snow Depths

The CS2 (*h(CS2)* and IS2 (*h(IS2)*) heights show a general pattern of lower CS2 heights in comparison to co-registered IS2 heights (Figure 34). The *h(IS2)-h(CS2)* differences range between -26.5 cm and 50.0 cm with a mean difference of 7.9 cm. 20% of the calculated differences are negative, with most of them being located closer to the coast i.e., closer to Sites 1 and 4 (Figure 34). The portions of the tracks having negative differences are excluded from the subsequent calculation of snow depths. The adjusted mean snow depth across the whole Cryo2Ice track is 10.4 cm, marginally lower than the in-situ mean snow depth of 11.9 cm (Figure 33). Snow depths shown in Figure 37(b) display a right-skewed distribution with a sharper and heavier tail compared to a normal distribution. This is consistent with the distributions obtained from the in-situ snow sites (Figure 36). A maximum snow depth of 48.1 cm is retrieved from Cryo2Ice, at a length scale of 300 m.

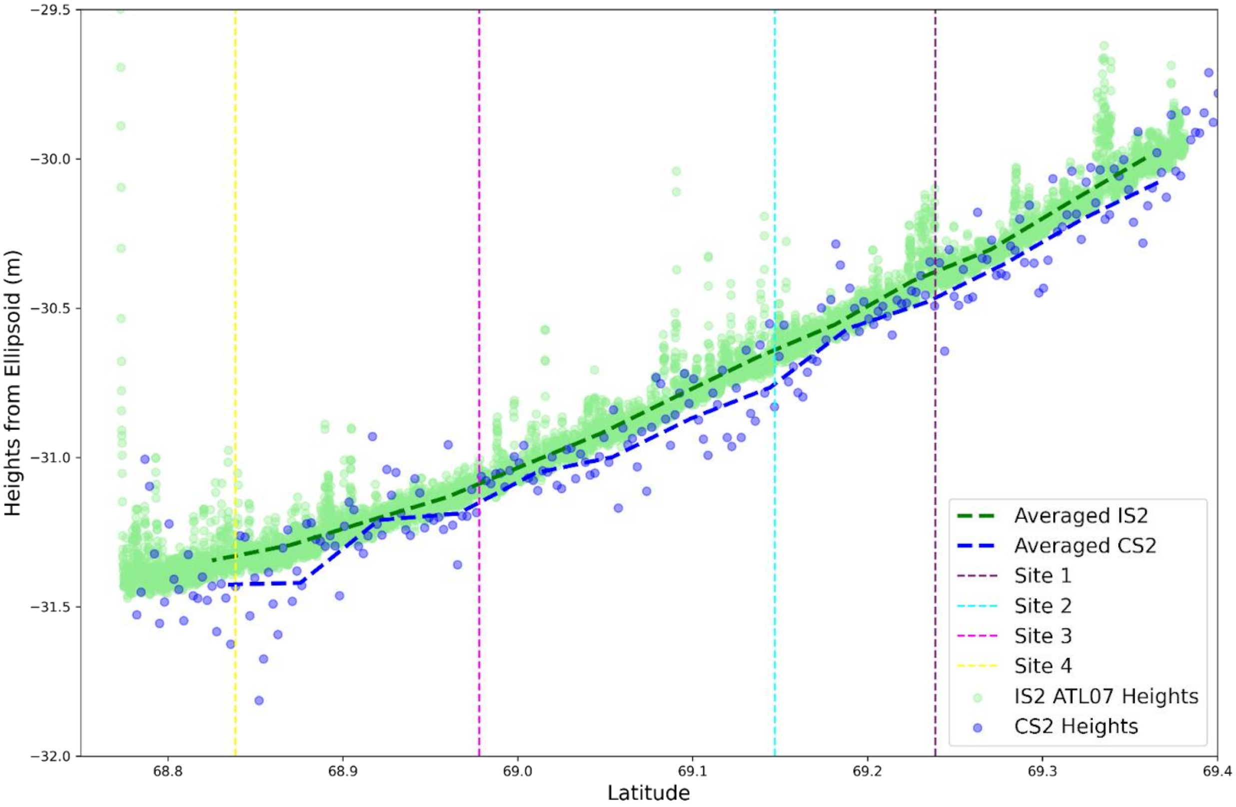

Figure 33 IS2 ATL07 sea ice heights plotted along with CS2 surface heights. Note, the reported heights are relative heights and can be negative because of the WGS84 ellipsoid reference heights

in the study area. The green and blue dashed lines indicate averaged heights over 5 km along-track distances.

The semivariogram analysis indicates that there is spatial autocorrelation among measured snow depths within ~1 km but there is no significant autocorrelation for larger distances, along this specific track . This also implies that there is significant spatial heterogeneity above the km-scale along the ~65 km track (Figure 35). The snow depths are correlated at scales under ~1 km which correspond with the lengths of the representative portions of the track delineated with similar roughness (Figure 35).

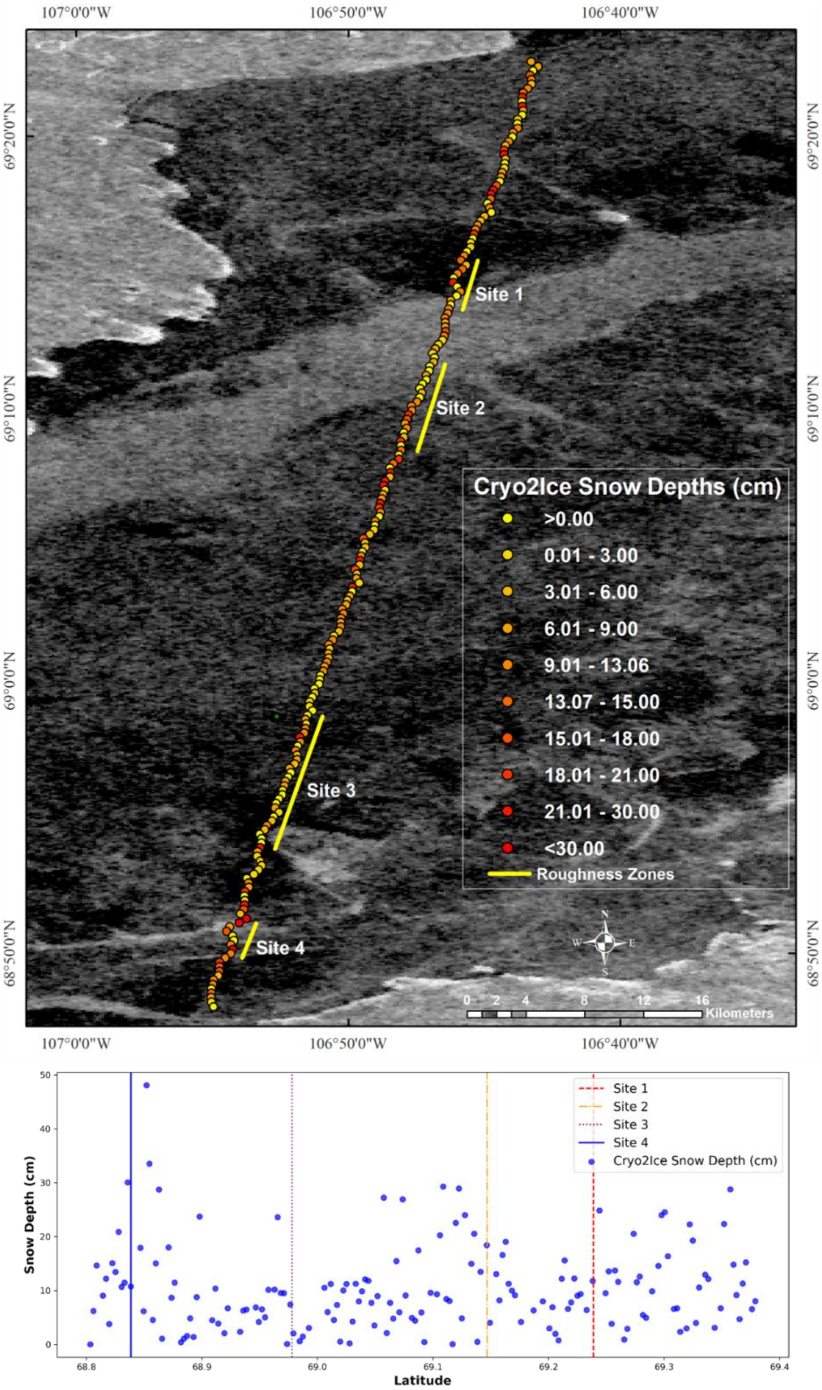

Figure 34 Spatial distribution of 300-m scale snow depths across the CS2 and IS2 derived track. The background image is a Sentinel-1 HH backscatter image from 5-05-2022. The bottom plot shows the along-track Cryo2Ice snow depth variation plotted against latitude.

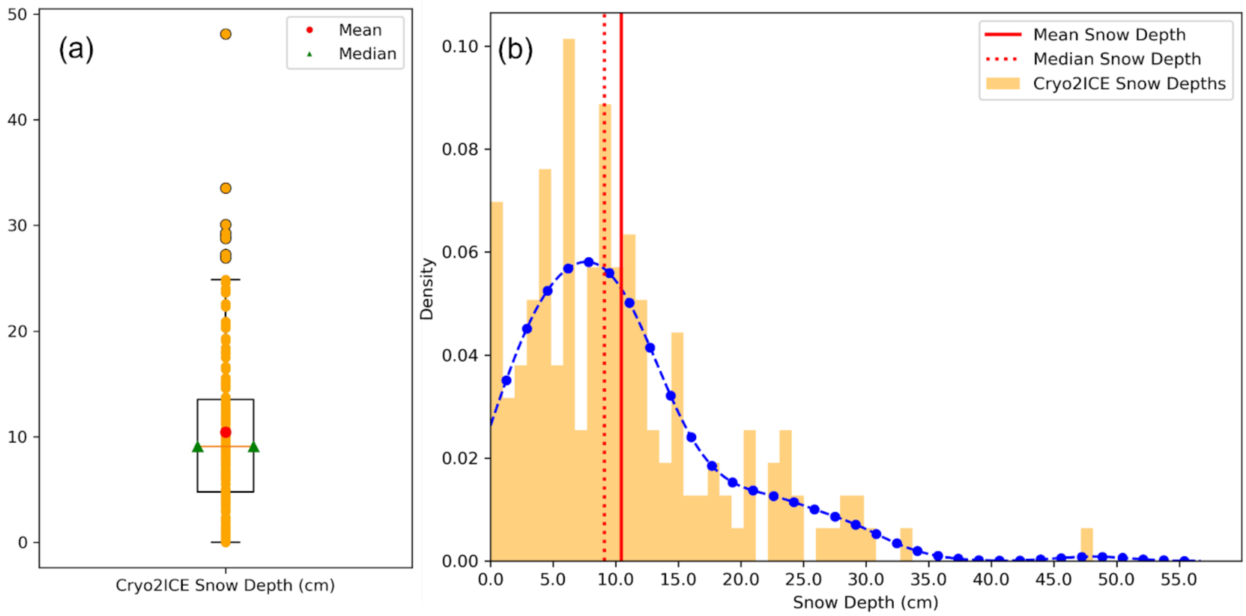

Figure 35 (a) Boxplot showing the distribution of Cryo2Ice snow depth along with the mean and median snow depths symbolized (b) Histogram showing the density distribution of the retrieved snow depth along the Cryo2Ice track with the mean and the median snow depths.

## 4.5 Discussion

### 4.5.1 Comparison with Past Studies

Previous field observations from Yackel et al. (2019) and Nandan et al. (2020) suggest that mean snow depth on FYI in Dease Strait during late winter ranges between 10 and 30 cm depth (Table 4). Both our mean in-situ snow depth measurements (11.9 cm) and Cryo2Ice retrieved mean snow depths (10.4 cm), are within the typical range reported in previous surveys (Table 4).

Table 4 In-situ snow depth measurements at Dease Strait. The range of mean snow depths represents the range of mean snow depths retrieved from the sampled sites.

| **Sampling Period** | **Mean Snow Depth (cm)** | **Number of Sites Sampled** | **Total Number of Samples** | **Sampling Technique** | **Reference** |
|---|---|---|---|---|---|
| 20 April to 9 June, 2014 | 13.5 | 24 | 24 | Snow Pits | Campbell et al., (2016) |
| 12 May to 17 June , 2014 | 20.8 | 2 | 60 | Meter Rule Sampling | Diaz et al., (2014) |
| 19-22 April, 2014 | 12.0/18.0 | 20 | 5200 | Meter Rule Sampling | Zheng et al., (2017) |
| 23-26 May, 2016 | 12.0/22.0 | 4 | 2100 | Meter Rule Sampling | Moon et al., (2019) |
| 01-08 April, 2017 | 17.0/ 35.0 | 5 | 2161 | Magnaprobe Sampling | Moon et al., (2019) |
| 17-19 May, 2018 | 20.9 / 21.8 | 3 |  | Magnaprobe Sampling | Yackel et al., (2019) |
| 1 May, 2022 | 11.9 | 4 | 1596 | Magnaprobe Sampling | This Study |
| Cryo2Ice Snow Depths | 10.4 (Mean), 48.1 (Maximum) |  |  |  |  |

### 4.5.2 Snow Depth: Cryo2Ice vs In-situ

Cryo2Ice snow depths showed similar relative patterns when compared to in-situ snow depth sampling. The thinnest (Site 3) and thickest (Site 4) mean snow depths found in the in-situ measurements are corroborated with Cryo2Ice snow depths as well (Table 5). The Kruskal-Wallis non-parametric test was conducted to assess statistically significant differences between the snow depths retrieved from the in-situ and Cryo2Ice. The test results show significant difference between in-situ sites which was also evident in the corresponding Cryo2Ice snow depths.

Although the mean snow depth for the entire studied Cryo2Ice track was 10.4 cm, the mean snow depth from Cryo2Ice samples at the site locations was 9.9 cm. This compares to a mean in-situ snow depth of 11.9 cm (Table 5). Cryo2Ice snow depths are on average 2.15 cm thinner than the in-situ data, which is a 0.5 cm larger difference than the manual tidal correction we applied to compare the CS2 and IS2 track heights (i.e., the largest known systematic uncertainty during processing). This pattern of a few cm mean snow depth underestimations by Cryo2Ice is consistently observed across three of the four sites: Sites 1, 2 and 3 (Figure 37).

Table 5 In-situ versus Cryo2Ice snow distribution statistics

| | | **Mean (cm)** | **Median (cm)** | **Lower Quartile (cm)** | **Upper Quartile (cm)** | **Inter-quartile range (cm)** |
|---|---|---|---|---|---|---|
| Site 1 | In-Situ | 12.2 | 7.8 | 4.1 | 16.3 | 12.2 |
| | Cryo2Ice | 8.9 | 8.8 | 5.8 | 10.2 | 4.4 |
| Site 2 | In-Situ | 9.7 | 5.2 | 3.7 | 9.2 | 5.5 |
| | Cryo2Ice | 8.1 | 7.4 | 5.2 | 11.1 | 5.9 |

| | | | | | | |
|---|---|---|---|---|---|---|
| Site 3 | In-Situ | 8.9 | 6.9 | 4.2 | 11.9 | 7.7 |
| | Cryo2Ice | 5.4 | 5.2 | 3.1 | 7.7 | 4.6 |
| Site 4 | In-Situ | 17.1 | 13.8 | 6.7 | 22.4 | 15.7 |
| | Cryo2Ice | 17.1 | 13.5 | 7.9 | 22.9 | 15.0 |

While the mean snow depth seems to be highly impacted by the presence of high snow depth sites especially around ridges, the median snow depth presents a more representative statistic for comparing the retrieved Cryo2Ice snow depth with the in-situ distribution. The median snow depths retrieved from Cryo2Ice are accurate to within ± 2.0 cm of median snow depths retrieved from all the different sites. There was an overestimation of the median snow depth by 1.0 cm and 2.2 cm for Sites 1 and Site 2 respectively while there was an overestimation of snow depths at Site 3 (1.7 cm). The best correspondence between the Cryo2Ice distributions in terms of median snow depth can be found in Site 4 which had a median snow depth much higher than the rest of the sites (Table 4).

We also notice that the impact of ridging on the overall accuracy of the technique was significant. The standard deviation of the in-situ snow depths is highest (Figure 36) and ridging is picked up from IS2 heights (Figure 34) at Site 2 where Cryo2Ice performs the worst. In terms of the overall shape of the distributions, the best match is found for Site 3 which has the lowest median snow depth among the sites. These mismatches may be caused by the difference in sampling length-scales between Cryo2Ice, which is at the kilometre scale, compared to in-situ measurements which are retrieved over 100s of metres. It is evident that while IS2 has a much finer resolution, the larger footprint of CS2 means that the spatial variability of snow depths under the kilometre scale are not well represented by Cryo2Ice. For instance, the Cryo2Ice snow depths are consistently truncated at the thick end of the distribution, with at least some portion of the in-situ distributions above ~30-50 cm seemingly unresolved from space (Figure 37).

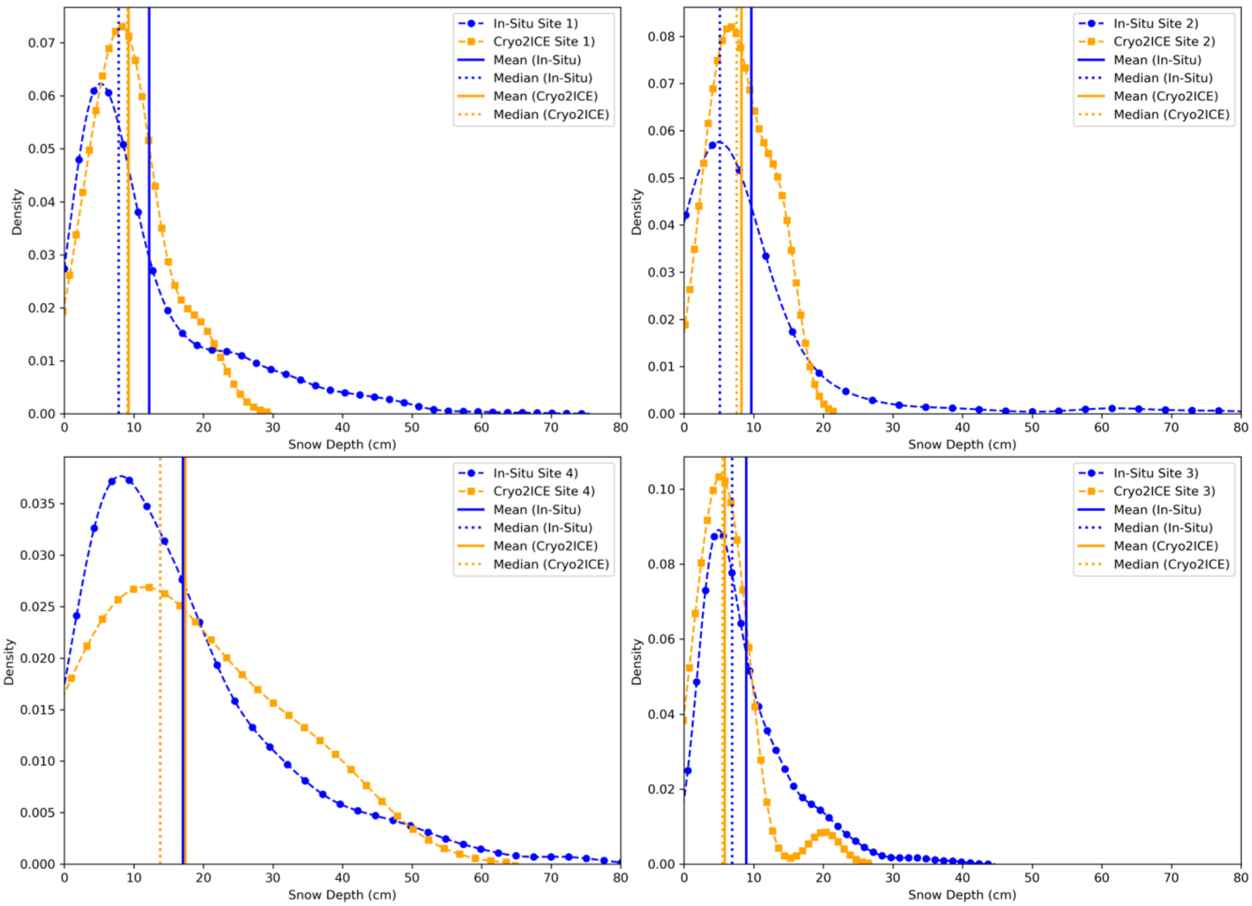

Figure 36 Probability Density plots comparing In-Situ snow depths to Cryo2Ice retrieved snow depths along with the median and mean values.

### 4.5.3 Snow Geophysical Properties and Cryo2Ice Retrievals

Both snow salinity and bulk density changes across the snowpack layer impacts the IS2 laser and CS2 radar waveform interactions with the snowpack. While the IS2 green laser is mostly impacted by the air-snow interface conditions, CS2 radar waveforms interact with different layers of the snowpack and the dominant scattering horizon and subsequently radar heights can potentially be impacted by the snow properties. There were significant differences among the snow salinity and density characteristics (Figure 33) between the surveyed sites. We notice that Cryo2Ice performs best in Site 4 which has the lowest mean snow salinity and has non-saline (<1 ppt) snow layers for the largest portion of the snow pack (Figure 33). Therefore, with 17 cm out of the 22 cm deep snowpack at Site 4 being non-saline, the maximum intensity of the CS2 backscatter may have been sourced from closer to the sea-ice interface. On the contrary, highly saline layers can potentially raise the height of dominant scattering intensity of the Ku-band radar leading to overestimated CS2 heights (*h(CS2)*) and subsequently lower mean snow depth compared to in-situ values. This phenomenon of snow depth underestimation was evident in Sites 1R, 1S and 2 potentially because of the sharp increase in snow salinity within the first 5 cm (from the air-snow interface) of the snowpack (Figure 33) and may have contributed to the 2-3 cm mean underestimation of Cryo2Ice snow depths.

The impact of snow bulk density on the Cryo2Ice retrievals was less likely except for the presence of wind-slab layers which are identified as stark increases in snow bulk densities within the snow pack. The wind-slab layers identified in Sites 1R, 2 and 4 reach to 0.425 g/cm$^3$ compared to 0.358 to 0.374 g/cm$^3$ on average throughout the snow pack which may have caused hindrance to Ku-band penetration. The presence of this high-density snow layer along with the reduction in Ku-band speed due to power attenuation of Ku-band microwaves may potentially cause a cumulative upward shift of the dominant scattering horizon resulting in underestimation of snow depths.

### 4.5.4 Sea Surface Height Estimation and Cryo2Ice Retrievals

Canadian Hydrographic Service (CHS) tidal predictions for 29 April 2022 suggest the satellite overpasses occurred during a low tide period. According to the predictions, the water level was 6 cm higher for the IS2 pass at 21:18 UTC than for the CS2 pass at 22:35 UTC (Appendix 3). This

6 cm water level difference should ideally be accounted for by the difference in IS2 and CS2 ocean tide corrections. The IS2 ATL07 heights were reduced by a mean ocean tide correction of -0.71 cm whereas the CS2 Heights reduced by an average ocean tide correction of -8.64 cm. Therefore, the difference between IS2 heights and CS2 heights was increased by 7.9 cm due to the ocean tide correction adjustment but the CHS predictions suggest it should have been only 6.0 cm. This 1.9 cm difference would introduce a 17% bias in retrieved snow depths, given the approx. mean snow depths we measured in-situ. This error could be attributed to the ocean tide corrections used in IS2 and CS2 originating from two different models i.e. GOT 4.8 (IS2) and FES 2004 (CS2). To put this source of error into wider context, past CS2 and IS2 coincident tracks from 15-04-2021 and 14-05-2021 were also analysed. We found a bias of 2 to 5 cm when compared with the CHS dataset, meaning that we can expect ~15-40% systematic uncertainty in Cryo2Ice retrieved snow depths owing to the uncertainty in tidal differences between satellite passes. This is a significant uncertainty, but it is systematic and varies at the length-scale of the tidal corrections (100s km), so it will not affect the *relative* variations in retrieved snow depth along track, only their *absolute* magnitude. Therefore, Cryo2Ice seems capable of measuring the relative variations in snow depth between different locations of the CAA without the availability of sea surface reference tie-points.

### 4.5.5 Surface Roughness and Cryo2Ice retrievals

Surface roughness calculated from IS2 was used to analyze the Cryo2Ice snow depths between sites with different roughness. There was only a weak positive correlation ($R^2$ 0.04) between surface roughness retrieved from IS2 and Cryo2Ice snow depths. Site 4 had the highest mean surface roughness (4.58 cm) whereas the other sites had roughness ranging between 2.4-2.7 cm. Although there was significant ridging in Site 2 and IS2 does pick up some of the ridges (Figure 34), the mean surface roughness is low (2.48 cm) because of the extensive areas of thin snow cover which dominates the laser returns. While Site 4 had the highest snow depth as well as highest surface roughness from IS2, the Cryo2Ice retrievals were most accurate both in terms of mean and median bias among all the four sites (Figure 37). However, one stark difference was the fact that there was no ridging in Site 4. Therefore, while there were extensive areas of rough sea ice with snow depths between 20 and 50 cm, there were hardly any snow depths greater than 80 cm (Figure 37). We also notice that for Site 2, the majority of the snow was very thin with only a few very high snow depth points especially around the ridges (Figure 37). The presence of isolated ridges and the deeper snow accumulated around them may have been missed by the CryoSat-2 radar given the larger impact of level ice versus ridges on the backscattered power. The ridge heights may also be underestimated with current ICESat-2 processing methods (Ricker et al., 2023) meaning that snow depths would be underestimated. The higher variability which is indicated by the standard deviation of snow depths translates to greater mean bias in snow depth (Figure 36).

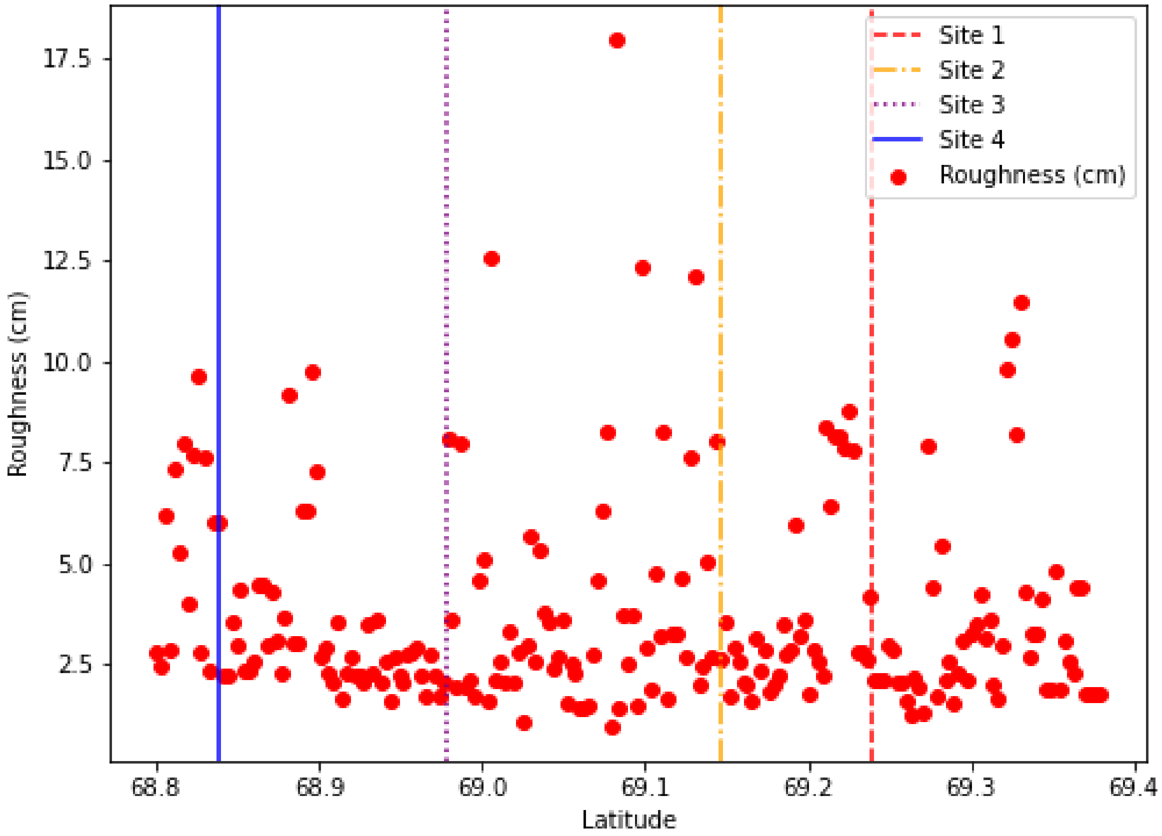

Figure 37 Variation in surface roughness along the Cryo2Ice track at the four in-situ snow thickness validation sites

### 4.6 Conclusion

Accurate snow depth monitoring over landfast ice in the Canadian Arctic Archipelago (CAA) is important for communities that rely on landfast ice for transportation and their livelihood (Mahoney et al., 2009). It is imperative to monitor snow depth in the CAA as there have been reports of declining snow depths at a rate of 0.8 cm per decade in Cambridge Bay and at other locations in the CAA (Howell et al., 2016; Lam et al., 2023). Moreover, they reported snow depth on sea ice trends were highly correlated to the declining sea ice thickness. Therefore, this study explores the potential of retrieving snow depth using Cryo2Ice in a lead-less regions of the Canadian Arctic Archipelago.

Snow depth from Cryo2Ice is retrieved based on the elevation difference between IS2 and CS2 sea ice heights from a common ellipsoid as opposed to the popular freeboard differencing method. The instantaneous difference in sea level between the ~1.5hour difference between the CS2 and IS2 passes is accounted for by adjusting the ocean tide corrections with local tide model predictions. The snow depths retrieved from Cryo2Ice compare favourably with in-situ snow depth measurements. The relative snow depth patterns from in-situ field sites were corroborated with Cryo2Ice measurements, i.e. the thinnest and thickest snow depth regions were picked up correctly by Cryo2Ice. The mean snow depth from Cryo2Ice of 10.4 cm is realistic compared to in-situ measurements from this study and previous studies conducted at the Dease Strait. The site-wise comparison between in-situ snow depths and Cryo2Ice snow depths from representative roughness zones demonstrates that the best correspondence is from sites which have the thickest snow and fewest ridges. Differences in the shapes of the distributions from in-situ sites and representative roughness zones of the Cryo2Ice are mostly a result of the difference in sampling resolutions of Cryo2Ice (~300 m) and the in-situ measurements (5 m). The tails of the in-situ snow depth distributions (> 40 cm) were largely missed by Cryo2Ice and the Cryo2Ice snow depth retrieval accuracy is impacted by the presence of sea ice ridges, with ridged sites having underestimated snow depths by as much as ~ 3.3 cm.

Snow geophysical properties especially snow salinity in the deepest few centimetres of the snow pack, may impact the dominant scattering centre of the CS2 radar return and can lead to underestimation of the snow depths. The snow depth was slightly underestimated in 3 out of 4 sites by 20.7% compared to in-situ measurements. However, median Cryo2Ice snow depths – reducing the impact of the missing thick snow tail in Cryo2Ice snow depth distributions – did not generally underestimate the in-situ values. Therefore, such physical factors (ridging, high salinity) did not seem to produce biases greater than the systematic uncertainty on the difference in ocean tidal corrections (1.90 cm), for our studied track. If these physical biases were larger for another scenario/track, when the tidal uncertainty is zero (i.e., in areas with leads) or snow pack thicker/roughness larger, they may have significant impacts on the retrieval process. However, it is difficult to attribute a few centimetres of bias to snow geophysical process, surface roughness and/or errors in the altimeters' tidal corrections. Therefore, further studies are required in different lead-less regions under varying snow conditions for improved insights into the sources of bias in snow depth retrievals from Cryo2Ice. Findings from this study are encouraging for estimating snow depth on landfast sea ice in lead-less regions using Cryo2Ice and for future coincident laser-radar or dual-frequency altimeter missions.

## References

Andersen, O. B., Nilsen, K., Sørensen, L. S., Skourup, H., Andersen, N. H., Nagler, T., Wuite, J., Kouraev, A., Zakharova, E., & Fernandez, D. (2019). Arctic freshwater fluxes from earth observation data: International Review Workshop on Satellite Altimetry Cal/Val Activities and Applications. *Fiducial Reference Measurements for Altimetry*, 97–103. https://doi.org/10.1007/1345_2019_75

Andreas, E. L. (2011). A relationship between the aerodynamic and physical roughness of winter sea ice. *Quarterly Journal of the Royal Meteorological Society*, *137*(659), 1581–1588. https://doi.org/10.1002/qj.842

Bagnardi, M., Kurtz, N. T., Petty, A. A., & Kwok, R. (2021). Sea Surface Height Anomalies of the Arctic Ocean From ICESat-2: A First Examination and Comparisons With CryoSat-2. *Geophysical Research Letters*, *48*(14), e2021GL093155. https://doi.org/10.1029/2021GL093155

Cafarella, S. M., Scharien, R., Geldsetzer, T., Howell, S., Haas, C., Segal, R., & Nasonova, S. (2019). Estimation of Level and Deformed First-Year Sea Ice Surface Roughness in the Canadian Arctic Archipelago from C- and L-Band Synthetic Aperture Radar. *Canadian Journal of Remote Sensing*, *45*(3–4), 457–475. https://doi.org/10.1080/07038992.2019.1647102

Campbell, K., Mundy, C. J., Belzile, C., Delaforge, A., & Rysgaard, S. (2018). Seasonal dynamics of algal and bacterial communities in Arctic sea ice under variable snow cover. *Polar Biology*, *41*(1), 41–58. https://doi.org/10.1007/s00300-017-2168-2

De Rijke-Thomas, C., Landy, J. C., Mallett, R., Willatt, R. C., Tsamados, M., & King, J. (2023). Airborne Investigation of Quasi-Specular Ku-Band Radar Scattering for Satellite Altimetry Over Snow-Covered Arctic Sea Ice. *IEEE Transactions on Geoscience and Remote Sensing*, *61*, 1–19. https://doi.org/10.1109/TGRS.2023.3318263

ESA. (2013). *CryoSat-2 Product Handbook*.

ESA. (2020). *About CRYO2ICE - Earth Online*. https://earth.esa.int/eogateway/missions/cryosat/cryo2ice

Farrell, S. L., Duncan, K., Buckley, E. M., Richter-Menge, J., & Li, R. (2020). Mapping Sea Ice Surface Topography in High Fidelity With ICESat-2. *Geophysical Research Letters*, *47*(21), e2020GL090708. https://doi.org/10.1029/2020GL090708

Fons, S. W., Kurtz, N. T., Bagnardi, M., Petty, A. A., & Tilling, R. L. (2021). Assessing CryoSat-2 Antarctic Snow Freeboard Retrievals Using Data From ICESat-2. *Earth and Space Science*, *8*(7), e2021EA001728. https://doi.org/10.1029/2021EA001728

Galley, R. J., Else, B. G. T., Howell, S. E. L., Lukovich, J. V., & Barber, D. G. (2012). Landfast Sea Ice Conditions in the Canadian Arctic: 1983-2009. *Arctic*, *65*(2), 133–144.

Howell, S. E. L., Laliberté, F., Kwok, R., Derksen, C., & King, J. (2016). Landfast ice thickness in the Canadian Arctic Archipelago from observations and models. *The Cryosphere*, *10*(4), 1463–1475. https://doi.org/10.5194/tc-10-1463-2016

Kacimi, S., & Kwok, R. (2020). The Antarctic sea ice cover from ICESat-2 and CryoSat-2: Freeboard, snow depth, and ice thickness. *The Cryosphere*, *14*(12), 4453–4474. https://doi.org/10.5194/tc-14-4453-2020

Kwok, R., Kacimi, S., Webster, M. a., Kurtz, N. t., & Petty, A. a. (2020). Arctic Snow Depth and Sea Ice Thickness From ICESat-2 and CryoSat-2 Freeboards: A First Examination. *Journal of Geophysical Research: Oceans*, *125*(3), e2019JC016008. https://doi.org/10.1029/2019JC016008

Kwok, R., & Markus, T. (2018). Potential basin-scale estimates of Arctic snow depth with sea ice freeboards from CryoSat-2 and ICESat-2: An exploratory analysis. *Advances in Space Research*, *62*(6), 1243–1250. https://doi.org/10.1016/j.asr.2017.09.007

Kwok, R., Petty, A. A., Bagnardi, M., Kurtz, N. T., Cunningham, G. F., Ivanoff, A., & Kacimi, S. (2021). Refining the sea surface identification approach for determining freeboards in the ICESat-2 sea ice products. *The Cryosphere*, *15*(2), 821–833. https://doi.org/10.5194/tc-15-821-2021

Kwok, R., Petty, A., Bagnardi, M., Wimert, J. T., Cunningham, G. F., Hancock, D. W., Ivanoff, A., & Kurtz, N. (2023). *Ice, Cloud, and Land Elevation Satellite (ICESat-2) Project Algorithm Theoretical Basis Document (ATBD) for Sea Ice Products, version 6*. https://doi.org/10.5067/9VT7NJWOTV3I

Lam, H. M., Geldsetzer, T., Howell, S. E. L., & Yackel, J. (2023). Snow Depth on Sea Ice and on Land in the Canadian Arctic from Long-Term Observations. *Atmosphere-Ocean*, *61*(4), 217–233. https://doi.org/10.1080/07055900.2022.2060178

Landy, J. C., Petty, A. A., Tsamados, M., & Stroeve, J. C. (2020). Sea Ice Roughness Overlooked as a Key Source of Uncertainty in CryoSat-2 Ice Freeboard Retrievals. *Journal of Geophysical Research: Oceans*, *125*(5), e2019JC015820. https://doi.org/10.1029/2019JC015820

Landy, J. C., Tsamados, M., & Scharien, R. K. (2019). A Facet-Based Numerical Model for Simulating SAR Altimeter Echoes From Heterogeneous Sea Ice Surfaces. *IEEE Transactions on Geoscience and Remote Sensing*, *57*(7), 4164–4180. https://doi.org/10.1109/TGRS.2018.2889763

Leuschen, C. J., Swift, R. N., Comiso, J. C., Raney, R. K., Chapman, R. D., Krabill, W. B., & Sonntag, J. G. (2008). Combination of laser and radar altimeter height measurements to estimate snow depth during the 2004 Antarctic AMSR-E Sea Ice field campaign. *Journal of Geophysical Research: Oceans*, *113*(C4). https://doi.org/10.1029/2007JC004285

Magruder, L. A., Brunt, K. M., & Alonzo, M. (2020). Early ICESat-2 on-orbit Geolocation Validation Using Ground-Based Corner Cube Retro-Reflectors. *Remote Sensing*, *12*(21), Art. 21. https://doi.org/10.3390/rs12213653

Mahoney, A., Gearheard, S., Oshima, T., & Qillaq, T. (2009). Sea Ice Thickness Measurements from a Community-Based Observing Network. *Bulletin of the American Meteorological Society*, *90*(3), 370–378. https://doi.org/10.1175/2008BAMS2696.1

Mallett, R. D. C., Lawrence, I. R., Stroeve, J. C., Landy, J. C., & Tsamados, M. (2020). Brief communication: Conventional assumptions involving the speed of radar waves in snow introduce systematic underestimates to sea ice thickness and seasonal growth rate estimates. *The Cryosphere*, *14*(1), 251–260. https://doi.org/10.5194/tc-14-251-2020

Maykut, G. A., & Untersteiner, N. (1971). Some results from a time-dependent thermodynamic model of sea ice. *Journal of Geophysical Research (1896-1977)*, *76*(6), 1550–1575. https://doi.org/10.1029/JC076i006p01550

Meier, W., & Stroeve, J. (2022). An Updated Assessment of the Changing Arctic Sea Ice Cover. *Oceanography*. https://doi.org/10.5670/oceanog.2022.114

Melling, H. (2002). Sea ice of the northern Canadian Arctic Archipelago. *Journal of Geophysical Research: Oceans*, *107*(C11), 2-1-2–21. https://doi.org/10.1029/2001JC001102

Moon, W., Nandan, V., Scharien, R. K., Wilkinson, J., Yackel, J. J., Barrett, A., Lawrence, I., Segal, R. A., Stroeve, J., Mahmud, M., Duke, P. J., & Else, B. (2019). Physical length scales of wind-blown snow redistribution and accumulation on relatively smooth Arctic first-year sea ice. *Environmental Research Letters*, *14*(10), 104003. https://doi.org/10.1088/1748-9326/ab3b8d

Mundy, C. J., Barber, D. G., & Michel, C. (2005). Variability of snow and ice thermal, physical and optical properties pertinent to sea ice algae biomass during spring. *Journal of Marine Systems*, *58*(3), 107–120. https://doi.org/10.1016/j.jmarsys.2005.07.003

Nandan, V., Geldsetzer, T., Yackel, J., Mahmud, M., Scharien, R., Howell, S., King, J., Ricker, R., & Else, B. (2017). Effect of Snow Salinity on CryoSat-2 Arctic First-Year Sea Ice Freeboard Measurements. *Geophysical Research Letters*, *44*(20), 10,419-10,426. https://doi.org/10.1002/2017GL074506

Nandan, V., Scharien, R. K., Geldsetzer, T., Kwok, R., Yackel, J. J., Mahmud, M. S., Rösel, A., Tonboe, R., Granskog, M., Willatt, R., Stroeve, J., Nomura, D., & Frey, M. (2020). Snow Property Controls on Modeled Ku-Band Altimeter Estimates of First-Year Sea Ice Thickness: Case Studies From the Canadian and Norwegian Arctic. *IEEE Journal of*

*Selected Topics in Applied Earth Observations and Remote Sensing, 13,* 1082–1096. https://doi.org/10.1109/JSTARS.2020.2966432

Neumann, T. A., Martino, A. J., Markus, T., Bae, S., Bock, M. R., Brenner, A. C., Brunt, K. M., Cavanaugh, J., Fernandes, S. T., Hancock, D. W., Harbeck, K., Lee, J., Kurtz, N. T., Luers, P. J., Luthcke, S. B., Magruder, L., Pennington, T. A., Ramos-Izquierdo, L., Rebold, T., … Thomas, T. C. (2019). The Ice, Cloud, and Land Elevation Satellite – 2 mission: A global geolocated photon product derived from the Advanced Topographic Laser Altimeter System. *Remote Sensing of Environment*, *233*, 111325. https://doi.org/10.1016/j.rse.2019.111325

Ricker, R., Hendricks, S., Helm, V., Skourup, H., & Davidson, M. (2014). Sensitivity of CryoSat-2 Arctic sea-ice freeboard and thickness on radar-waveform interpretation. *The Cryosphere*, *8*(4), 1607–1622. https://doi.org/10.5194/tc-8-1607-2014

Rotermund, L. M., Williams, W. J., Klymak, J. M., Wu, Y., Scharien, R. K., & Haas, C. (2021). The Effect of Sea Ice on Tidal Propagation in the Kitikmeot Sea, Canadian Arctic Archipelago. *Journal of Geophysical Research: Oceans, 126*(5), e2020JC016786. https://doi.org/10.1029/2020JC016786

Tilling, R. L., Ridout, A., & Shepherd, A. (2018). Estimating Arctic sea ice thickness and volume using CryoSat-2 radar altimeter data. *Advances in Space Research*, *62*(6), 1203–1225. https://doi.org/10.1016/j.asr.2017.10.051

Ullaby, F. T., Moore, R. K., & Fung, A. K. (1987). Microwave Remote Sensing. Active and Passive. *Geological Magazine, 124*(1), 88–88. https://doi.org/10.1017/S0016756800015831

Webster, M., Gerland, S., Holland, M., Hunke, E., Kwok, R., Lecomte, O., Massom, R., Perovich, D., & Sturm, M. (2018). Snow in the changing sea-ice systems. *Nature Climate Change*, *8*(11), Art. 11. https://doi.org/10.1038/s41558-018-0286-7

Willatt, R., Laxon, S., Giles, K., Cullen, R., Haas, C., & Helm, V. (2011). Ku-band radar penetration into snow cover on Arctic sea ice using airborne data. *Annals of Glaciology*, *52*(57), 197–205. https://doi.org/10.3189/172756411795931589

Xu, C., Mikhael, W., Myers, P. G., Else, B., Sims, R. P., & Zhou, Q. (2021). Effects of Seasonal Ice Coverage on the Physical Oceanographic Conditions of the Kitikmeot Sea in the Canadian Arctic Archipelago. *Atmosphere-Ocean*, *59*(4–5), 214–232. https://doi.org/10.1080/07055900.2021.1965531

Yackel, J., Geldsetzer, T., Mahmud, M., Nandan, V., Howell, S. E. L., Scharien, R. K., & Lam, H. M. (2019). Snow Thickness Estimation on First-Year Sea Ice from Late Winter Spaceborne Scatterometer Backscatter Variance. *Remote Sensing*, *11*(4), Art. 4. https://doi.org/10.3390/rs11040417

Zheng, J., Geldsetzer, T., & Yackel, J. (2017). Snow thickness estimation on first-year sea ice using microwave and optical remote sensing with melt modelling. *Remote Sensing of Environment*, *199*, 321–332. https://doi.org/10.1016/j.rse.2017.06.038

## Appendix

Appendix 1: Geophysical corrections applied on the IS2 ATL07 product. The range represents the typical variation in the corrections as reported in the IS2 Algorithm Theoretical Basis Document (ATBD).

| **Geophysical Correction** | **Typical Range** | **Source** |
|---|---|---|
| Solid Earth Tide | -19 to +27 cm | IERS 2010 (Applied in ATL03) |
| Solid Earth Pole Tides | -0.6 to +0.7 cm | IERS 2010 (Applied on ATL03) |
| Ocean Pole tides | +/- 2 mm | IERS 2010 (Applied in ATL03) |
| Ocean loading | -9.7 to +9.3 cm | GOT4.8 Ocean Tide Model (Applied in ATL07) |
| Ocean Tides | -6.2 to +6.2 m | GOT4.8 Ocean Tide Model<br>(Applied in ATL07) |
| Long period equilibrium tides | -7.1 to +6.0 cm | GOT4.8 Ocean Tide Model<br>(Applied in ATL07) |
| Inverted barometer | -53 to +94 cm | ATL09/GEOS5 FP-IT<br>(Applied in ATL07) |

Appendix 2: Geophysical Corrections applied in the CS2 Level 2 product. The typical range values are reported in the Cryosat-2 Baseline E Level 2 Product Handbook.

| **Geophysical Correction** | **Typical Range** | **Source** |
|---|---|---|
| Ocean Tide | -50 to +50 cm | Finite Element Solution FES 2004 Tide Model |

| | | |
|---|---|---|
| Long-Period Equilibrium Ocean Tide | < 1cm | Finite Element Solution FES 2004 Tide Model |
| Ocean Loading | -2 to +2 cm | Finite Element Solution FES<br>2004 Tide Model |
| Solid Earth Tide | -30 to +30 cm | Cartwright Tide model (Cartwright & Edden, 1973) |
| Geocentric Polar Tide | -2 to +2 cm | Historical Pole Positions from CNES |
| Inverved Barometer | -15 to +15 cm | Dynamic Surface Pressure from Meteo France |

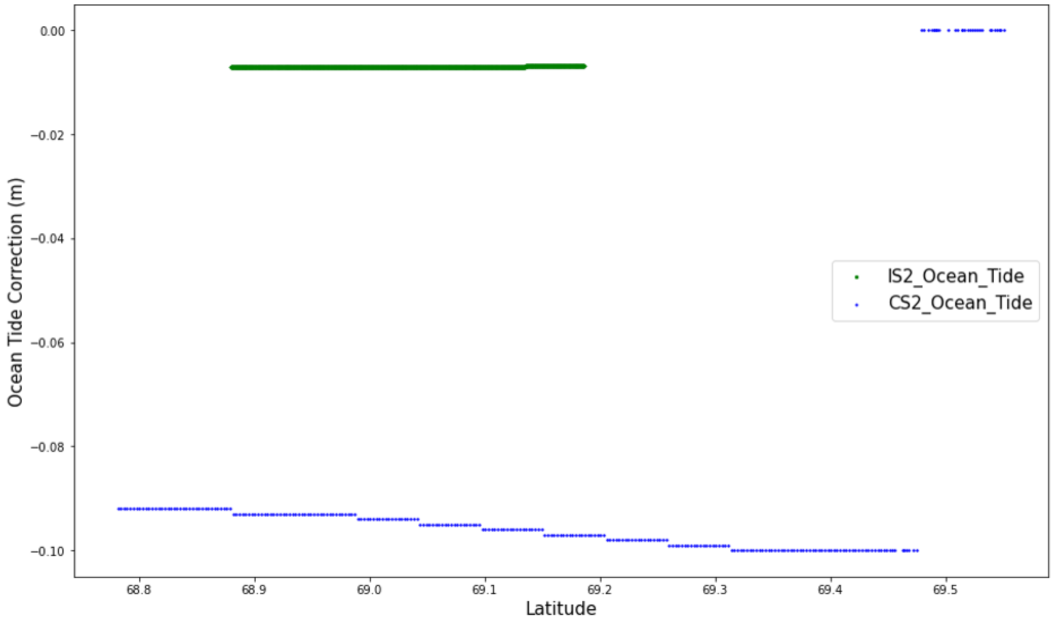

Appendix 3: Ocean tidal correction used in the IS2 and CS2 tracks. The IS2 ocean tide corrections are shown in green while the CS2 ocean tide corrections are shown in blue.

# Chapter 5

# Conclusion

## 5.1 Summary

This thesis focuses on investigating the application of satellite altimetry to estimate snow depth on sea ice in the Canadian Arctic. Satellite altimetry has been considered to be the most viable observation technique for monitoring snow depth on sea ice which has been the most critical uncertainty for estimating sea ice thickness in the Arctic. However, satellite altimetry approaches have vital uncertainties especially related to the position of the dominant scattering horizon of the Ku-band radar interacting with the snow depth on sea ice in addition to uncertainties related to spatial resolution of the sensors, impact of snow geophysical properties on Ku-band interaction and the impact of surface roughness. The dual-frequency and coincident laser/ radar approaches for estimating snow depth on sea ice are explored in Chapter 3 and Chapter 4 respectively. Thesis Objective (i) which aimed towards analyzing surface based dual microwave (Ku and Ka band) interaction over sea ice and lake ice is addressed in Chapter 3 while thesis Objective (ii) aimed towards retrieving and validating satellite based coincident laser and radar (Ku band) snow depth measurements is addressed in Chapter 4.

Chapter 3 presents results from the first deployment of a surface based KuKa fully polarized radar over landfast first-year sea ice and lake ice. Critical observations about the position of the dominant scattering horizon of Ku and Ka band microwave are made from surface based radar altimeter mimicking the satellite dual-frequency radar altimeters. The impact of the presence of brine on the snow pack is compared to a non-saline snow on lake ice having similar snow depth and density. The position of the dominant scattering for both the Ka and Ku band is significantly different for snow on brine-wetted sea ice and fresh snow on lake ice. Both Ka and Ku co-polarized HH polarized waveforms have maximum scattering closer to the air-snow interface over brine wetted snow on sea ice which contradicts the general assumption of Ku band scattering from the snow-ice interface. However, a fresh snow pack over lake ice allows both the Ka and Ku to scatter beyond the snow-ice interface as deep as the ice-water interface. In contrast to the co-polarized Ku and Ka band waveforms used in the satellite level, the cross-polarized Ku waveforms used in conjunction with the co-polarized waveforms perform better at retrieving snow depth on first-year landfast sea ice. We notice that there are significant differences in interaction of both co-polarized HH and cross-polarized VH Ku and Ka band over both snow on sea ice and lake ice.  We notice that while currently active satellite altimeters operate in the co-polarized (HH) polarization for Ku and Ka band, a combined approach considering both HH and VH waveforms for Ka and Ku seem to give the best estimates of snow depth on sea ice. However, it is also apparent that considering Ku HH and VH polarizations as proposed by Willatt et al., (2023) seem to perform the best for estimating snow depth on sea ice.

While surface based observations are critical to test Ka and Ku band interactions with the snow pack, the difference in footprint size with satellite observations means that satellite measurements are more complex to interpret. Therefore, Chapter 4 presents the first near-coincident validation of snow depth retrieved from a combination of a near-coincident Cryosat-2 (Ku band) and ICESat-2 (green laser) over snow depth on landfast sea ice in the Canadian Arctic. The findings present the first evaluation of snow depths retrieved from Cryosat-2 and ICESat-2 over a lead-less landfast sea ice zone. The results suggest that reliable snow depth on sea ice may be derived using Cryo2Ice even in the lead-less Canadian Arctic Archipelago but the accuracy of the technique varies depending on the roughness, snow geophysical properties and also the difference in spatial resolution between the footprint of the altimeters. The study identifies the impact of surface roughness on the Cryo2Ice retrievals where the presence of ridges causes a large portion of the higher snow depth areas to be missed leading to a general underestimation of the snow depth. Moreover, the difference in spatial resolution between Cryosat-2 and ICESat-2 is attributed to be the cause behind snow depths greater than 30 cm to be generally missed by Cryo2Ice. We notice that snow salinity and density causes biases in the retrieved snow depths. The general underestimation of Cryo2ice snow depths compared to in-situ snow depths and the fact that all snow packs had saline basal snow layers demonstrates that Ku-band dominant scattering horizon may be significantly shifted up leading to a general underestimation of snow depths from Cryo2Ice in case of a saline snow pack. The findings from Chapter 4 are vital for current Cryo2Ice and future satellite altimeter missions such as Copernicus Polar Ice and Snow Topography Altimeter (CRISTAL) where the Ku-band will be used.

Overall, both studies explore two different scales (surface and satellite) and techniques (dual radar and coincident laser/radar) for estimating snow depth on sea ice. While the two studies were conducted on two different locations, i.e. Churchill and Cambridge Bay, both studies were over first-year landfast sea ice. Therefore, cumulatively, this thesis presents both surface based and satellite based altimeter observations over first-year landfast sea ice. While Chapter 4 provides observations on retrieved satellite products over the kilometre scale, Chapter 3 provides a much finer surface based observations. We notice from both studies that Ku-band microwave which is generally assumed to penetrate the snow pack completely only partially penetrates a saline snow pack which is often found on first-year sea ice. The study also shows that co-polarized (HH) Ku band waveforms which is currently used in satellites has a dominant scattering closer to the air-snow interface as opposed to the general assumed snow-ice interface especially when the snowpack is saline. Both studies demonstrate that snow geophysical properties especially snow salinity plays a determining role on the interaction of Ku band microwave with the snow pack. Surface roughness is also seen to be a major factor especially in the satellite level. However, as demonstrated in Chapter 4, the difference in spatial resolutions both between satellite altimeters and between satellite and surface (Chapter 3) play vital roles in the snow depth retrieval process involving Ku-band for both the dual-radar and coincident laser/radar approaches. However, further investigations on both the surface based and satellite levels are required for addressing uncertainties in snow depth estimations from satellite altimeters.

## 5.2 Limitations and Future Studies

### 5.2.1 Limitations

#### 5.2.1.1 Surface-Based Study (Chapter 3)

(a) Surface-based KuKa measurements were taken ~2km from the shore and therefore surface based measurements were difficult to compare to the satellite retrievals which are often impacted by land contamination.

(b) Difference in footprint size between surface based Ku and Ka band compared to corresponding satellites mean that these measurements can’t be directly compared.

(c) Co-locating the snow pit measurements with the exact KuKa waveform was difficult due to difference in GPS.

(d) Lake Ice thickness was not obtained from the field which meant that it was difficult to verify the ice-water interface.

#### 5.2.1.2 Satellite-Based Study (Chapter 4)

(a) Cryosat-2 and ICESat-2 have very different footprint sizes which introduces a systematic bias towards the retrieved snow depths.

(b) Although the study assumes Cryosat-2 and ICESat-2 to be exactly coincident, the difference in footprint sizes would mean that the snow depth observed from the two altimeters is slightly different.

(c) It was difficult to attribute centimetre scale biases identified in the satellite level to factors such as systematic errors between the sensors, impact of tides, surface roughness or snow geophysical properties.

(d) Snow geophysical properties obtained from single snow pits from particular sites made it difficult to make generalized conclusion on Ku-band interaction with snow from different conditions

(e) In-situ validation conducted in the scale of ~200 metre in 4 different sites does not represent the snow spatial heterogeneity over the entire ~75 kilometre Cryo2Ice track.

### 5.2.2 Future Studies

Although the two studies presented here in this thesis provide a fairly comprehensive look into the state of art for snow depth estimations using altimeters in terms of scale (surface and satellite) and type of approaches (dual-radar and coincident laser/radar), further investigation is required to resolve uncertainties in snow depth estimation from altimetry. The study shows the need for a comprehensive field campaign where surface, satellite as well as air-borne altimeters may be deployed. This would help resolve uncertainties due to scale of measurements and help ascertain uncertainties due to physical factors such as surface roughness. Further investigations including field based lake ice thickness exploring Ku and Ka band interaction over snow on lake ice can inform us more about the impact of brine.

Additionally, further investigations into satellite based approaches for obtaining snow depth from Cryo2Ice need to be conducted where we can test the proposed workflow in Chapter 4 over different landfast sea ice locations. This could potentially lead to be a basin-scale snow depth on sea ice product from Cryo2Ice which could help address the massive data gaps in regions of landfast sea ice such as the Canadian Arctic Archipelago.